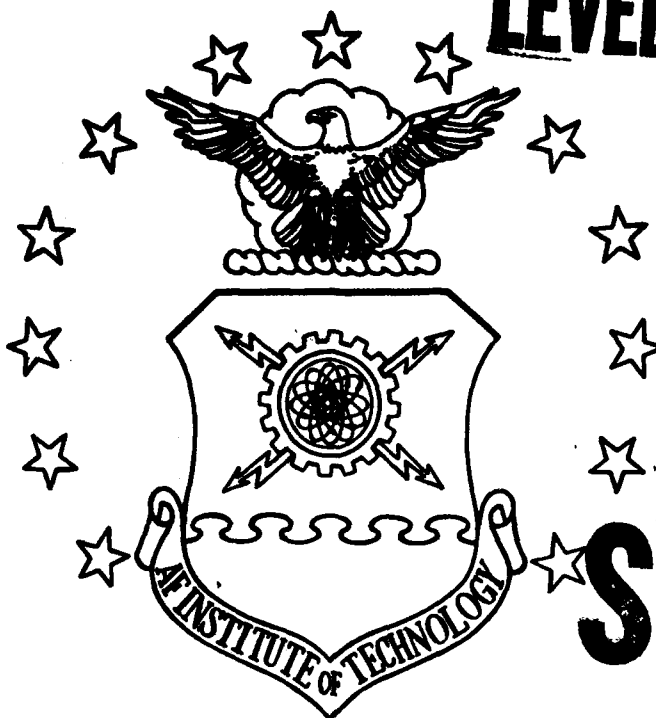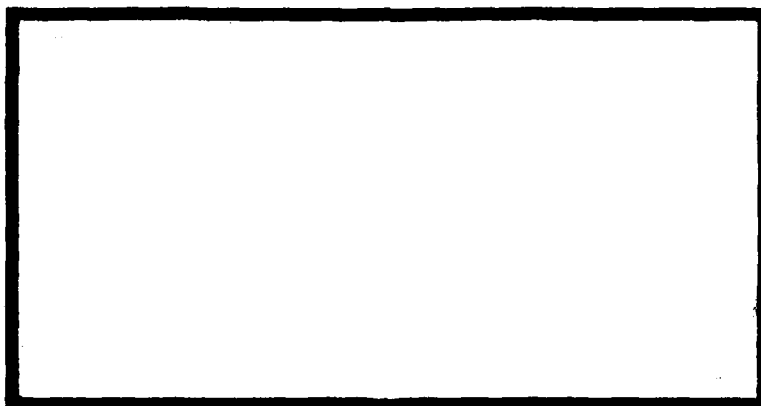LEVEL II

DTIC
ELECTE
FEB 1 9 1982
S
E
D

UNITED STATES AIR FORCE
AIR UNIVERSITY
AIR FORCE INSTITUTE OF TECHNOLOGY
Wright-Patterson Air Force Base, Ohio

82 02 18 129

LEVEL II

DTIC
FEB 19 1982

EXPERIMENTAL ANALYSIS OF THE
EFFECTS OF SWEEP AND ASPECT RATIO
ON INCOMPRESSIBLE FLOW ABOUT
FORWARD SWEPT WINGS

THESIS

GAE/AA/81D-26   Paul W. Savage

EXPERIMENTAL ANALYSIS OF THE

EFFECTS OF SWEEP AND ASPECT RATIO

ON INCOMPRESSIBLE FLOW ABOUT

FORWARD SWEPT WINGS

THESIS

Presented to the Faculty of the School Engineering

of the Air Force Institute of Technology

Air University

in Partial Fulfillment of the

Requirements for the Degree of

Master of Science

by

Paul W. Savage, B.S.A.E.

Graduate Aeronautical Engineering

December 1981

Preface

This report provides experimental incompressible, aerodynamic data on the effects of sweep and aspect ratio on forward swept wings. The data have been compared to the empirically based large aircraft performance prediction program LACBIN.

The Air Force Flight Dynamics Laboratory, Vehicle Synthesis Branch (FIMB) uses LACBIN to predict the performance of new aircraft designs. The recent use of forward swept wings in the design of aircraft led FIMB to question the ability of LACBIN to accurately predict forward swept wing aerodynamic characteristics. In order to test LACBIN, experimental data for varying wing parameters at several Mach numbers was needed. It was found that there was a significant lack of aerodynamic data on thin forward swept wings. Since the area of thin forward swept wings was of primary interest to FIMB, this test program was initiated to attain experimenrtal data for use in evaluating LACBIN. Although the data attained in this test program is only a portion of that requested by FIMB, it has provided a starting point for further testing and has shed some light on LACBIN's ability to predict aerodynamic characteristics of forward swept wings.

I would like to thank my thesis advisor, Major Michael L. Smith, for suggesting the topic and for his advice and guidance throughtout this effort. I would also like to thank Professor Harold C. Larsen for sharing his vast depth of knowledge with me. Special thanks to Wales S. Whitt and Nicholas Yardich for their tunnel operation and the Model Fabrication Division for their excellent model construction. Lastly, thanks to my wife who doubled as typist.

Contents

Contents

List of Figures

List of Tables

AR	Aspect ratio
c	Chord, in
C_D	Wing drag coefficient
C_L	Wing lift coefficient
C_M	Wing moment coefficient
C_{MAC}	Wing moment coefficient about the aerodynamic center
C_{MTR}	Wing moment coefficient about the trunnion
C_r	Root chord, in
C_t	Tip chord, in
M_{AC}	Moment about aerodynamic center, in-lbs
M_{TR}	Moment about trunnion, in-lbs
t	Section thickness, percent c
α	Angle of attack, deg
Λ	Leading edge sweep angle, deg, – equals forward sweep, + equals aft sweep

Abstract

Low speed wind tunnel tests were conducted on nine wing planforms to determine the effect of sweep and aspect ratio on forward swept wings in incompressible flow. Sweep angles tested were -15, -30 and -45 degrees. Aspect ratios ranged from 2.05 to 4.79. A NACA 0006 airfoil section perpendicular to the leading edge was used for all models. Results showed increasing negative sweep decreased lift curve slope and shifted the aerodynamic center rearward. Increasing aspect ratio increased lift curve slope, decreased drag coefficient and shifted the aerodynamic center rearward. The wind tunnel aerodynamic data were compared to the Air Force Flight Dynamics Laboratory's Large Aircraft Performance Prediction Program to determine the program's ability to predict forward swept wing aerodynamic coefficients. At incompressible Mach numbers, the program was found to be accurate in predicting lift curve slope in the linear range using a positive sweep input. Drag Polar slope and moment coefficient were accurately predicted for lift coefficients below 0.4 using a negative sweep angle input. Neither positive nor negative angle input predicted maximum lift coefficient accurately.

EXPERIMENTAL ANALYSIS OF THE EFFECTS OF SWEEP

AND ASPECT RATIO ON INCOMPRESSIBLE FLOW

ABOUT FORWARD SWEPT WINGS

I. Introduction

Objective

The objective of this thesis is to provide experimental aerodynamic
data on thin forward swept wings with varying sweep and aspect ratio for the
purpose of evaluating the accuracy of the Large Aircraft Performance
Prediction Program LACBIN.

Background

While the advantages of forward swept wings have been known for years,
structural limitations have prevented their use. But, recent advances in
the use of composite materials have made possible the incorporation of
forward swept wings in the design of aircraft without the prohibitive weight
increase associated with conventionally designed forward swept wings.

Even with these recent developments there is a lack of aerodynamic data
available on forward swept wings. Forward swept wings were tested in the
late 1940's by NACA, but not to the same extent as aft swept wings.
Again, this was due to the structural limitations imposed by the divergent
twisting moment of forward swept wings which appeared to make their use
unfeasible. To compound this lack of data problem, thin wings ($t/c \leq 0.1$),
which are in major use today, were not extensively tested.

This lack of data on thin forward swept wings came to the attention of
the Vehicle Synthesis Branch (FIMB) of the Air Force Flight Dynamics

1

Laboratory which is responsible for accessing aircraft performance. With recent use, by several manufacturers, of forward swept wings in fighter aircraft design, FIMB questioned whether their performance prediction program (LACBIN) could accurately predict the aerodynamic characteristics of forward swept wings. However, the lack of experimental data with a systematic varying of wing parameters prevented an accurate analysis.

Scope

FIMB is interested in a full range of experimental data from low speed to supersonic Mach numbers for comparison with their performace program. The following are the planform parameter ranges of interest to FIMB:

Aspect ratio, AR	2.0	to	5.5
Sweep angle, Λ	0°	to	-70°
Thickness ratio, t/c	0.04	to	0.06
Taper ratio, C_t/C_r	0	to	0.5

In addition to these parameters, the effects of high lift devices and canard configurations are also of interest.

Aerodynamic data desired include lift, drag, and pitching moment for the above mentioned parameters. Also, spanwise location of the center of pressure is desired. The problem was broken up into several areas. The area of interest for this thesis, includes the design of several wind tunnel test models that can be used in follow-on studies, as well as being used to investigate a range of sweep and aspect ratios at incompressible Mach numbers.

Lift, drag and pitching moment data were to be taken for all sweep angles and aspect ratios. The reduced wind tunnel data would then be compared to FIMB's program results and evaluated.

Approach

Three models were constructed, each with a different sweep angle. The angles were; -15, -30 and - 45 degrees. Each model had a basic tip and two extensions to allow investigation of three aspect ratios for each sweep. The nine aspect ratios varied from 2.05 to 4.79. Each model had a constant thickness ratio and taper ratio. The basic wing, extension one and extension two had the same area for each sweep angle (i.e. the basic wing area for the -15, -30, and -45 degree models was the same, etc.). The models were constructed of sufficient strength so as to decrease aeroelastic effects.

Tests were conducted in the Air Force Institute of Technology (AFIT) Five-Foot Wind Tunnel. Test Reynolds numbers based on chord length, ranged from 571,000 to 809,000. Mach number varied from 0.134 to 0.135. This latter variation was considered insignificant.

Model lift, drag and pitching moment were obtained using a wire balance system. Data were gathered from an angle of attack of -4 deg to well above the onset of tip flutter (from 14 to 16 deg). All data were then reduced to coefficient form.

Wing parameters for each model and extension were then input into FIMB's performance program which yielded C_L, C_D, and C_m data. These coefficients were then compared to the reduced wind tunnel data for accuracy.

II. Wind Tunnel Test Program

Test Models

All model construction was done by the AFIT Model Fabrication Division. Three basic constant chord forward swept wing planforms were constructed (Fig 1). Each model was built around a 3.0 in by 0.125 in steel spar which was centered at the quarter chord. The rest of the model was made of solid aluminum based epoxy resin. The spar was allowed to extend 0.375 in from both tips on each model. A tip was constructed to cover the spars of each basic model. It was secured to the spar by three screws. This is called the basic model for each of the three sweep angles. Two extensions for both tips on each wing were also constructed. These were of constant chord and each extension added 0.2 square feet to the planform area. They were also attached to the spar by three screws. A six percent thick airfoil section was used for all models. See Appendix A for airfoil and planform dimensional data.

Wind Tunnel

The AFIT Five-Foot Wind Tunnel was used for all tests. It is an open return, closed test section wind tunnel with a circular cross-section (Fig 2) . Two counter rotating 12-foot fans, powered by four 400-horsepower d.c. motors provide a speed capability of 300 mph. However, it has been down rated to a top speed of 200 mph. Forces for this experiment were measured by a wire balance system using three springless scales: front lift, rear lift and drag. The balance wires were aligned using an inclinometer and a plumb bob to insure the orthogonality of the system components.

4
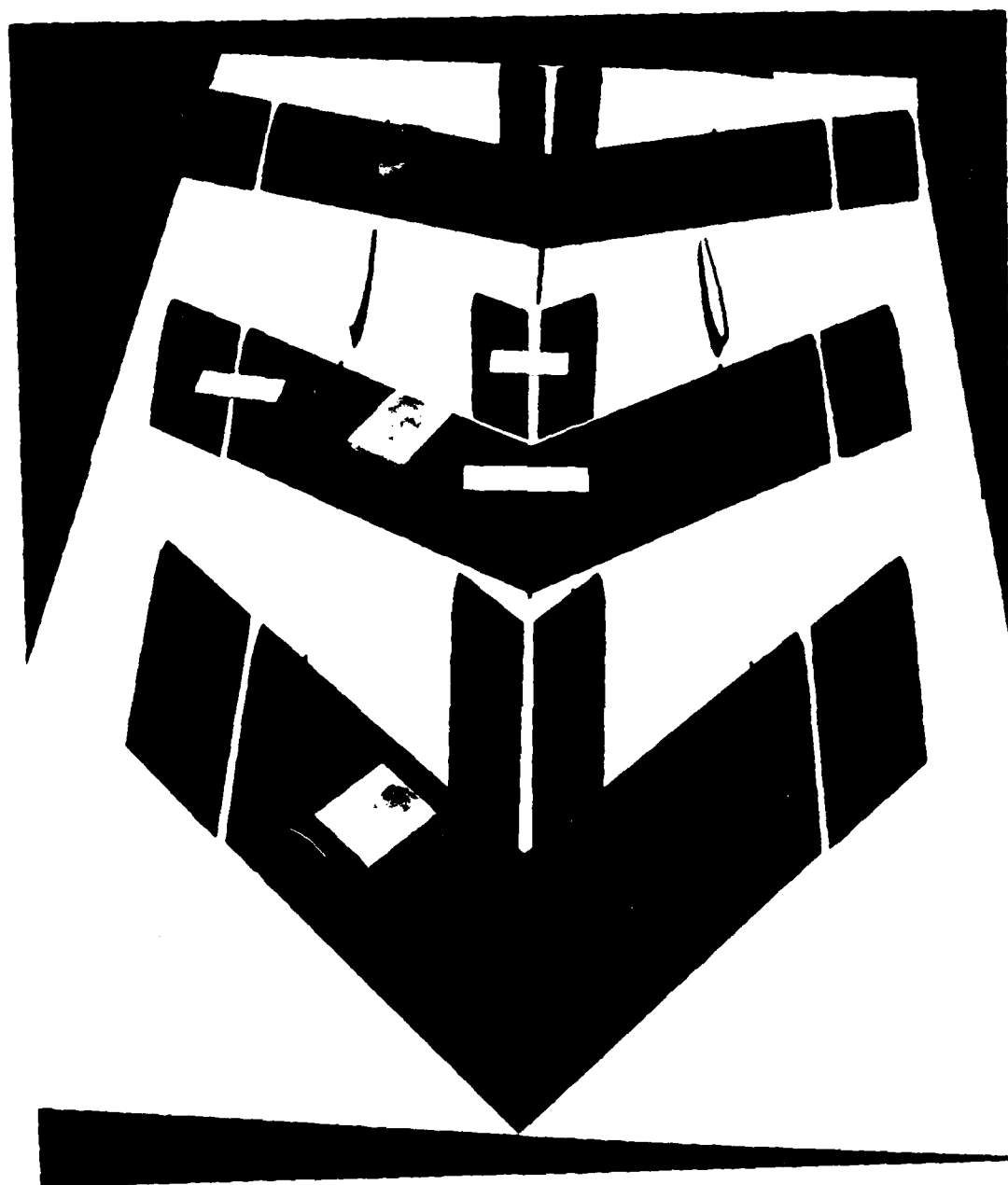
Fig. 1.
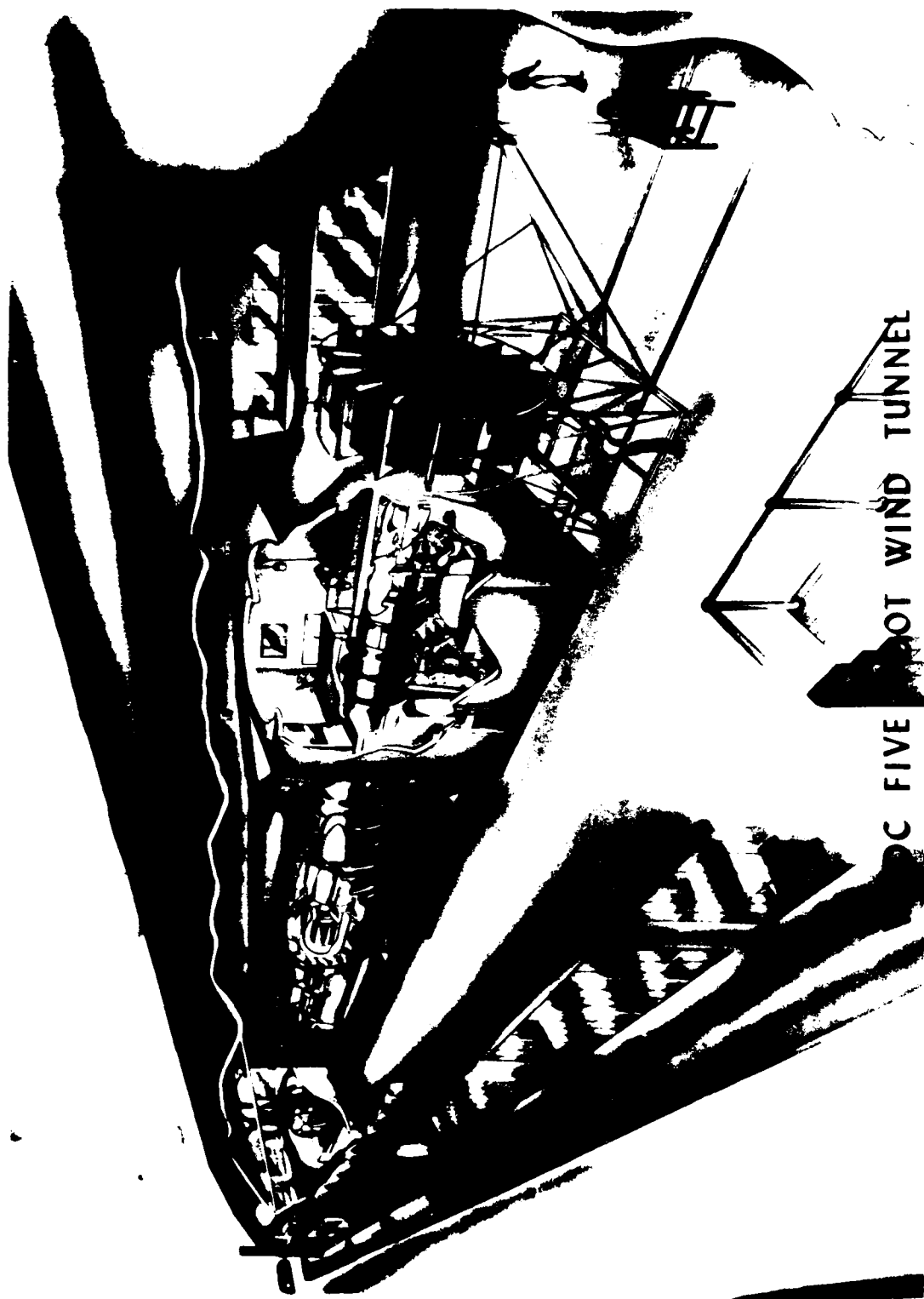
C FIVE FOOT WIND TUNNEL

Fig. 2. AFIT Five Foot Wind Tunnel

Model Installation

A typical model installation can be seen in Figs 2 and 3. Each model was equipped with two slotted, drilled and tapped steel screws embedded in epoxy, in the leading edge of the model, along the chord line. Each screw was placed 9 in outboard of the wing centerline allowing for an 18 in distance between wires. The front lift and drag wires were attached to each screw by means of a trunnion fitting which was attached to the slotted screw with a threaded pin.

The -15 and -30 degree models were equipped with a slotted, tapped and drilled sting which extended out the centerline aft of the model, along the chord line. The rear lift wire was attached to the sting by a threaded pin. The -45 degree model was equipped with a screw fitting in the model centerline itself. The fitting projected out the top and bottom of the wing and each side was slotted, drilled and tapped. The rear lift wire was cut and the upper portion of the wire connected to the top of the fitting while the lower portion was connected to the bottom of the fitting.

Test Conditions

All tests were run at 4.92 in of water (25.6 psf). This yielded an airspeed of approximately 100 mph (Mach 0.135). This speed was well within the incompressible flow regime and presented the least amount of turbulence for this tunnel, aiding in the repeatability of data. Because of the unstable twisting moment of forward swept wings, it was desired to keep the loads on the fittings as well as on the model as low as possible. This insured the safety of the tunnel and reduced aeroelastic effects on the data. See Appendix B for safety analysis. No attempt was made to trip the
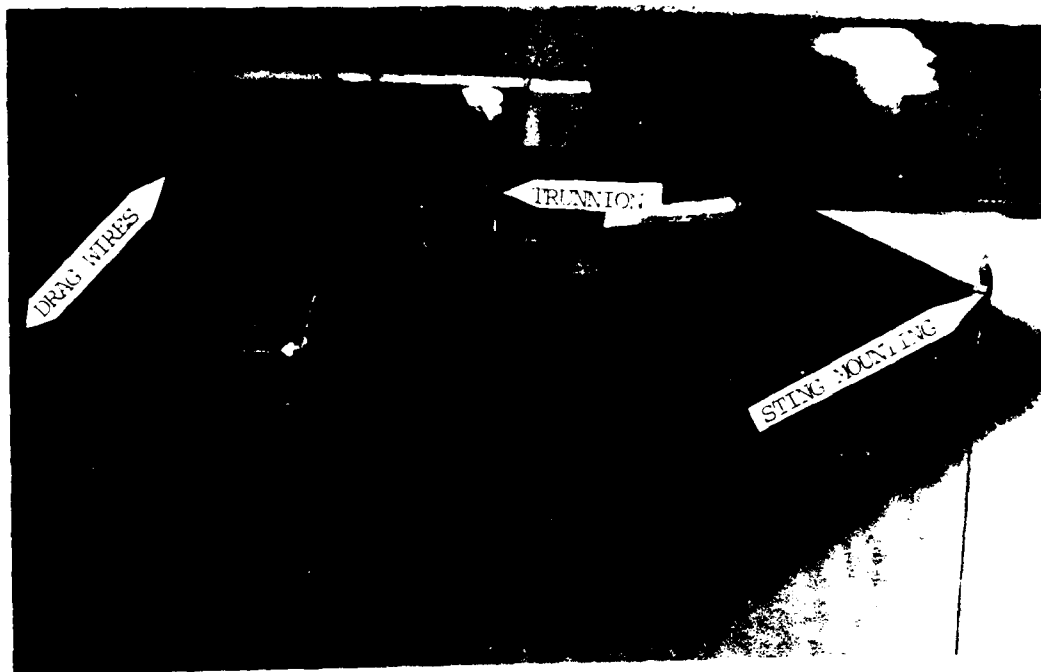
Fig. 3(a). Side View. -30° Model Installation

boundary layer as this would have increased the difficulty of finding comparable experimental data. In addition, FIMB's program predicts drag for laminar, transition and turbulent boundary layer. Angle-of-attack varied from -4 deg to the onset of significant flutter, from 14 to 16 deg.

Test Procedure

Each model was precisely measured on a surface plate, prior to installation in the tunnel, using an inclinometer and a height gage. These measurements were used for angle-of-attack calibration, and to determine if there was an angle between the front and rear fitting (angle of the balance). These measurements were also used in the data reduction. Angle of balance and associated distance values are defined in Appendix C. The model was leveled on the surface plate to within ±1 min of arc. Readings on the height gage were accurate to ±.001 in.

The model was then suspended on the wire balance in the tunnel as described above. Next, the angle of attack was calibrated, using an inclinometer, to within ±5 min of arc.

Prior to taking data, each basic wing was given a shakedown run at 76 mph to determine if there was any erratic behavior. After this run, the model was thoroughly inspected for any structural damage.

Static wind-off readings for every angle of attack were recorded before and after each data run. Three readings for every angle of attack were recorded. During wind-on runs, 5 readings were taken per data point. Each of the three scales printed the load on a paper tape. The multiple readings helped to reduce data scatter.

During the before static readings, ambient pressure was recorded using a mercury barometer to within ±.001 in. The reading was corrected for

temperature and instrument constant. Stagnation temperature was also recorded using a mecury thermometer located on the guide vanes in front of the tunnel. This was accurate to ±0.25 F. These quantities were used in determining Reynold's number and Mach number.

Wind-on data points were taken at two degree increments of angle-of-attack from -4 to +10 deg. One degree increments were then taken until 14 or 16 deg. This was based on data from Ref 9. Repeat data were taken at 12, 8, 4 and 0 deg. Angle of attack was manipulated by vertical translation of the rear lift wire. Hysteresis effects were avoided on the repeat data points by always approaching the angle of attack desired from below.

Because of the forward sweep in the models, the center of rotation (front trunnion fitting) could not be seen through the telescope. To correct this, a cross-hair was placed on the front lift wire below the wing model to maintain the center of rotation. The center of rotation was adjusted at each angle of attack prior to taking data. During wind-on runs, angle of attack was accurate to within ±10 min of arc.

After the basic wing, extension 1 and extension 2 were tested, the basic wing was inverted and tested to determine the tunnel flow angularity. Flow angularity for these tests was -0.1 deg. Since this was greater than the angle-of-attack calibration accuracy, the data was modified to reflect this.

Finally, a repeat run of the basic wing was accomplished to insure the repeatability of the data and to determine that there was no slippage in the wire balance system. All repeat runs matched the original data within three percent.

The above procedure was done for all three models, except the -45 degree model which was not run in the inverted position.

Tunnel dynamic pressure was maintained to within ±0.01 in of water during testing by use of a Meriam manometer.

Wire balance drag was determined, based on dynamic pressure, from a 1976 experiment (Ref 7). Data are available at the tunnel. Sting drag was considered negliglible for these models.

Data Reduction

Raw data from each run were printed on a paper tape. One tape for each scale. The three readings per data point for the before and after statics were averaged. The five wind-on readings per data point were also averaged. The front lift scale least division was 0.05 lb_f, while the drag and rearlift least division was 0.02 lb_f. The data were rounded to the nearest 0.01 lb_f.

The raw data were reduced to aerodynamic coefficient form by the use of a computer program written by Mr. Duane R. Burnett and Mr. George W. Leptein of the Aeromechanics Division of the Air Force Flight Dynamics Lab. The program was modified and updated by the author. A listing of the program and input variables can be found in Appendix F. The program computes wing lift and drag coefficient (C_L and C_D) and moment coefficient about the trunnion (C_{MTR}) and aerodynamic center (C_{MAC}). Reynolds number and Mach number were also computed (see Appendix D).

The program also applied wind tunnel boundary corrections to the raw data. These included corrections made for solid and wake blocking, streaming curvature, and downwash as developed in Ref 4. These corrections are presented in Appendix E.

11

The C_{MAC} for the wing was found as follows. Using
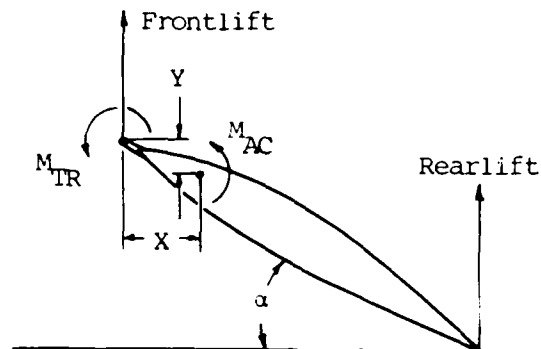
Fig. 4. Force and Moments for C_{MAC} Computation.

Fig. 4, the following equation (in coefficient form) was developed to determine C_{MAC}:

$$C_{MAC} = C_{MTR} - X(C_L \cos\alpha + C_D \sin\alpha) - Y(C_D \cos\alpha - C_L \sin\alpha) \qquad (1)$$

(Ref 4:213). To find x and y the fact that $\dfrac{dC_{MAC}}{dC_L} = 0$ was used.

12

$$\frac{dC_{MAC}}{dC_L} = 0 = \frac{dC_{MTR}}{dC_L}$$

$$- \left[(1 + C_D \frac{d\alpha}{dC_L}) \cos\alpha + (\frac{dC_D}{dC_L} - C_L \frac{d\alpha}{dC_L}) \sin\alpha\right] x$$

$$- \left[(\frac{dC_D}{dC_L} - C_L \frac{d\alpha}{dC_L}) \cos\alpha - (1 + C_D \frac{d\alpha}{dC_L}) \sin\alpha\right] y$$

This equation was solved by substitution of data from two α locations in the linear range. dC_{MTR}/dC_L and $d\alpha/dC_L$ are constants in this range. dC_D/dC_L was found by plotting the corrected C_D and C_L data. The slope at the two points selected was determined using the mirror method. This yielded two equations and two unknowns which was solved by substitution in the data reduction program. The values of x and y were then substituted into eq (1) to give C_{MAC}.

13

III. Experimental Results

This section presents the experimental aerodynamic data collected and compares it with theory and previous experimental data. All wing data are plotted in coefficient form. The effects of forward sweep angle on lift coefficient, drag coefficient and moment coefficient are plotted for each set of basic wings and extensions. A typical set of data is shown in Figs 5a through c. Aspect ratio effects on lift, drag and moment coefficients were evaluated at each sweep angle by comparing the basic wing, extension-1 and extension-2. A typical set of data is presented in Figs 6a through c. Previous experimental data is also provided in Figs 7a and b for comparison purposes. All curves were approximated by a cubic spline curve fit. The remaining data, which takes the form of Figs 5 and 6 can be found in Appendix G.

Sweep Effects

Lift

Figure 5a shows the effects of forward sweep angle on lift coefficient. Lift curve slope decreases with increasing forward sweep angle, from 0.067 for the -15 degree model to 0.047 for the -45 degree model. This trend was consistent for all models tested (see Appendix G).

Basic theory for swept wings as developed in Ref 14 is based on the concept that only the component of velocity normal to the wing leading edge determines the chord wise pressure distribution.
Therefore, the direction of sweep is unimportant. Using the assumption that the spanwise pressure distribution is rectanglular
the following equation was developed to determine lift curve slope:

CL –VS– ALPHA (EXT-2)

o – 15° – Experimental Data
Λ – 30° – Experimental Data
+ – 45° – Experimental Data

LIFT COEFFICIENT (CL)

ALPHA (DEGREES)
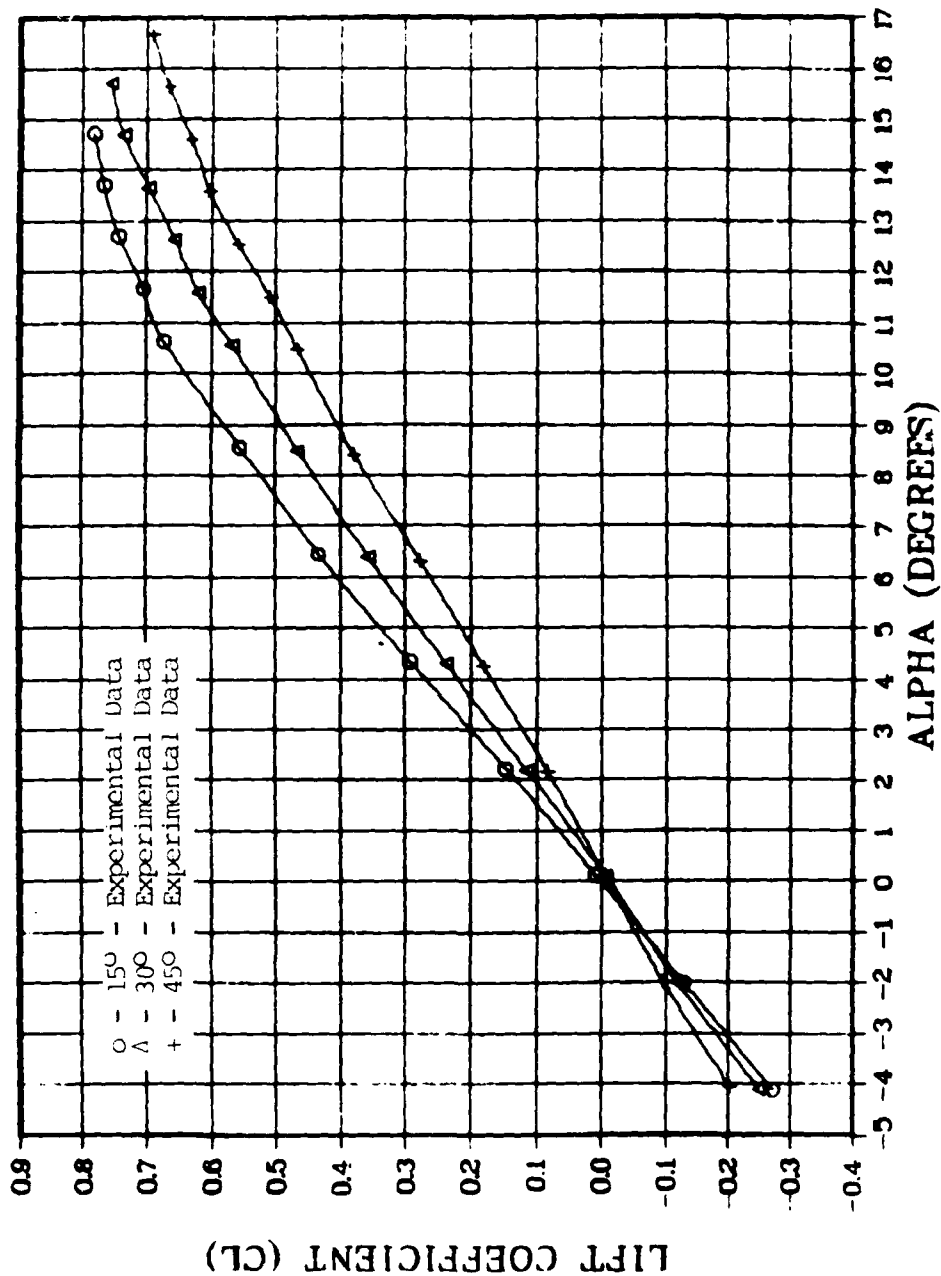
Fig. 5a. Lift Coefficient Versus Angle of Attack For
Increasing Forward Sweep Angles (Distortion-' model-1)

$$C_{L_\iota} = (C_{L_\iota})_{\Lambda=0} \cos \Lambda$$

where $(C_{L_\iota})_{\Lambda=0}$ is the lift curve slope for an unswept wing with the same

aspect ratio and taper ratio as the swept wing. Results of this

equation as compared to experimental data are shown in Ref 14, Fig 42.

This figure indicates a decrease in lift curve slope with increasing

sweep angle. Lift curve slope for the experimental data on the -30 and

-45 degree models agreed well with theory, while lift curve slope for

the 15 degree model was just slightly higher than theory (see Table I).

Overall agreement of the experimental data and theory for lift curve

slope appears to be excellent.

Table I

C_{L_ι} – Theory vs Experiment

	-15°			-30°			-45°		
	Basic	Ext-1	Ext-2	Basic	Ext-1	Ext-2	Basic	Ext-1	Ext-2
Theory	.060	.062	.066	.054	.056	.058	.043	.045	.047
Experiment	.064	.065	.067	.055	.055	.057	.043	.045	.047

Maximum lift coefficient was not attained for the wings

tested. This was due to the large magnitude of flutter at high angles

of attack. Although Reynolds number variation has only a very small

effect on lift curve slope, maximum lift coefficient is unreliable in

terms of scaling to other geometries. This was because of the low

Reynolds numbers of this experiment.

According to previous experiments (Ref 15:6), the angle ot

attack for maximum lift increases with increasing sweep. This trend can

be seen in Fig 5a, at high angles of attack. At this point, the slopes

of the curves increase with sweep angle. The -15 degree wing has almost

reached maximum lift coefficient, while the other curves continue to

rise, the -45 degree model rising at a slightly higher rate then the 30

degree model. Previous experiments also indicate an increase in maximum

lift coefficient with increasing sweep. In Fig 5a this appears to be

the case for the -15 and -30 degree wing. As the -15 degree wing curve

is peaking, the -30 degree wing's lift curve slope is still fairly

steep, indicating it would exceed the maximum lift coefficient of the

-15 degree wing. However, this trend is not predictable with the -45

degree wing data.

Drag

Values for drag coefficient are plotted versus lift

coefficient in Fig 5b for all three models with extension-2. Area was

held constant for all three models; therefore, in addition to sweep

effects, there are also aspect ratio effects influencing the data. For

the curves plotted in Fig 5b aspect ratio varies from 2.58 for the -45

degree wing to 4.79 for the -15 degree wing.

Figure 5b indicates for a fixed value of lift coefficient,

drag coefficient increases as forward sweep increases and aspect ratio

decreases. Again, these trends are consistent with other experimental

data from Ref 14. However, in the lower lift range there is a crossover

of the drag curves. This occurs for the basic wing and extension-1

comparisons as well (see Appendix G).   Figure 5b indicates the -15

degree model has the highest zero-lift drag, while extension-1 and extension-2 are practically equal. The curves themselves appear to be very inconsistent below a lift coefficient of 0.35. There are several reasons for this inconsistency.

These anomalies can be explained by examining the boundary layer. The Reynolds number range (5.4 to 8.0 x 10^5) for this experiment indicates that the laminar flow regime extends over a significant portion of all the models tested, at low angles of attack. This partially accounts for the very low values of zero-lift drag coefficient. In fact, because of the laminar flow, a drag bucket at low lift coefficients is expected. However, data scatter and the nature of the cubic spline curve fit prevent seeing this. This scatter at low lift coefficients has several sources. First, it was difficult to obtain accurate data for models of the size tested because of the relatively large drag tare of the wire balance. The drag tare has not been experimentally determined since 1976. Clutter in the open return section of the tunnel influences these values. Lastly, there are inherent inaccuracies in subtracting large scale readings to attain low drag values.

The higher zero-lift drag coefficient attained for the lower sweep, higher aspect ratio wing can be explained, again, by examining the boundary layer. Assuming a transition Reynolds number of 500,000, calculation shows that approximately 92 percent of the -15 degree wing was in the laminar flow range as compared to approximately 63 percent for the -45 degree wing. Reference 6 develops an expression for turbulent skin friction coefficient as a function of Mach number and the reciprocal of Reynolds number. The Reynolds number is based on
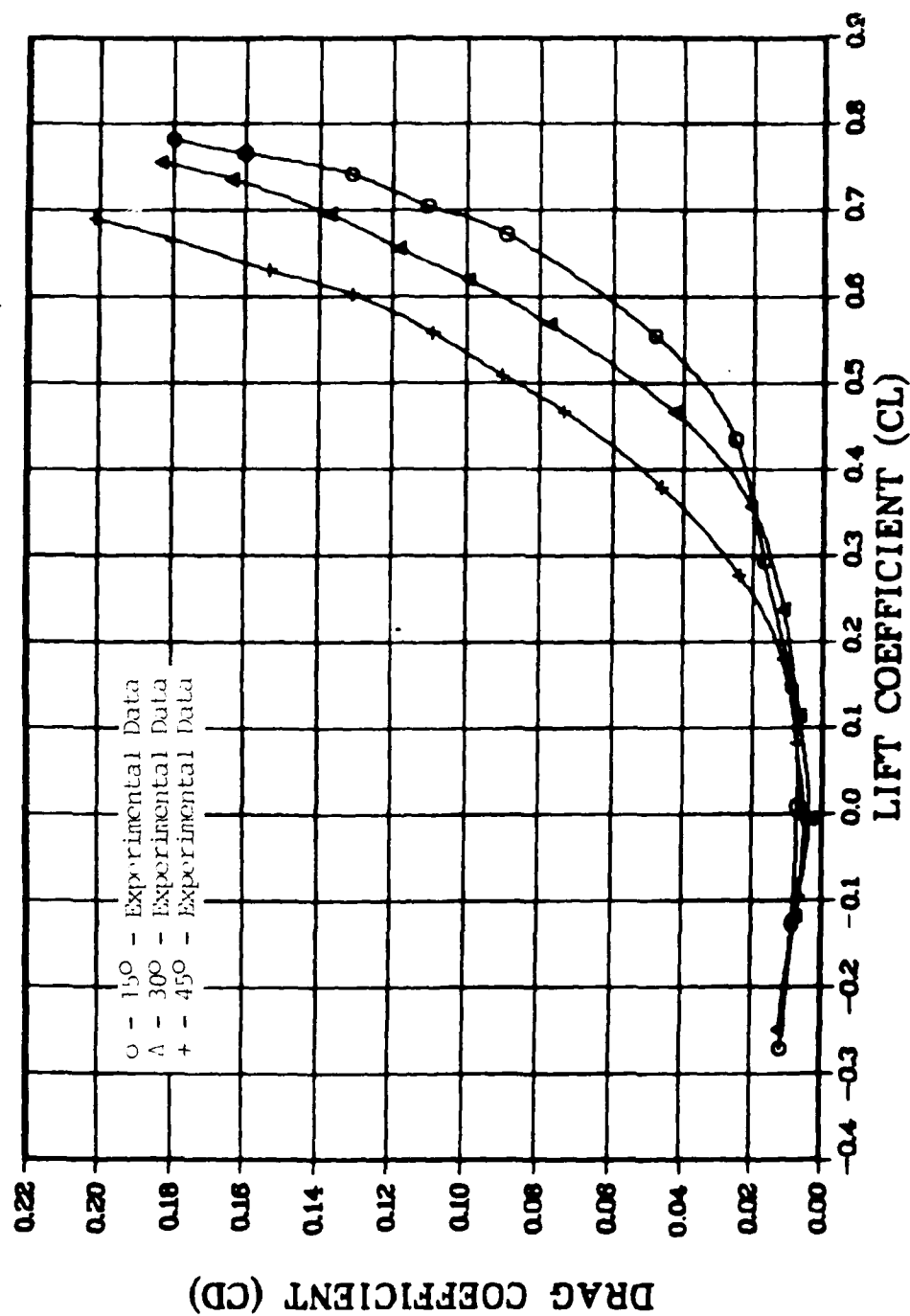
Fig. 5b. Drag Coefficient Versus Lift Coefficient For Increasing Forward Sweep Angles (Extension 2 Models)

component length. Component length for the -15 degree model was 7.82

inches and 10.69 inches for the -45 degree model. Applying the equation

from Ref 6 yields a lower skin friction coefficient for the higher

sweep wing. Therefore, given the same wetted area, the friction drag

coefficient is smaller for the higher sweep, lower aspect ratio wing.

Now, as lift coefficient increases spanwise flow effects on drag (which

increase with increased sweep) become dominant and account for the

crossover of the curves.

Moment About Aerodynamic Center

Moment coefficient about the aerodynamic center is plotted

versus lift coefficient in Fig 5c. Location of the aerodynamic center

for all models is listed in Table II.

Location of the aerodynamic center appears to be very good

(see Fig 5c). Moment coefficient values are very nearly zero for all

models tested. A break point occurrs for all models in a lift

coefficient range of .55 to .60. This is in excellent agreement with

previous experimental data (Ref 10 and 17). The shift is most likely

due to the onset of stall at the wing root and leading edge separation.

The slope at the break point is a function of aspect ratio and sweep

angle. Combinations of aspect ratio and sweep angle for stable and

unstable pitch excursions are presented in Ref 15. All -45 degree

models are in the unstable (positive slope) or marginally stable areas.

The -30 degree models are very close to the marginally stable area and

all -15 degree models are well within the stable area (negative slope).

The data in Table II indicate that the aerodynamic center

moves rearward with increasing sweep. This trend is consistent with

CMAC –VS– CL (EXT–2)
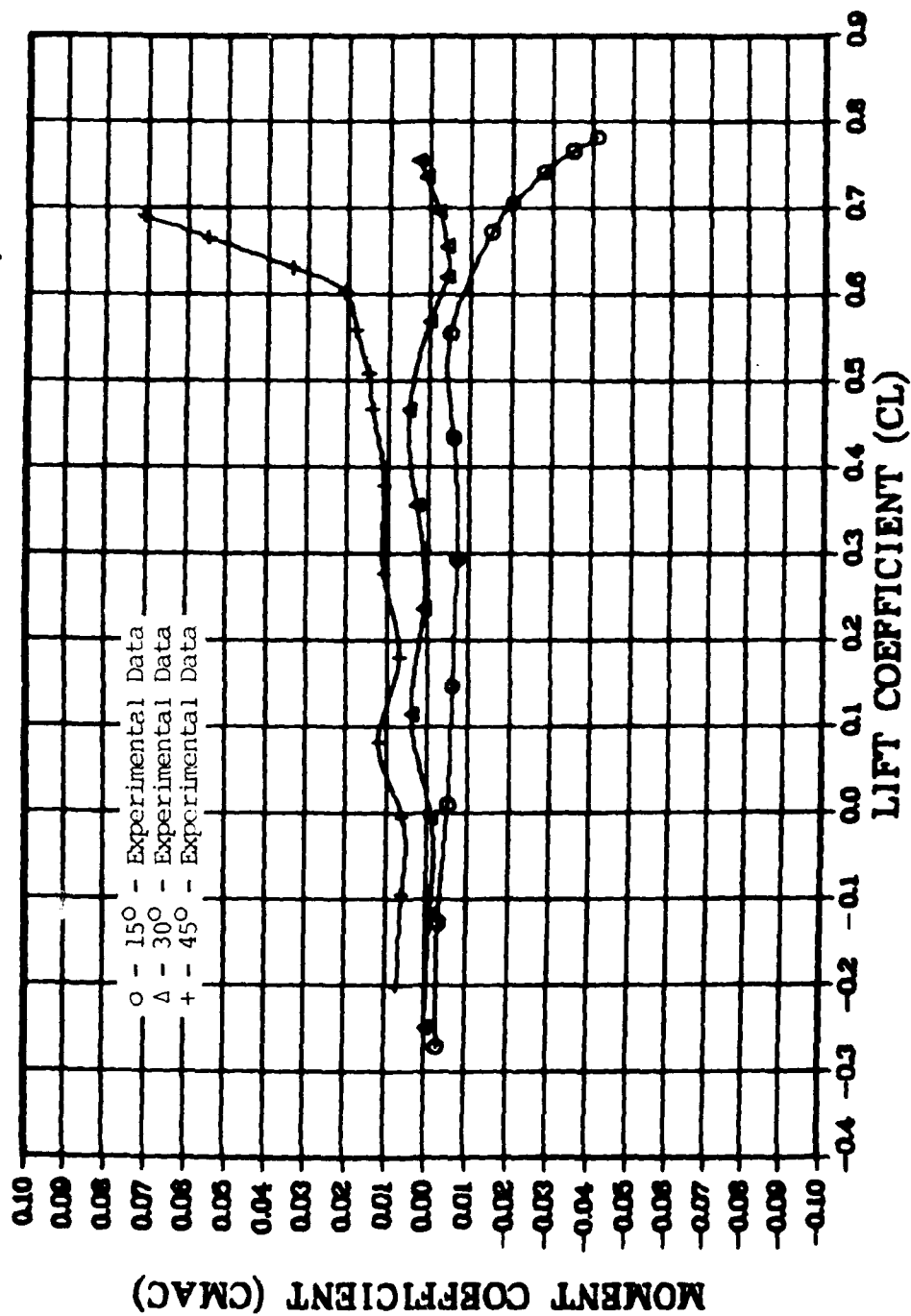
o – 15° – Experimental Data
Δ – 30° – Experimental Data
+ – 45° – Experimental Data

LIFT COEFFICIENT (CL)

MOMENT COEFFICIENT (CMAC)

Fig. 5c. Moment Coefficient About the Aerodynamic Center Versus Lift Coefficient
For Increasing Forward Sweep Angles (Extension-2 Models)

21

the theory developed in Ref 15, as well as the experimenta   :: . :

the same source.

Table II

Aerodynamic Center Location

Sweep Angle	Basic Wing AR/%MAC	Extension-1 AR/%MAC	xtension-2 AR/%MAC
-15	3.83/.326	4.32/.327	..79/.320
-30	3.21/.337	3.54/.'4:	'.87/.353
-45	2.05/.370	2.31. .:.' '	'.58/.389

Aspect Ratio Effects

Lift

        The effects of aspect ratio on lift coefficient are presented

in Fig 6a. It is apparent from this and other aspect ratio comparisons

that the variation in aspect ratio is too small for these models.

However, the small magnitude of scatter in the data for the -45 degree

models allow observation of aspect ratio effects.

The curves in Fig 6a indicate an increase in lift curve slope with

increasing aspect ratio. Also, at a fixed, high angle of attack, Fig 6a

indicates a decrease in lift curve slope as aspect ratio decreases.

This points toward a lower maximum lift coefficient as aspect ratio

decreases. Experimental data from Ref 14 verifies these trends for both

forward and aft swept wings.

CL –VS– ALPHA (45-DEG FSW)
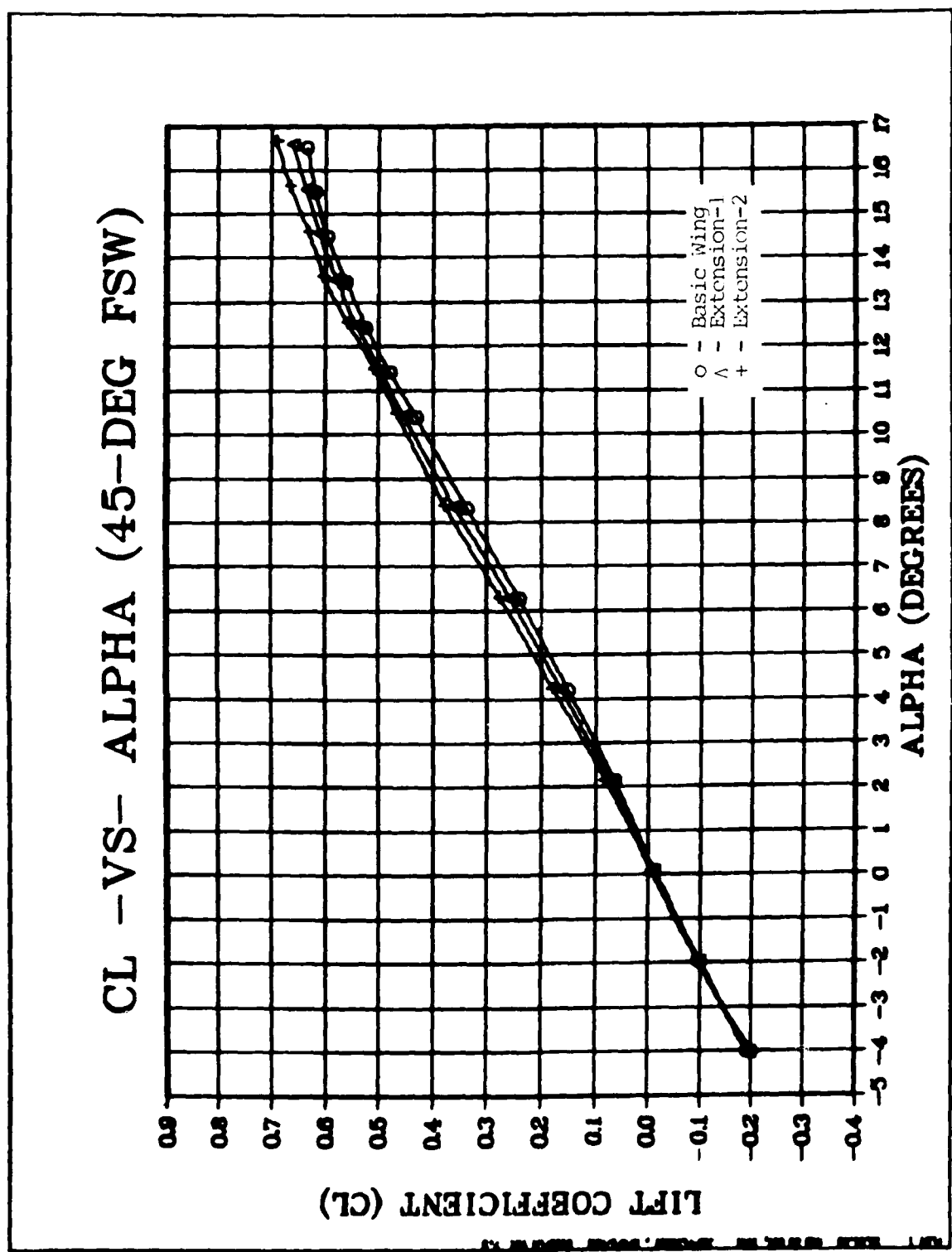
Fig. 6a. Lift Coefficient Versus Angle of Attack For
Increasing Aspect Ratio (45 Degree Models)

Drag

Drag coefficient variation with aspect ratio is summarized in Fig 6b. Again, the small change in aspect ratio (0.53) makes interpretation difficult. However, at high lift coefficients it can be seen that the drag coefficient increases as aspect ratio decreases. This variation is confirmed in Ref 14. Changes for zero-lift drag with aspect ratio are not distinguishable. Any variation present is within the 0.01 lb_f accuracy of the wire balance. An increase in zero-lift drag with aspect ratio is expected due to the increase in friction drag and spanwise flow with each extension.

Moment About Aerodynamic Center

Moment coefficient about the aerodynamic center for the -45 degree models is plotted in Fig 6c against lift coefficient. As in Fig 5c the location of the aerodynamic center is very accurate. From the break slopes of the three curves it is obvious that the pitching moment becomes less unstable as aspect ratio decreased. Again, this agreed with data from Ref 15.

Values of the aerodynamic center location listed horizontally in Table II generally indicate an aft shift of the aerodynamic center with increasing aspect ratio. The only exception to this trend is the -15 degree model with the second extension. It has a slightly more forward location than the other two -15 degree models. This can be attributed to the small change in aspect ratio coupled with data scatter.

Experimental Comparison

Aerodynamic data collected in this program were compared to previous experimental data which most closely matched the geometry and
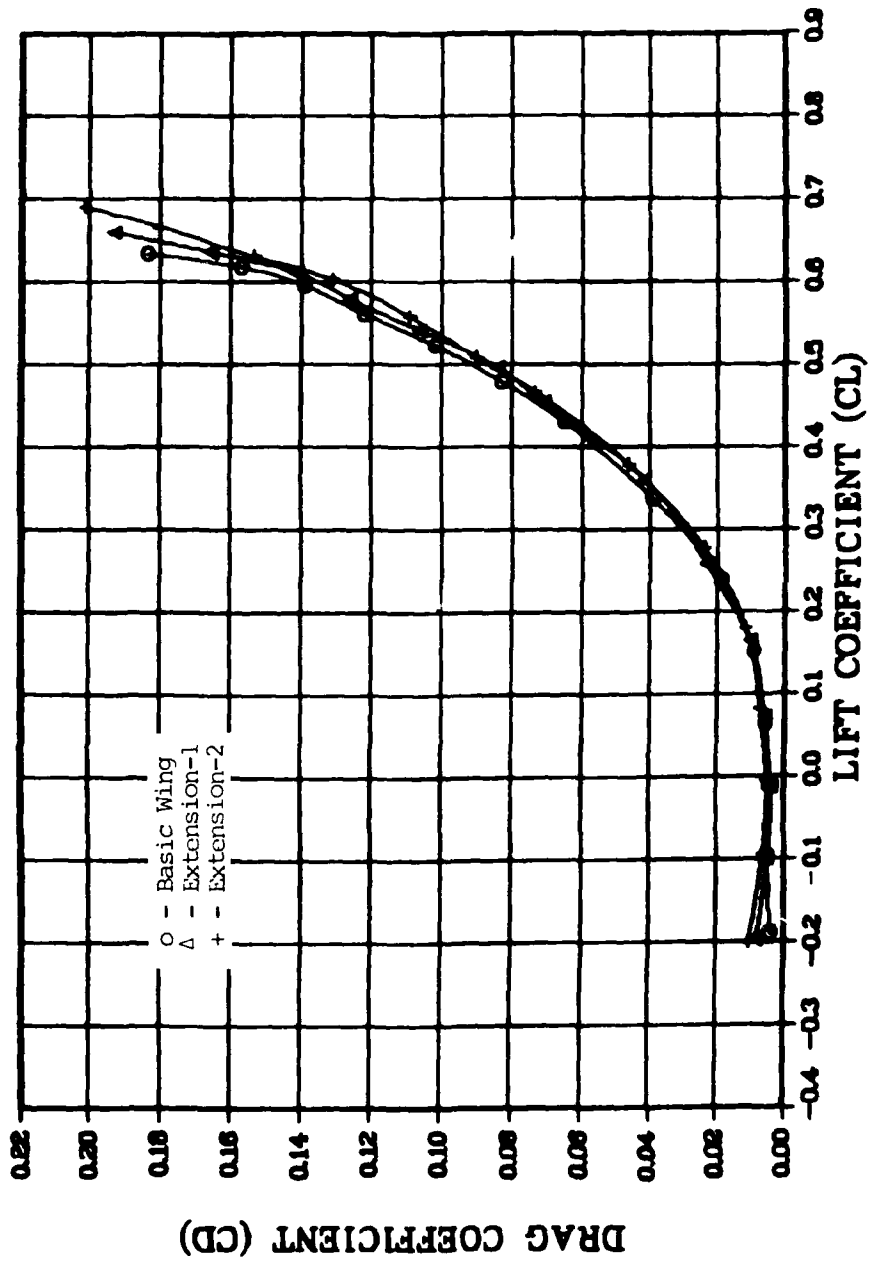
Fig. 6b. Drag Coefficient Versus Lift Coefficient For Increasing Aspect Ratio (45 Degree Models.)

CD -VS- CL (45-DEG FSW)

O - Basic Wing
Δ - Extension-1
+ - Extension-2

LIFT COEFFICIENT (CL)

DRAG COEFFICIENT (CD)

CMAC –VS– CL (45–DEG FSW)
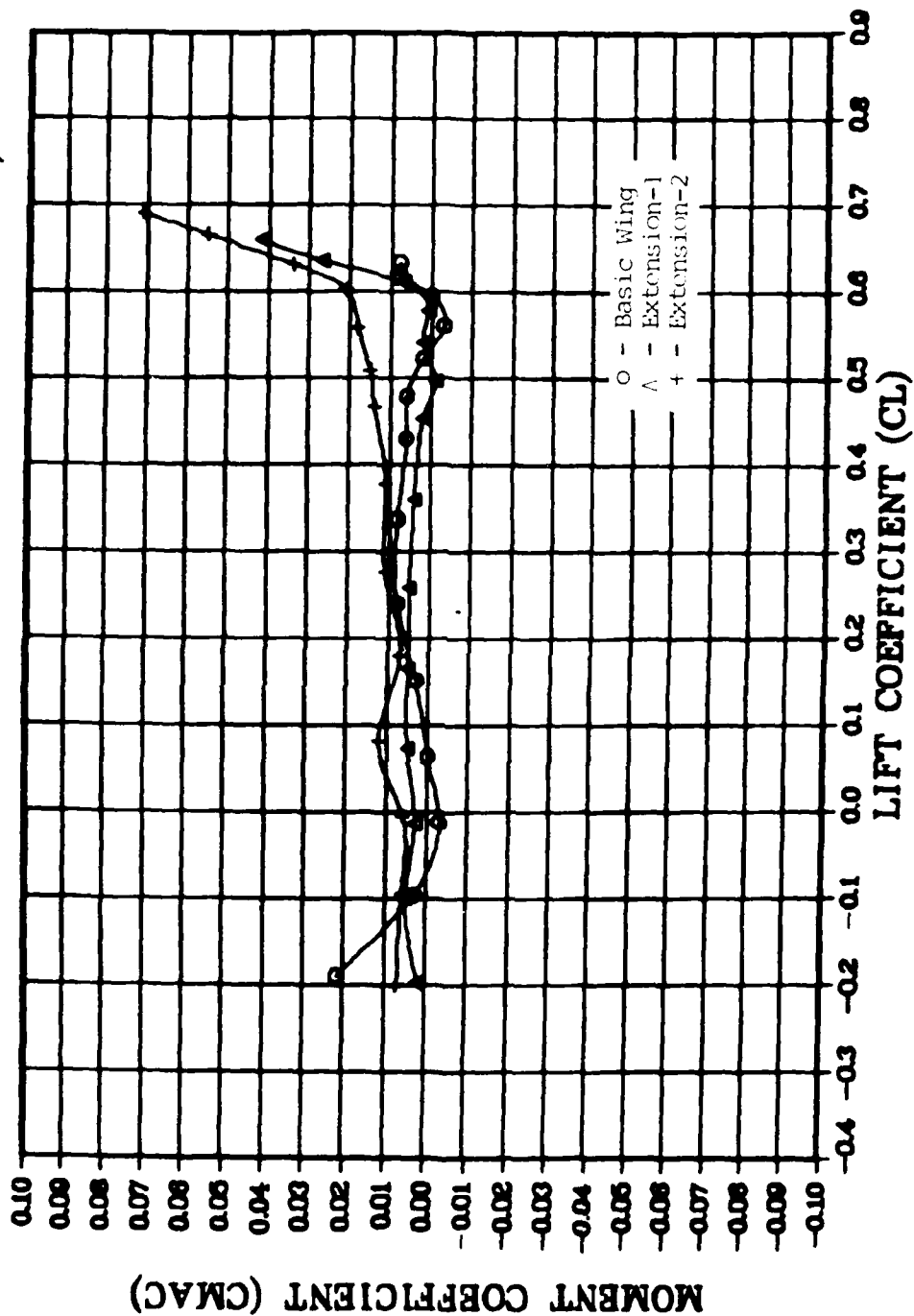
Fig. 6c. Moment Coefficient About the Aerodynamic Center Versus
Lift Coefficient For Increasing Aspect Ratio (45 Degree Models)

26

test conditions of this experiment. These comparisons are shown in Figs. 7a and b. These data represent the best available for comparison.

Characteristics of the two comparison models are listed in Table III.

Table III

Comparison Model Characteristics

	AR	C_t/C_r	$\Lambda_{c/4}$	Thickness Distribution	$R_e \times 10^6$
Model 1 (FSW)	3	.6	-45	65A006	1.5
Model 2 (ASW)	3	.5	45	0006	1.65

In addition to these characteristics, the aft swept wing has a leading edge radius of .005c compared to .007c for the models in this experiment. The model which most closely matches these characteristics is the -45 degree forward swept wing with extension-2. This model has an aspect ratio of 2.58, a taper ratio of one and was tested at a Reynolds number of 8.07×10^5.

Lift

Figure 7a compares lift coefficient versus angle of attack for all three models. Lift curve slopes were as follows:

Model-1 - 0.049

Model-2 - 0.050

45-Deg. Ext-2 - 0.047

CL –VS– ALPHA (EXP. COMP)
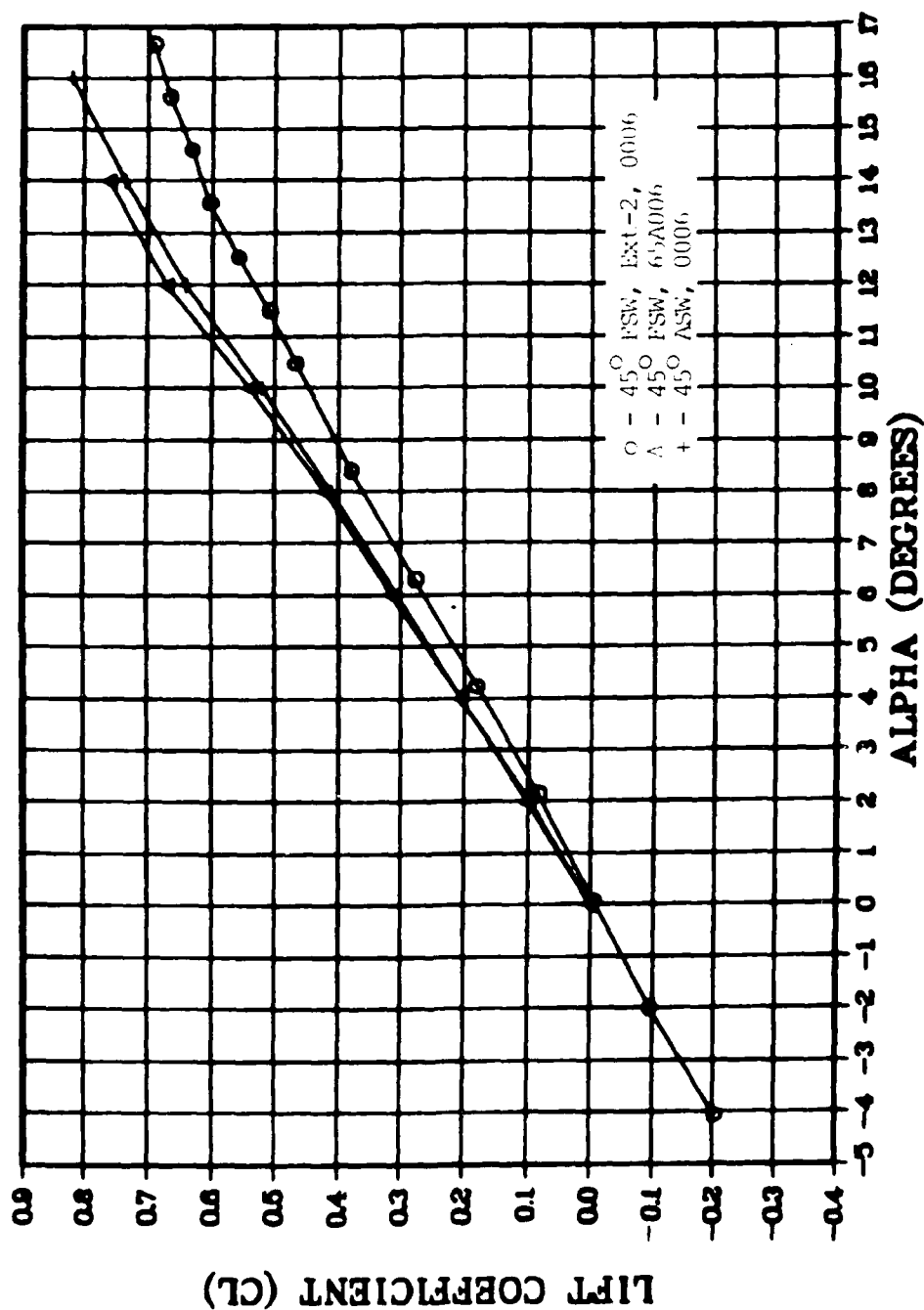
Fig. 7a. Lift Coefficient Versus Angle of Attack For
Experimental Data Comparisons.

CD —VS— CL (EXP. COMP.)

O — 45° FSW, Ext-2, 0006
Δ — 45° FSW, 65A006

LIFT COEFFICIENT (CL)

DRAG COEFFICIENT (CD)
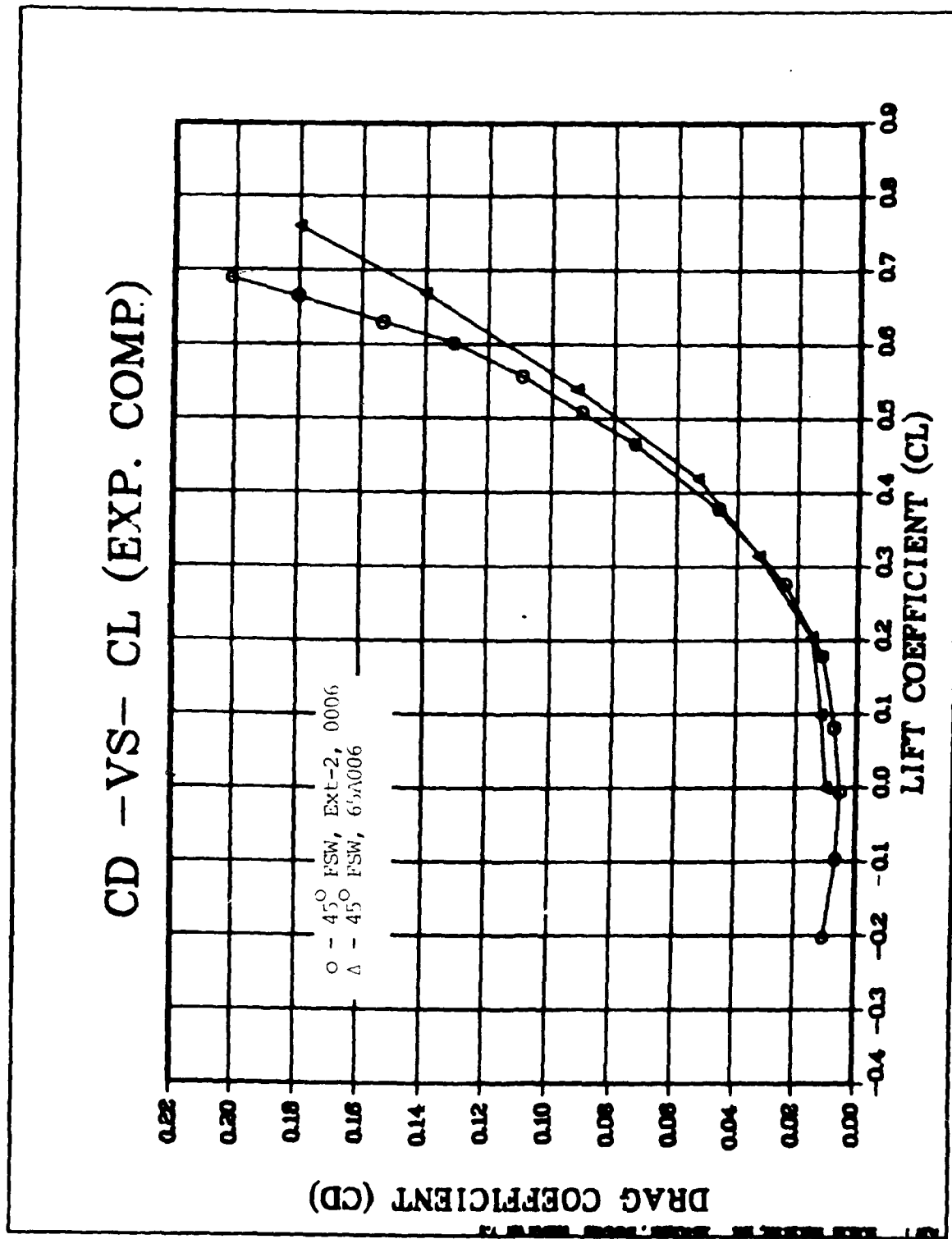
Fig. 7b. Drag Coefficient Versus Lift Coefficient
For Experimental Data Comparisons

The greater slope for model one compared to the -45 degree extension-2 model, can be attributed mainly to its higher aspect ratio. Also, slight increases in the lift curve slope are caused by the higher Reynolds number. This would bring better agreement among the data.

Model two, the aft swept model, again, has a higher aspect ratio and test Reynold's number which would increase its slope relative to the extension-2 model. However, experimental data from Ref 16 indicated that the lift curve slope for a forward swept wing is slightly lower compared to an aft swept wing of the same angle and geometry.

The tapering off of lift curve slope to a lower maximum lift coefficient for the extentsion-2 model can be directly attributed to the lower test Reynolds number, i.e. in this Reynolds number range increasing Reynolds number increases maximum lift coefficient.

Drag

Figure 7b presents the experimental comparison of drag coefficient versus lift coefficient. No drag data are available for model two.

Model one was a NACA 65A006. The location for maximum thickness was .40c as compared to the 0.30c maximum thickness location for the NACA 0006 section of the extension-2 wing. The aft movement of maximum thickness presents a more favorable condition for maintaining a laminar boundary layer, thus decreasing skin friction drag. Because of the low test Reynolds number for the extension-2 wing the laminar boundary layer extended over a majority of the surface. This, coupled with the inaccuracies of the drag balance in this area of data, produced a lower zero-lift drag for the extension-2 model.

In the higher lift range drag decreased for model one relative to the extension-2 model. This was due to the taper ratio effects on model one which tended to decrease induced drag. Therefore, as lift increases the increase in induced drag was greater for to the extension-2 model (Ref 14:14).

Comparison of the data collected from this test program with theory and previous experimental data and trends indicate that it represents a valid basis of comparison for evaluating the Large Aircraft Performance Prediction Program, LACBIN. Results of this comparison are presented in the following section.

IV. Experimental Data vs. Performance Program Data

The performance program (LACBIN) used by FIMB, was executed to empirically determine the aerodynamic lift, drag and moment coefficients of the forward swept wind tunnel test models. These coefficients are then compared graphically to the corrected wind tunnel data.

Inputs to the program included configuration geometry and aerodynamic conditions. A list of input variables, input program and output listing are provided in Appendix H. The main program listing can be found in Ref 6.

The performance program was run for both aft and forward swept wings. Aft sweep being a positive angle and forward sweep being negative. All other geometry was kept consistent. The two angles did not produce the same data. Accuracy of the program has been checked through past comparisons of the predicted results with experimental data for several configurations. These comparisons have shown the program is accurate in many areas, while improvement is needed in others (see Ref 6). However, no comparisons to experimental forward swept wing data have been made prior to this. The experimental data are plotted against data generated by the computer program for both negative and positive sweep angles. Additional graphs are provided in Appendix I.

Program Comparison

Lift

Comparisons of lift coefficient versus angle of attack are presented in Figs 8a through d. Initial lift curve slope values are presented in Table IV. Both the positive and negative angle input produced the same initial lift curve slope.

CL –VS– ALPHA (PROG. COMP.)
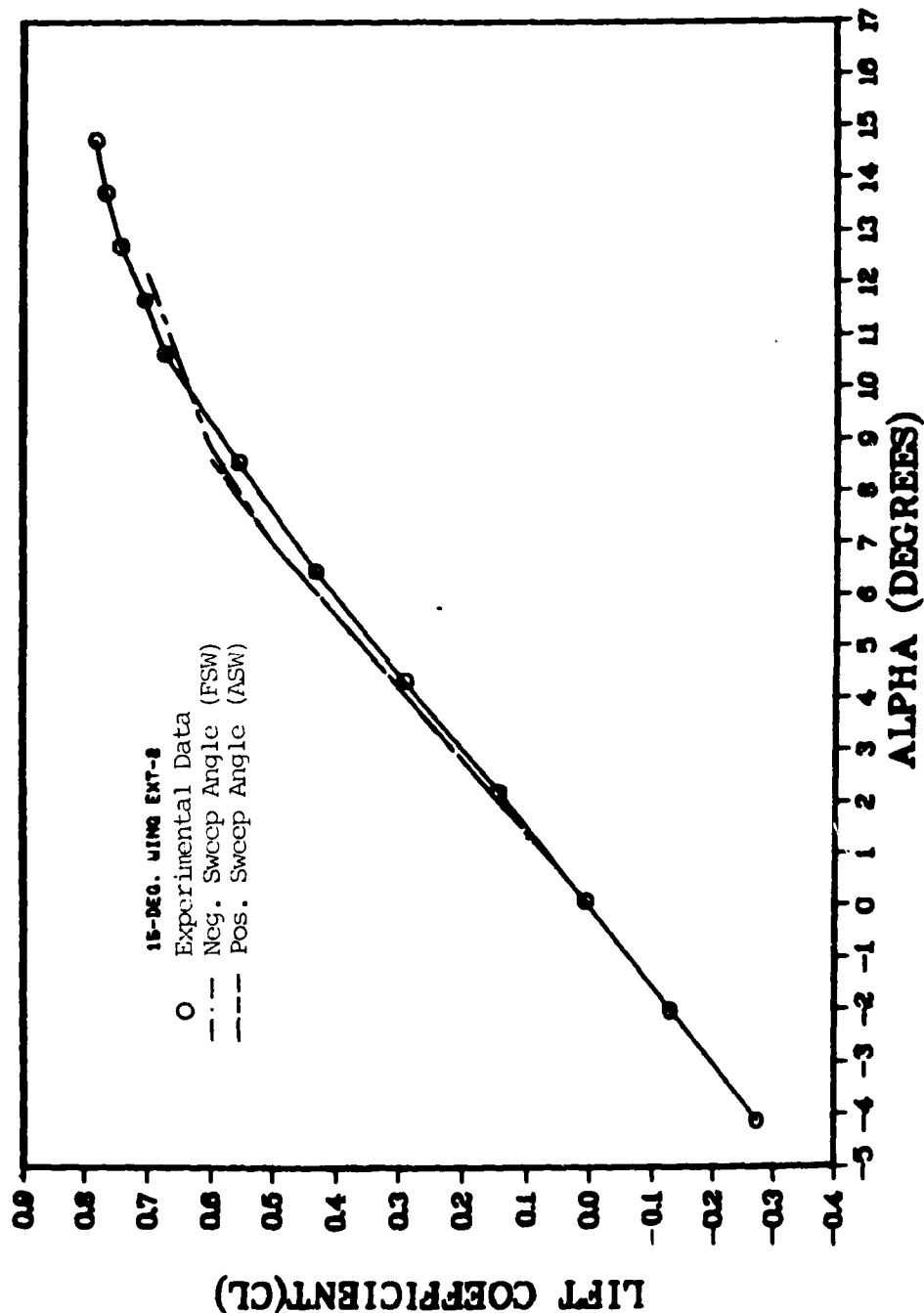
Fig. 8a. Program Comparison of Lift Coefficient Versus Angle of Attack for the 15 Degree Extension-2 Model.

33

CL –VS– ALPHA (PROG. COMP.)
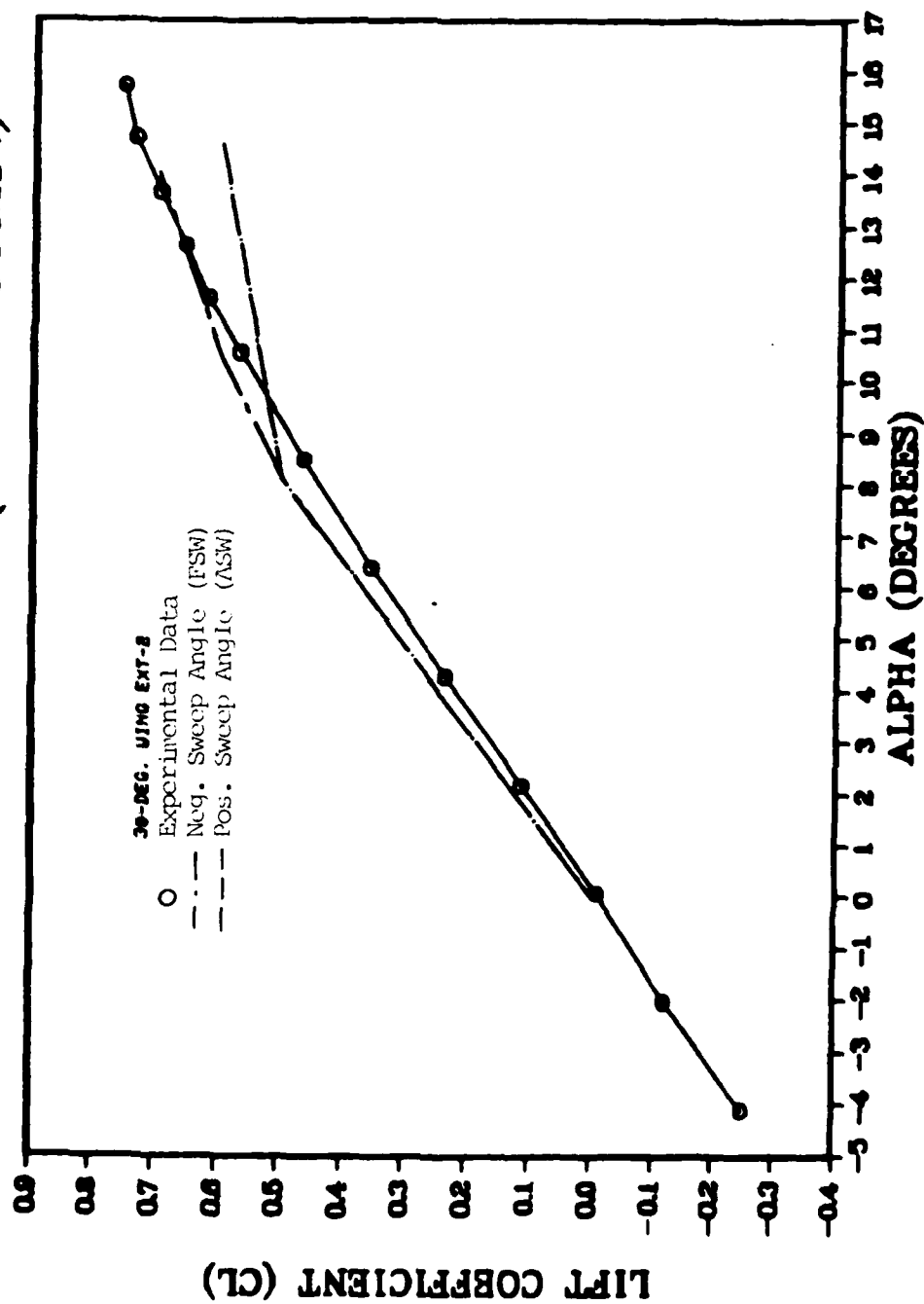
Fig. 8b. Program Comparison of Lift Coefficient Versus Angle of Attack
for the 30 Degree Extension 2 Model.

34
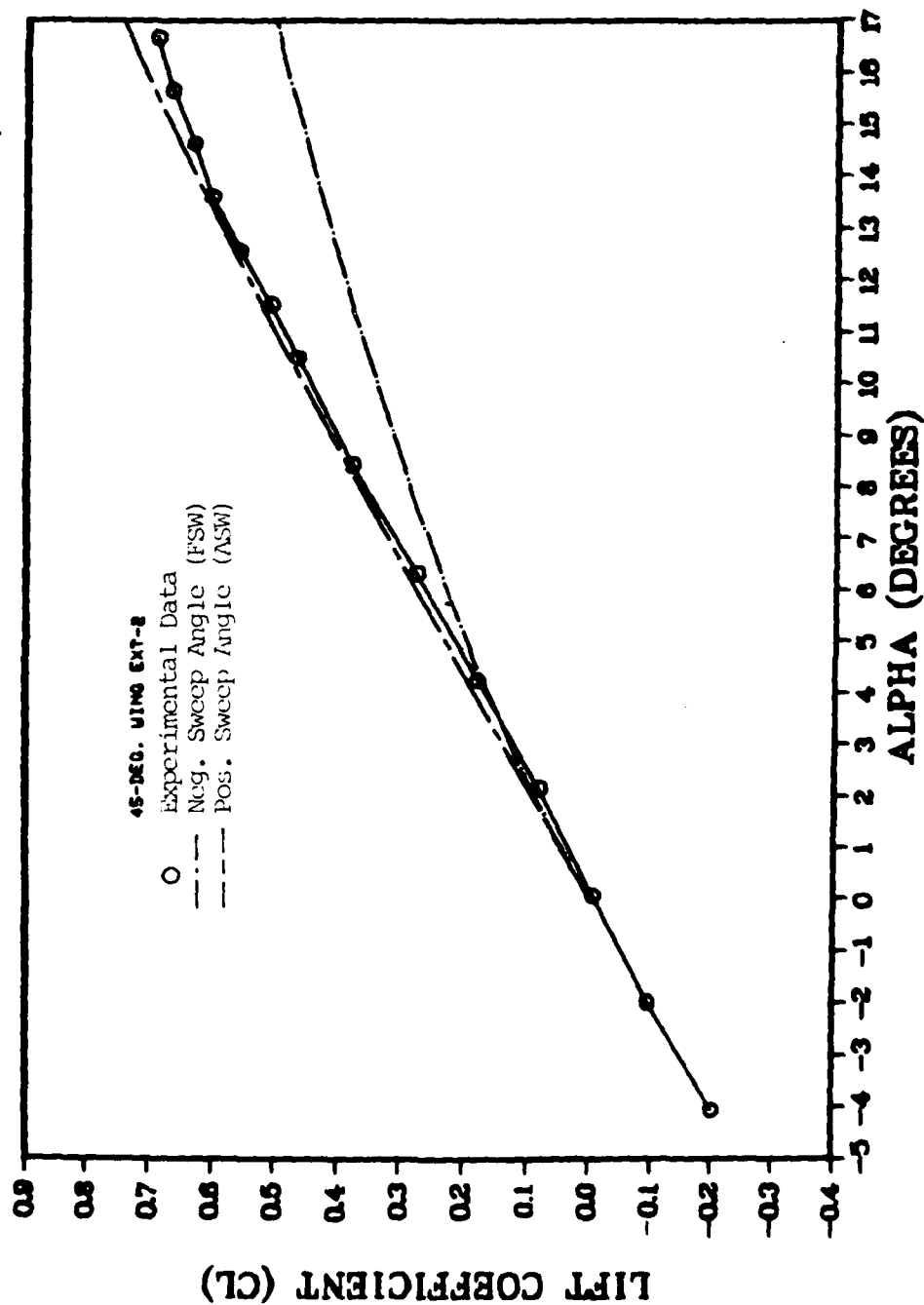
Fig. 8c. Program Comparison of Lift Coefficient Versus Angle of Attack for the 45 Degree Extension-2 Model.

Table IV

Initial C_{L_α} - LACBIN vs Experimental Data

		Neg. Angle Input (FSW)	Pos. Angle Input (ASW)	Experimental Data
-15°	Basic	.066	.066	.064
	Ext-1	.069	.069	.067
	Ext-2	.072	.072	.067
-30°	Basic	.056	.056	.055
	Ext-1	.059	.059	.055
	Ext-2	.062	.062	.057
-45°	Basic	.041	.041	.043
	Ext-1	.044	.044	.045
	Ext-2	.046	.046	.047

Figures 8a through c indicate the prediction of lift curve slope became less accurate with increasing negative sweep angle for a negative sweep angle input into LACBIN. Also, maximum lift coefficient was consistently underestimated by the negative angle input. The program fairs a continuous curve between the lift curve slope estimation and the maximum lift coefficient (which occurs at an estimated angle-of-attack). Since the maximum lift curve slope was low for the negative input, the curve broke inward early. The maximum lift prediction grew worse as forward sweep angle increased. This made the lift curve slope break away earlier as forward sweep increased. There was one exception to these trends. This was the -45

degree basic wing shown in Fig 8d. In this case the negative angle
overpredicted maximum lift coefficient. Data for the positive sweep angle
input produced consistent results for all comparisons. However, it slightly
overpredicted lift curve slope for the -15 and -30 degree models. This
overprediction was expected after comparing forward and aft swept wing
experimental data which showed this same trend (Fig 7a). Maximum lift
coefficient appears to be underestimated for the -15 and -30 degree sweep
comparisons and overestimated for the -45 degree model. The program was
suspect for these poor estimations because of the unreliable maximum lift
coefficient predictions in subonic flow against other experimental data,
(Ref 6, Vol 2., p. 32).

Drag

Drag coefficient comparisons are presented in Figs 9a through c.

Drag coefficient predictions by the program for a negative sweep
angle follow the slope of the experimental data very accurately up to a lift
coefficeint of at least 0.4. The positive angle predicts slightly higher
drag values. Above lift coefficients of 0.4 , both the positive and
negative curves, break away from the experimental data. The reason for this
break was not determined.

The program manual, Ref 6, states the skin friction coefficient may be
obtained using a laminar, transition and turbulent boundary layer
calculation. Transition location was specified as a percentage of chord.
Transition locations calculated in Section Three were used for this purpose.
The degree of accuracy of the boundary layer transition location can be
determined by comparing the zero-lift drag of the experimental data and the
predicted data. This is done in Table V. These drag data compaired fairly
well. However, the accuracy of the drag balance in the low drag area is

CL –VS– ALPHA (PROG. COMP.)

45-DEG. BASIC WING

- ○ Experimental Data
- —·— Neg. Sweep Angle (FSW)
- — — Pos. Sweep Angle (ASW)

LIFT COEFFICIENT (CL)

ALPHA (DEGREES)
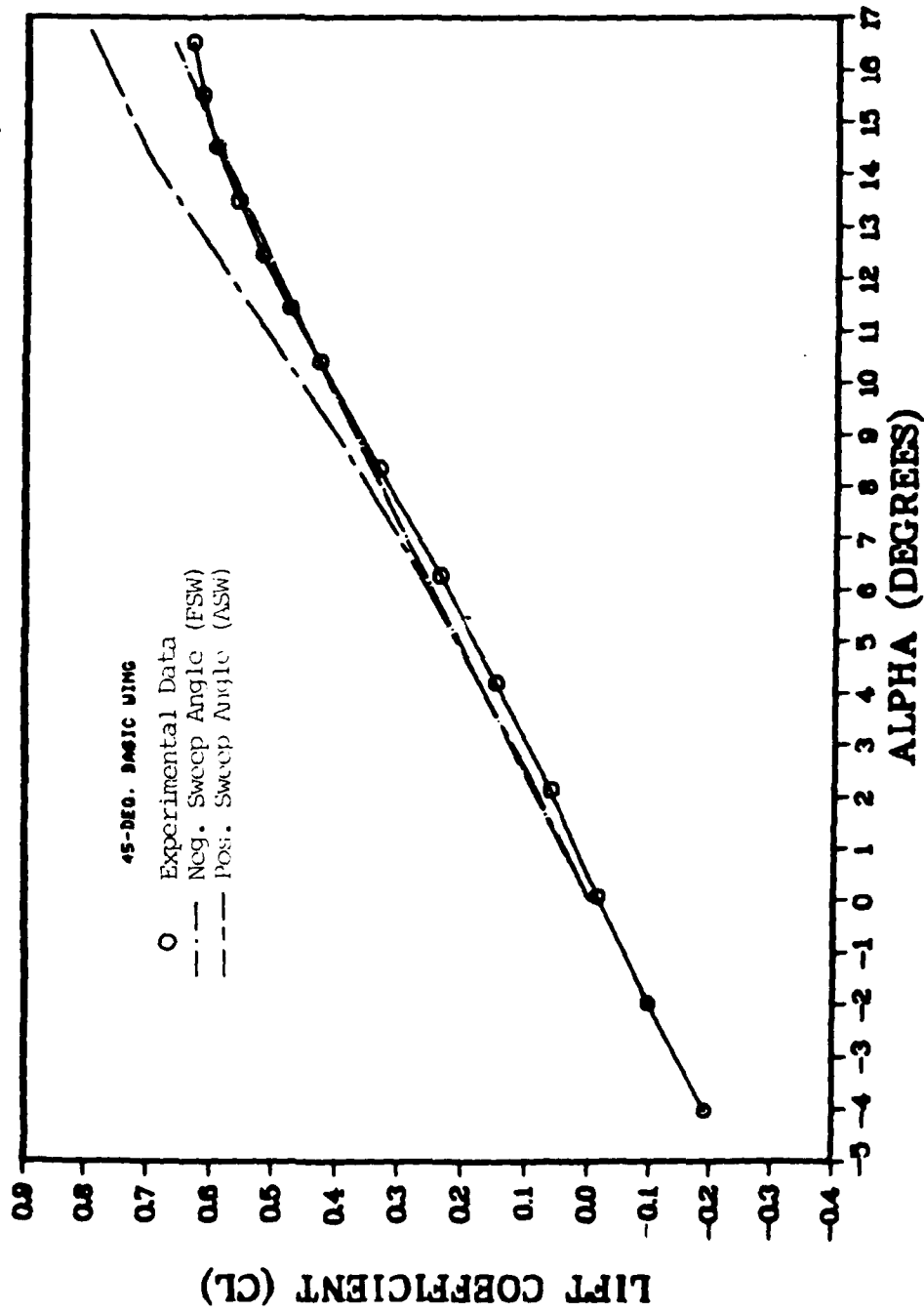
Fig. 8d. Program Comparison of Lift Coefficient Versus Angle of
Attack for the 45 Degree Basic Wing Model.

38

CD -VS- CL (PROG. COMP.)

15-DEG. WING EXT-2

○   Experimental Data
-·-   Neg. Sweep Angle (FSW)
---   Pos. Sweep Angle (ASW)

LIFT COEFFICIENT (CL)

DRAG COEFFICIENT (CD)
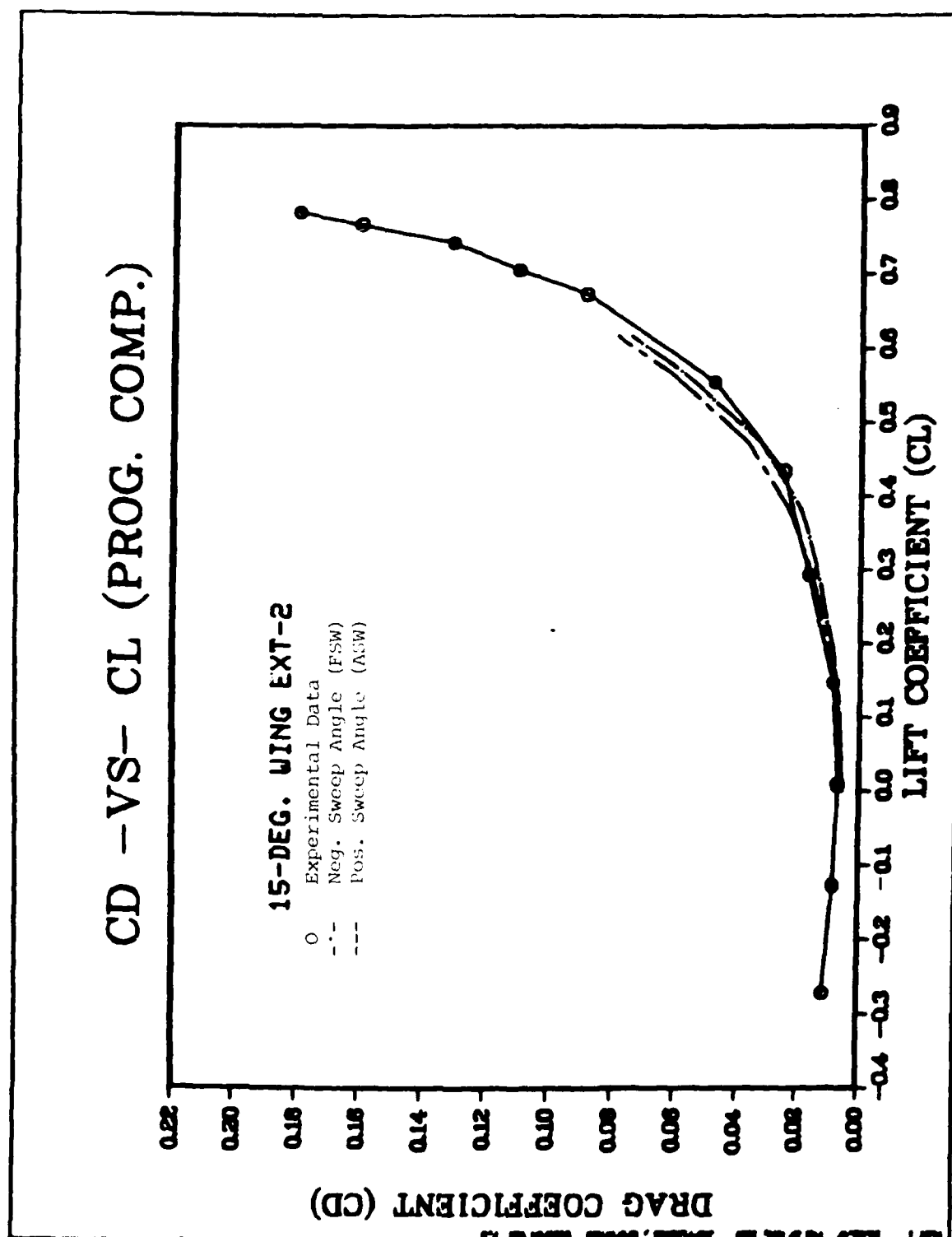
Fig 9a.   Program Comparison of Drag Coefficient Versus Lift
Coefficient for the 15 Degree Extension-2 Model.

CD –VS– CL (PROG. COMP.)

30-DEG. WING EXT-2

O   Experimental Data
-·-   Neg. Sweep Angle (FSW)
---   Pos. Sweep Angle (ASW)

LIFT COEFFICIENT (CL)

DRAG COEFFICIENT (CD)

Fig. 9b.   Program Comparison of Drag Coefficient Versus Lift
Coefficient for the 30 Degree Extension-2 Model.

40

CD –VS– CL (PROG. COMP.)

45-DEG. WING EXT-2

○   Experimental Data
–·–   Neg. Sweep Angle (FSW)
– –   Pos. Sweep Angle (ASW)

LIFT COEFFICIENT (CL)

DRAG COEFFICIENT (CD)

Fig. 9c.   Program Comparison of Drag Coefficient Versus Lift
Coefficient for the 45 Degree Extension-2 Model.

Table V

Zero-Lift Drag Comparison

		Pos. Angle Input (ASW)	Neg. Angle Input (FSW)	Experimental Data
-15°	Basic	.0057	.0054	.0060
	Ext-1	.0057	.0054	.0063
	Ext-2	.0057	.0054	.0068
-30°	Basic	.0063	.0063	.0050
	Ext-1	.0063	.0063	.0051
	Ext-2	.0063	.0063	.0040
-45°	Basic	.0066	.0066	.0046
	Ext-1	.0066	.0066	.0042
	Ext-2	.0066	.0066	.0051

highly dependent on the accuracy of the wire drag tare. Therefore, these values could change.

Moment About Aerodynamic Center

Comparison of moment data about the aerodynamic center is presented in Figs 10a through c. Locations of the aerodynamic center attained from the experimental data reduction program were used as the moment reference points for the models in the performance prediction program. Because of the different geometry and spanwise pressure

CMAC —VS— CL (PROG. COMP.)
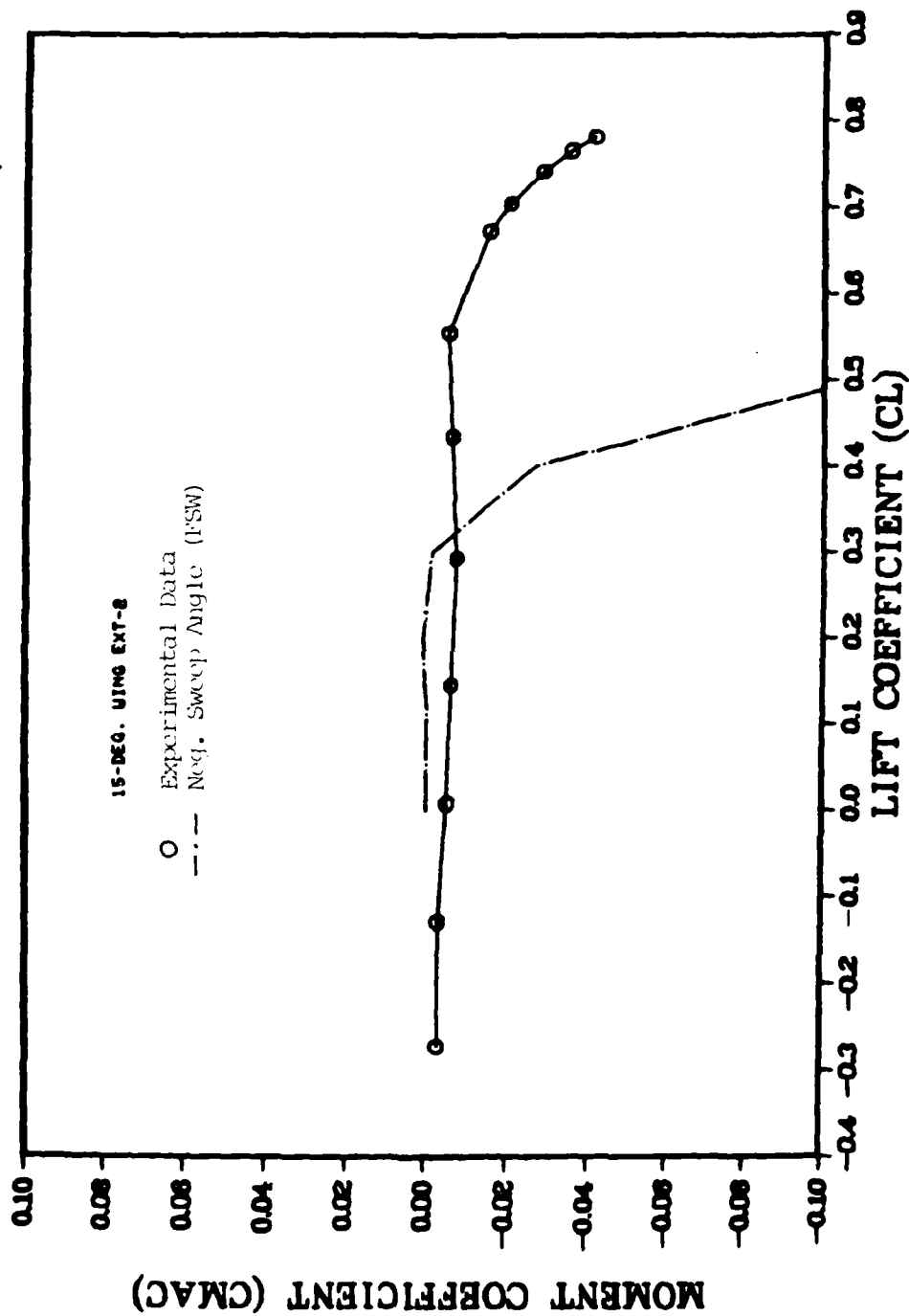
15-DEG. WING EXT-2

   o   Experimental Data
—·— Neg. Sweep Angle (FSW)

LIFT COEFFICIENT (CL)

MOMENT COEFFICIENT (CMAC)

Fig. 10a. Program Comparison of Moment Coefficient versus
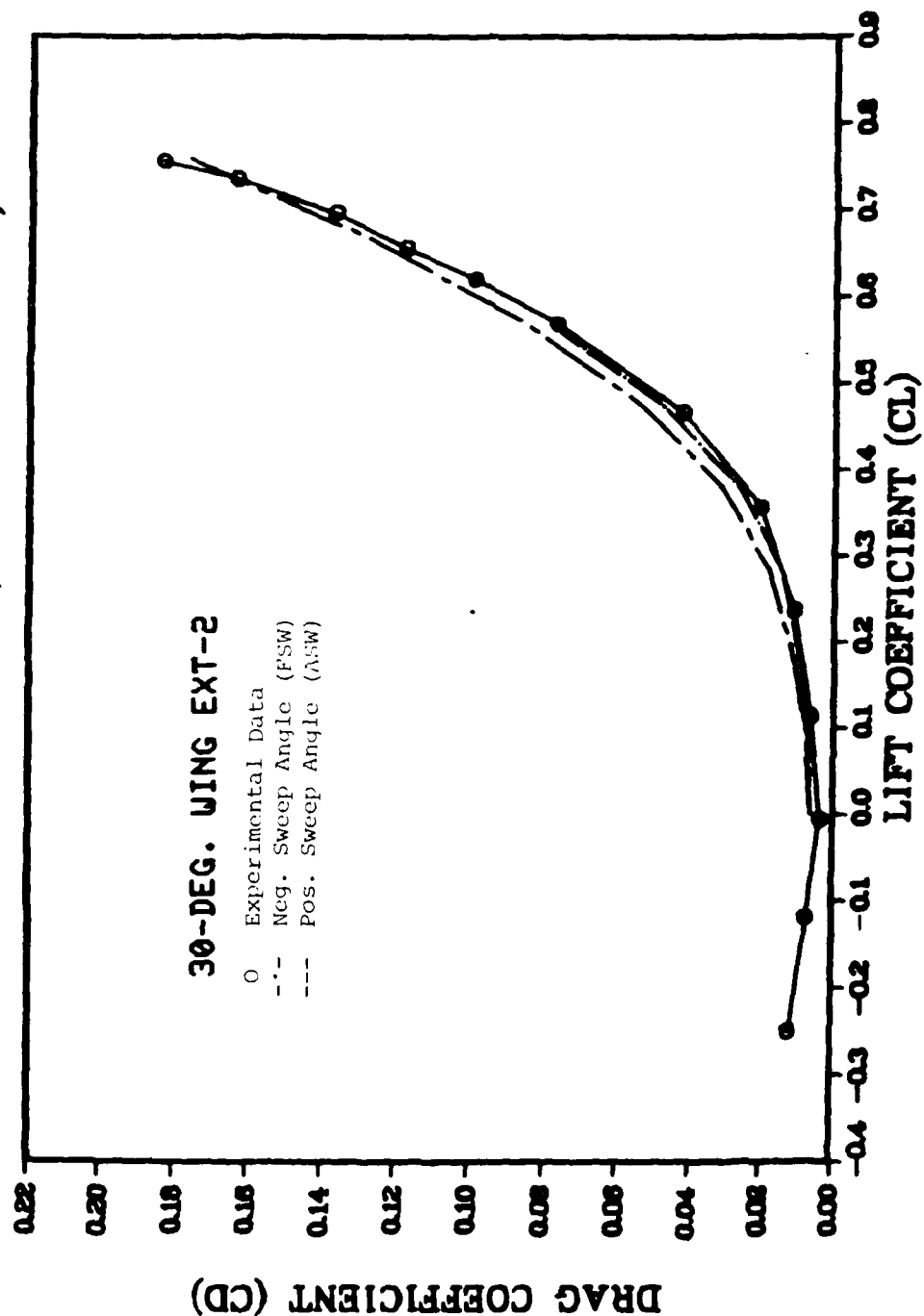Lift Coefficient for the 15 Degree Extension-2 Model.
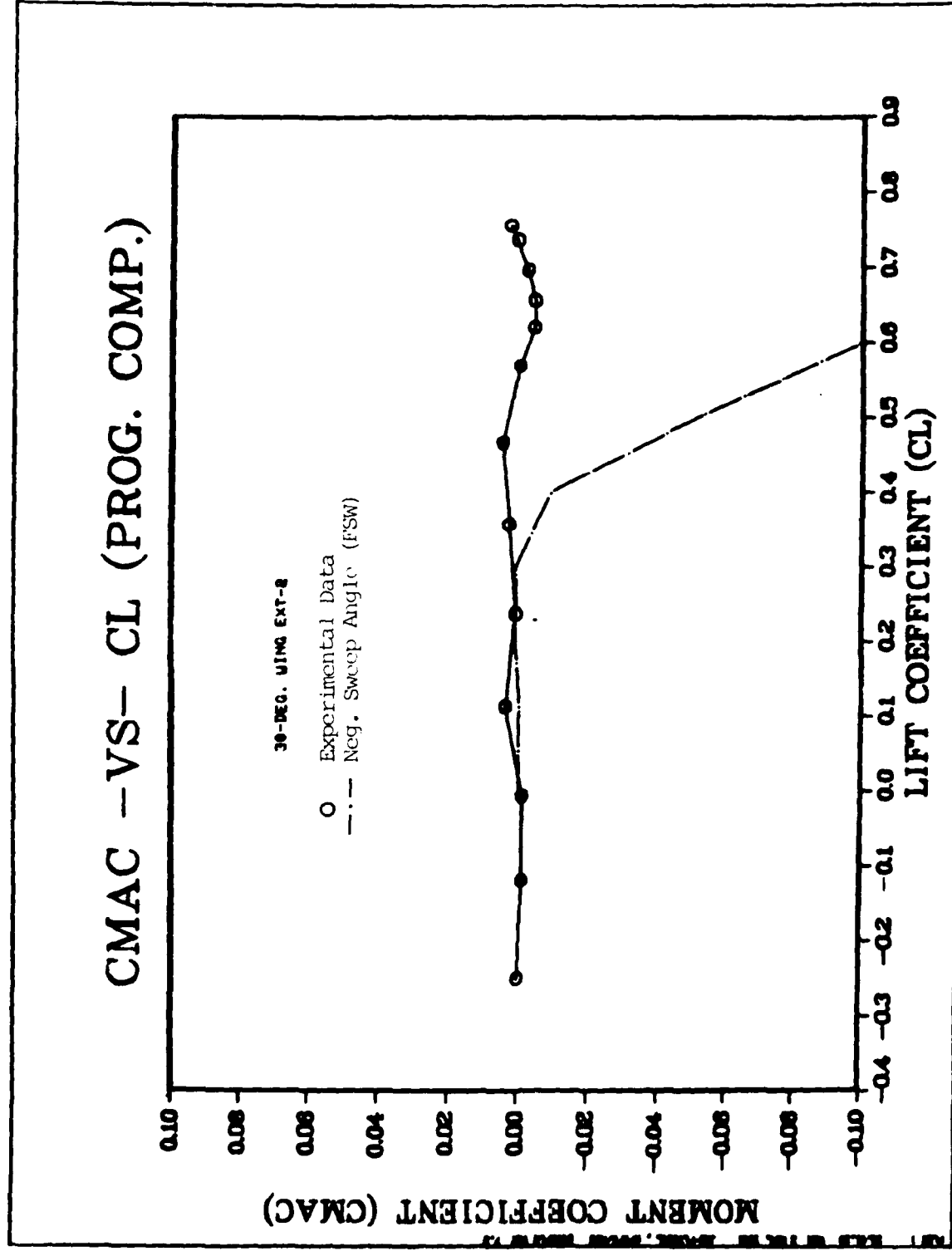
Fig. 10b. Program Comparison of Moment Coefficient Versus Lift Coefficient for the 30 Degree Extension-2 Model.

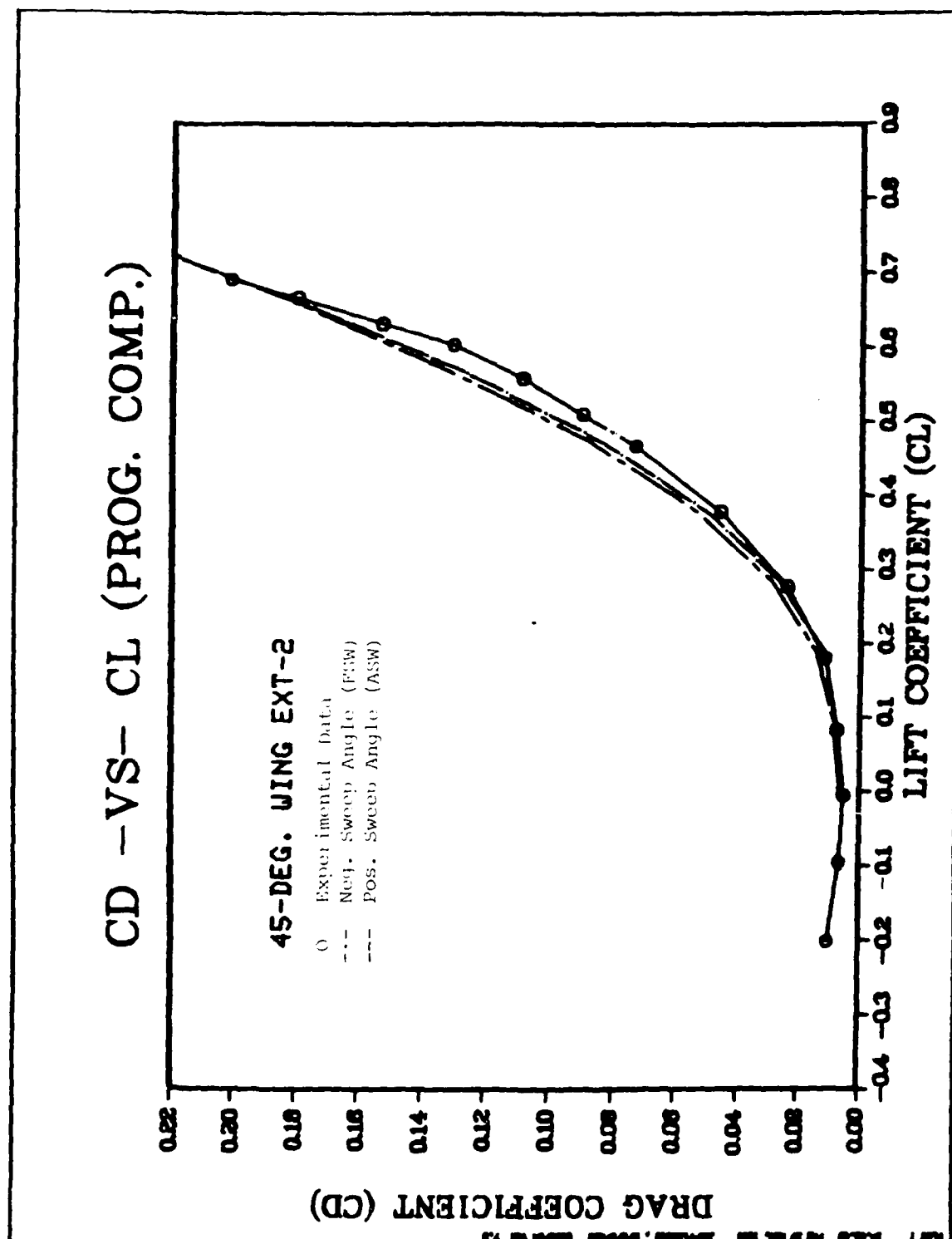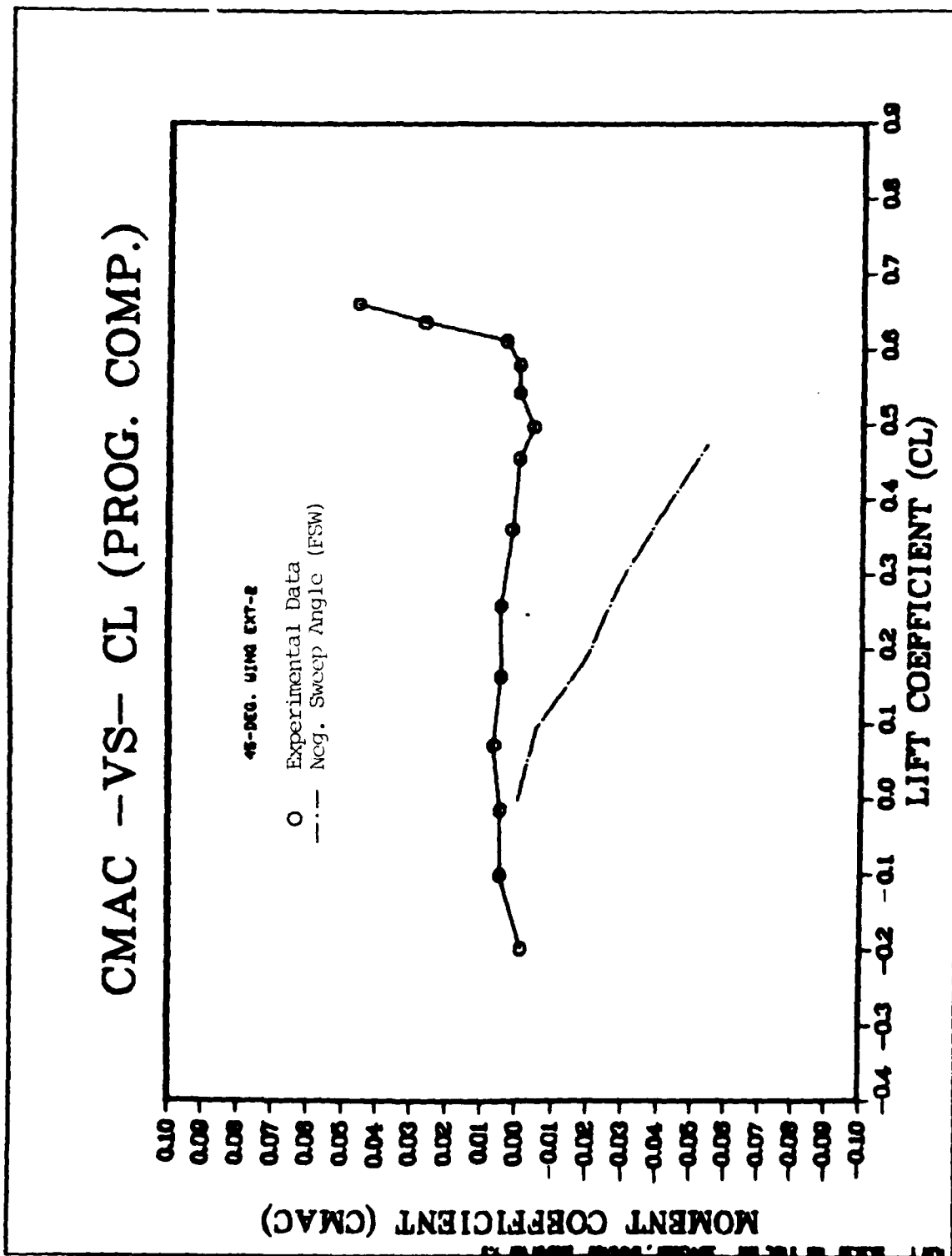Fig. 10c. Program Comparison of Moment Coefficient Versus Lift
Coefficient for the 45 Degree Extension-2 Model.

distributions of aft swept wings, location of the aerodynamic center for the positive angle case was not possible.

At low lift coefficients (below $C_L = 0.3$), Figs 10a and b show excellent agreement for moment coefficient. This indicated an accurate aerodynamic center location. The early, sharp departure of the data predicted for the negative sweep angle is the result of low maximum lift coefficient prediction by the program.

Aerodynamic center location of the -45 degree model was not accurate for use in the prediction program (Fig 10c). Predicted data indicates the aerodynamic center based on the experimental data was too far forward. Whether this disagreement is due to the prediction program or the experimental data is not known. It is possible that the wing twisting moment could account for this. The positve twisting moment of the forward swept wing increases in severity as forward sweep angle increases. If the structure did not damp this out, the aerodynamic center may have to shift forward to compensate.

The results of the program comparison show several areas in which the performance prediction program, LACBIN provided accurate results and others where its utility was marginal compared to the test data in the incompressible flow regime.

Allowing for a small overprediction in lift curve slope the positive sweep angle input into LACBIN provided an accurate and consistent prediction for forward swept wings in the linear range. Neither sweep angle input provided an accurate estimation of non-linear lift curve slope for maximum lift coefficient. This was due to inherent inaccuracies in the program.

Using the negative sweep angle provided an accurate prediction of drag polar slope below 0.04 lift coefficient. Assuming a fairly accurate boundary layer transition location, both input angles predicted zero-lift drag fairly well.

Moment coefficient prediction for lift coefficients below 0.04 was very accurate for the negative sweep angle. But, until errors in maximum lift coefficients are corrected, the estimation of moment coefficient at high lift coefficients is not reliable.

V. Conclusions and Recommendations

Conclusions

1. The effects of sweep and aspect ratio on the aerodynamic characteristics of forward swept wings in incompressible flow, are similar, in trend, to their effects on the characteristics of aft swept wings. Increasing forward sweep angle decreases lift curve slope and moves the aerodynamic center rearwards. Increasing aspect ratio increases lift curve slope, decreases drag coefficient and moves the aerodynamic center rearward.

2. Data collected for various forward sweep angles and aspect ratios provided a valid base for comparison to the Large Aircraft Performance Prediction Program (LACBIN) in incompressible flow.

3. LACBIN predicts lift curve slopes accurately in the linear range using a positive sweep angle input. Drag polar is accurately predicted below a lift coefficient of 0.4, using a negative angle input. Moment about the aerodynamic center is also accurately predicted below a lift coefficient of 0.4 using a negative sweep angle input. This indicates accurate aerodynamic center prediction. Maximum lift coefficient is very inaccurate for both positive and negative sweep angle inputs into LACBIN.

Recommendations

1. In the short term, using LACBIN to predict aerodynamic characteristics of forward swept wings in incompressible flow, must be done with care. This study may be used a guideline for this purpose.

2. Follow-on studies are needed to provide a complete data base for comparison to LACBIN. Data from this study and follow-on studies may be used to provide an empirical base for forward swept wings to incorporate

into LACBIN. This would provide a long term solution for predicting forward swept wing aerodynamics.

3. It is recommended that a pressure model be constructed to evaluate spanwise flow effects.

4. In order for follow-on experimental data to be reliably scaled to higher Reynolds numbers, for comparison purposes, it is recommended that half-span models with splitter plates be used in addition to operating at higher speeds.

BIBLIOGRAPHY

1. Roark, R. J. and W. C. Young. Formulas for Stress and Strain (5th edition). New York: McGraw-Hill Book Company, 1975.

2. Lawrence, J. R. Development of a Half-Span Model Test System for the AFFDL-TAGJ. Contract F-33615-74-C-3085, Vol. 2, Fort Worth, Texas: General Dynamics Corporation, September 1975.

3. U.S. Standard Atmosphere, 1962. Prepared under sponsorship of NASA, USAF, U.S. Weather Bureau, December 1962.

4. Pope, Alan and John J. Harper. Low-Speed Wind Tunnel Testing, John Wiley and Sons, New York, 1966.

5. Abbott, I. H. and A. E. Von Doenhoff. Theory of Wing Sections, Dover Publications, Inc., New York, 1959.

6. Schemensry, Roy T. Develompent of an Empirically Based Computer Program to Predict the Aerodynamic Characteristics of Aircraft Vols. I & II. Contract F33615-73-C-3043. Fort Worth, Texas: General Dynamics, November 1973.

7. Sarver, Russell H. Low Reynolds Number Characteristics of Selected Airfoils as Determined From Wind Tunnel Tests. Thesis, Air Force Institute of Technology, Wright-Patterson AFB, Ohio, December 1976.

8. Lipson, Charles and Robert C. Juvinall. Handbook of Stress and Strength. The Macmillan Co., New York, 1963.

9. McCormack, Gerald M. and Woodrow L. Cook. A Study of Stall Phenomena on a 45° Swept-Forward Wing. NACA-TN-1797, December, 1948.

10. Schneider, William C. Effects of Reynolds Number and Leading Edge Shape on the Low Speed Longitudinal Stability of a 6-Percent-Thick 45° Swept Back Wing. NACA-RM-L56B14, April 18, 1956.

11. Brebner, G. G. Low Speed Wind-Tunnel Tests on the Effect of Planform Design, and Chamber and Twist on Sweptback Wing Characteristics. RAE-TN-65145, July, 1965.

12. Cahill, Jones F. and Stanley M. Gottlieb. Low Speed Aerodynamic Characteristics of a Series of Swept Wings Having NACA 65A006 Airfoil Sectons. NACA RM L50F16, October 17, 1950.

13. Sims, K. L. An Aerodynamic Investigation of a Forward Swept Wing. Thesis, Air Force Institute of Technology, Wright-Patterson, AFB, December, 1974.

14. Purser, Paul E. and M. Leroy Spearman. Wind Tunnel Tests at Low
    Speeds of Swept and Yawed Wings Having Various Plan Forms. NACA TN
    2445, Langley, Virgina, May 22, 1947.

15. Hopkins, Edward J. Lift Pitching Moment, and Span Load
    Characteristics of Wings at Low Speed as Affected by Variations of
    Sweep and Aspect Ratios. NACA TW-2284, Ames Research Center,
    California, November 17, 1950.

16. Hogard, M. Page and John R. Hagerman. Downstream and Wake Behind
    Untapered Wings of Various Aspect Ratios and Angles of Sweep. NACA
    TN-1703, Langley Field, Virgina, June 3, 1948.

17. Connter, William D. and Patrick A. Cancro. Low Speed
    Characteristics in Pitch of a 34° Swept Forward Wing With
    Circular-Arc Airfoil Sections. NACA RM-L7F04A, Langley, Virgina,
    January 9, 1948.

Table VI

NACA 0006 Coordinates

(L. E. radius: .007 c)

X/C	X (IN)	Z (IN)
0	0	
.005	.0375	
.0125	.094	.071
.025	.188	.098
.050	.375	.133
.075	.563	.158
.10	.75	.176
.15	1.125	.200
.20	1.50	.215
.25	1.875	.223
.30	2.25	.225
.40	3.00	.218
.50	3.75	.199
.60	4.5	.171
.70	5.25	.137
.80	6.0	.098
.90	6.75	.054
.95	7.125	.030
1.00	7.56	.005

(Ref 5:311)

52

Appendix A

Model Geometry

Airfoil Coordinates

$$\overline{C} = 7.56 \text{ inches}$$
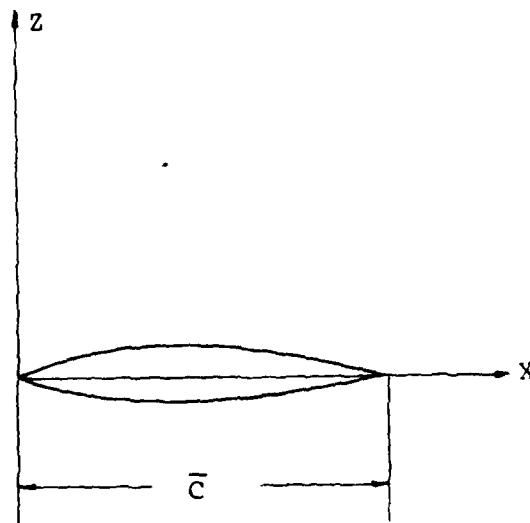
Fig. 11a. Airfoil Coordinate System

Planform Coordinates
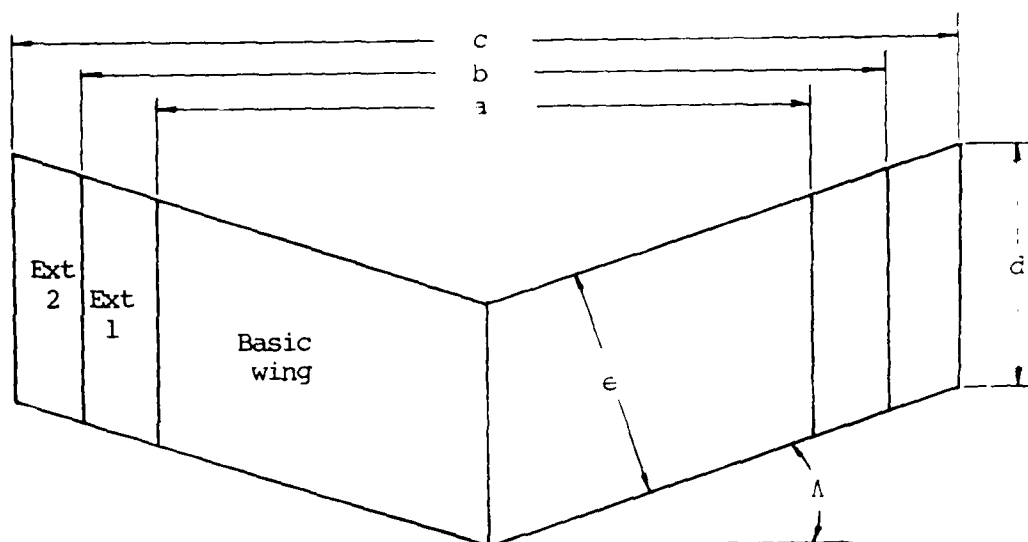
Fig.   11b.   Planform Geometry

Table VII

Planform Coordinates (Dimensions in inches)

Λ	a	b	c	d	e
-15°	30.0	33.75	37.5	7.82	7.5ɔ
-30°	26.95	30.29	33.62	8.73	7.56
-45°	22.0	24.73	27.45	10.69	7.56

Table VIII

Wing Area and Volume

	Basic Wing	Extension-1	Extension-2
Area (ft. sq)	1.63	1.83	2.03
Vol. (cu. ft.)	.044	.050	.056

Table IX

Wing Aspect Ratio

Λ	Basic Wing	Extension-1	Extension-2
-15	3.33	4.32	4.79
-30	3.21	3.47	3.85
-45	2.05	2.31	2.55

Appendix B

Model Safety Analysis

Due to the divergent nature of the forward swept wing twisting moment, a stress analysis was preformed to insure each model could withstand the loads expected during wind tunnel testing.

Another area of interest was the aeroelastic effects on the data. Obviously, these needed to be kept to a minimum. While weight was not a critical design factor, the models had to be light enough to provide ease of installation for one person.

To yield a conservative estimate on the ultimate factor of safety, two basic assumptions were adhered to throughout the analysis. First, a uniform (rectangular) pressure distribution was used. Second, wing loading was concentrated at the centroid, instead of the theoretical center of pressure. Both of these assumptions provide higher bending moments and tip loads than would be expected for a forward swept wing.

In this analysis, two models were considered. The first was the 15° model with the second extension. This model had the largest bending moment. The second model was the 45° model with the second extension. The largest twisting moment was experienced by this model. Loads were calculated at three sections on each wing. Referring to Fig 12 section A-A experienced the maximum bending moment. Section B-B was located along the front trunnion line, where the opposing moments of the tip and inboard sections were concentrated. Lastly, section C-C was the point where the metal spar ended, and the solid epoxy carried the full load. Each wing was modeled as a simply supported beam with overhanging ends.
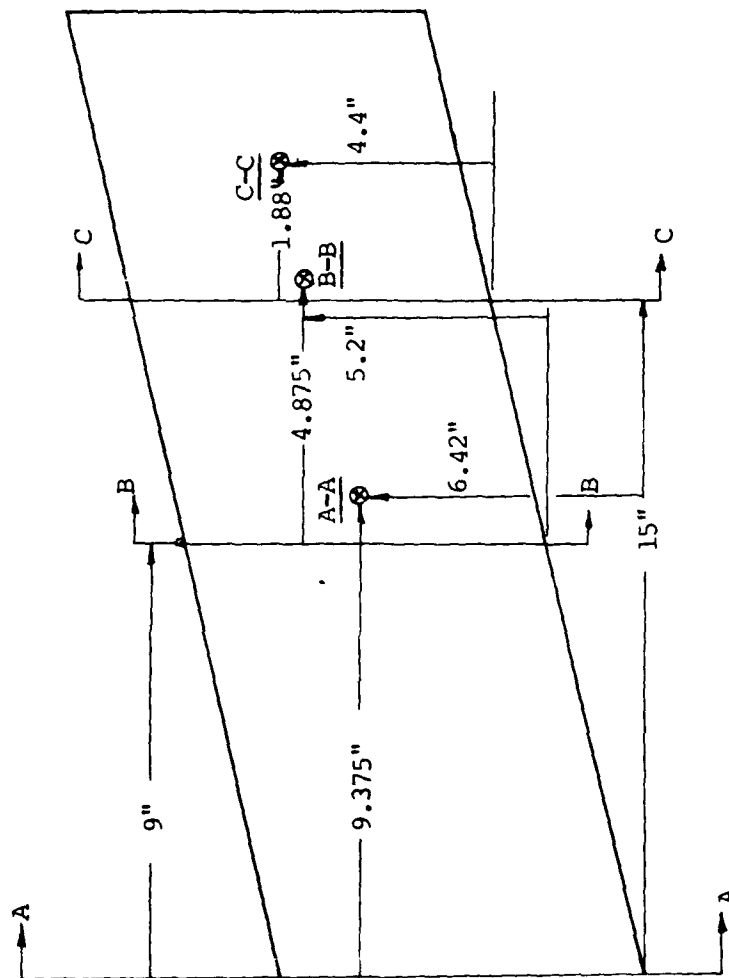
Fig. 12. 15° Ext-2 Model, Centroid and Section Locations

57
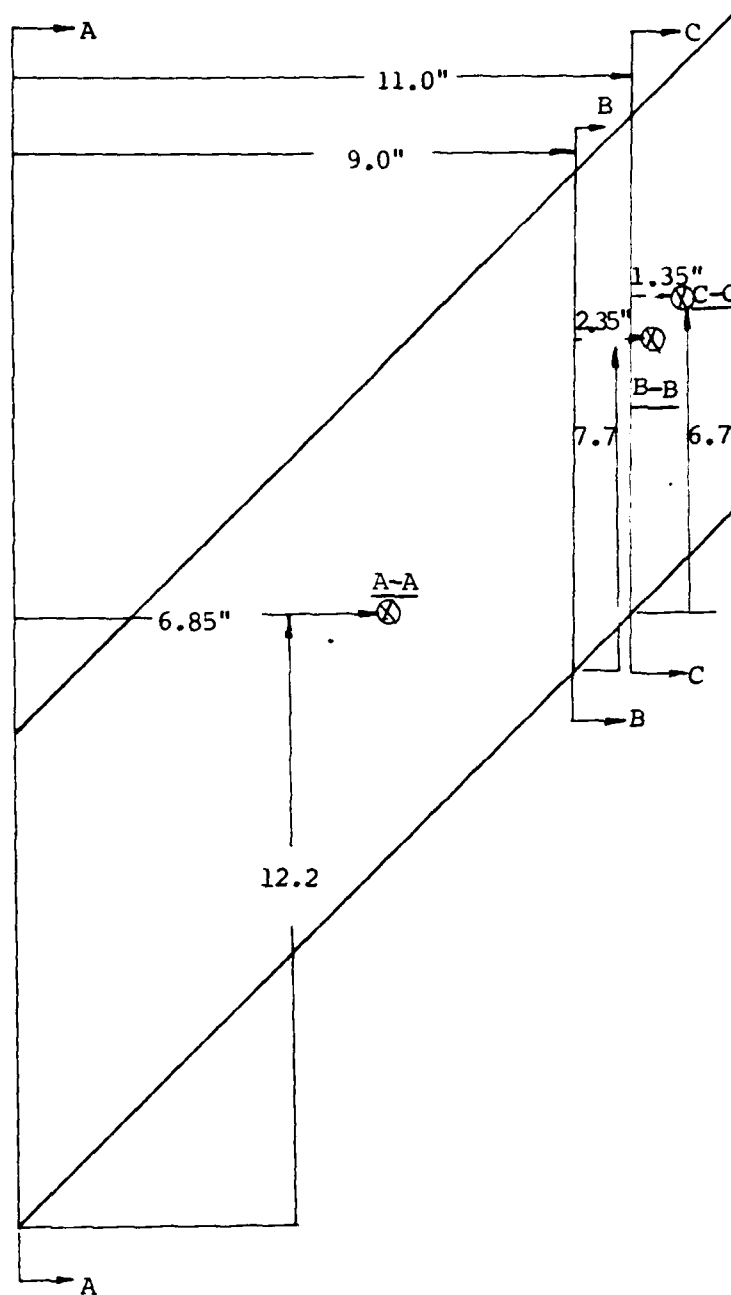
Fig. 13. 45° Ext-2 Model, Centroid and Section Locations

Maximum Loads

The maximum aerodynamic load expected for each wing was determined using a $C_{L_{max}} = 1.4$

$$L_{max} = C_{L_{max}} qS$$

where

$q = 25.58$ psf for all tests

$S = 2.03$ ft^2 for both models analyzed

L_{max} equaled 72.25 lbf* for each model.

Referring to Fig 14, the maximum aerodynamic load is a function of angle of attack.
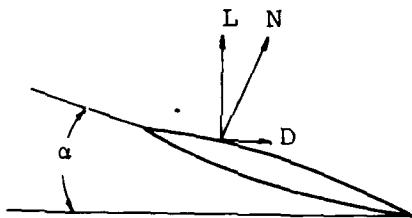
Fig.14. Load Diagram of Wing Section

$$N = \frac{L}{\cos\alpha}$$

where N is the maximum normal aerodynamic force. For $\alpha = 14.5°$, N is 74.63 lbf for each model.

The average pressure acting over the wing in accordance with assumption one, is:

$$P_{avg} = \frac{N}{S}$$

*This was based on the load recorded on the first 15° basic wing, which failed at $\alpha = 14.5°$. This was obviously an aeroelastic model and loads on it were 30% greater than any load recorded during the remainder of testing. This added to the conservative nature of this analysis.

59

P_{avg} was 36.76 psf for this analysis.

Section A-A

Bending Stress

The aerodynamic force acting outboard of section A-A is given by

$$N_{A-A} = P_{avg} S_a$$

where

$$S_a = 1.02 \text{ sq. ft.}$$

A normal force of 37.3 lbf was obtained for both wing models.

The bending moment for section A-A was computed using N_{A-A} multiplied by the y distance to the centroid minus the restoring moment of the trunnion fitting.

$$M_{A-A} = N_{A-A} \bar{Y} - 21.14 \text{ ft} - \text{lbf}$$

This resulted in a bending moment of 96.84 in-lbf for the 15° model and 1.2 in-lbf for the 45° model.

To evaluate the stresses at sections A-A, the steel spar was modeled as a thin beam as shown in Fig 15. The beam was assumed to carry the entire load.
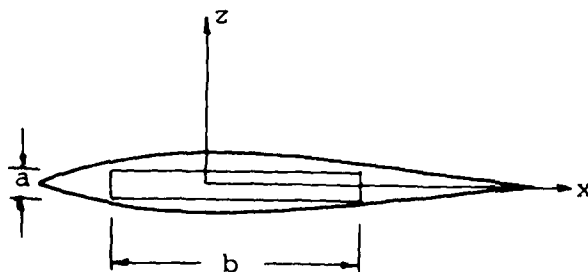
Fig. 15. Wing Modeled as a Thin Beam

The expression for the moment of inertia about the x-axis is

$$I_x = \frac{a\,b^3}{12}$$

where a and b are the cross-sectional dimensions of the beam. At any point on the beam, the bending stress, σ is given by:

$$\sigma = \frac{M}{I_x}\,Z$$

where z = b/2, for the maximum stress at the surface. Substituting yielded the following expression for σ_{max}:

$$\sigma_{max} = \frac{6M}{ab^2}$$

which gave the maximum stress on the beam. For both models, a was 3.0 inches, and b was .125 inches. This yielded a maximum bending stress of 12,345 psi for the 15° model and 154 psi for the 45° model for section A-A.

Shearing Stress

The maximum shearing stress, using the thin beam model is:

$$\tau_{max} = (\frac{3a + 1.8b}{a^2\,b^2}) \tag{1}$$

where

$$T = N\,(\widetilde{Y} - d_c) \tag{2} \qquad \text{(Ref 1:194)}$$

where d_c is the distance to the center of flexure as measured from the same reference system used to locate the centroid. For the 15° model d_c was 5.13 in. This gave a maximum shearing stress of 2628 psi. For the 45° model, d_c

61

was 6.81 in. yielding 79.68 in-lbf for the twisting moment and 5666 psi for the maximum shearing stress.

Factors of Safety

The spar material was 1020 cold drawn steel. It has the following properties:

yield tensile stress (yts) = 60000 psi

ultimate tensile stress (uts) = 78000 psi

yield shearing stress (yss) = 36000 psi

ultimate shearing stress (uss) = 60000 psi

$$(Ref \ 8:434)$$

The ultimate factor of safety is given by:

$$FS = \frac{1}{\sqrt{(\frac{\sigma_{max}}{uts})^2 + (\frac{\tau_{max}}{uss})^2}} \qquad (3) \qquad (Ref \ 2:20)$$

For the 15° model, the factor of safety was 6.09 and 10.5 for the 45° model at section A-A.

Section B-B

Bending Stress

For both models, the normal force acting outboard of section B-B was given by:

$$N_{B-B} = P_{avg} \ S_B$$

where the area outboard of B-B was .53 sq. ft. for both models. N_{B-B} for both models was 232.78 lbf.

The bending moment for section B-B was due to aerodynamic forces alone and was given by:

$$M_{B-B} = N_{B-B} \, \overline{Y}$$

M_{B-B} was 93.12 in-lbf for the 15° model and 30.0 in-lbf for the 45° model. The wing was again modeled as a thin beam (Fig 15). The maximum bending stress was 4,975 psi for the 15° model and 3858 psi for the 45° model.

Shearing Stress

Eq (1) was used again to find the maximum shearing stress. N_{B-B} was used in eq (2), as well as the correct value of y to determine the twisting moment. The twisting moment for the 15° model was 432 in-lbf. For the 45° model, it was 6.84 in-lbf. Substituting these yeilded 94.8 psi and 48.75 psi. for the maximum shearing stress of the 15° and 45° model respectively.

Factors of Safety

These values gave an ultimate factor of safety of 6.5 for the 15° model and 19.9 for the 45° model using eq (3).

Section C-C

Again, for both models, the normal force was given by:

$$N_{C-C} = P_{avg} \, S_C$$

where S_C was .2 sq. ft. for both models. N_{C-C} was 87.84 lbf for both models.

The bending moment was given by:

$$M_{C-C} = N_{C-C} \, \overline{Y}$$

M_{C-C} was 13.56 in-lbf and 9.84 in-lbf for 15° and 45° model respectively.

There was no spar in this section of the model, but the wing was still modeled as a thin beam only with slightly larger dimensions. The dimension a was changed to 4 inches and b to .25 inches. This gave a maximum bending of 325.44 psi for the 15° model and 237.22 psi for the 45° model.

Shearing Stress

The twisting moment, eq (2), was modified to reflect the movement of the center of flexure to the 30% chord position (Ref 1). This was done due to the elimination of the spar in this section of the model. This changed d_c by a small amount. These changes yielded a twisting moment of 5.1 in-lbf for 15° model and .84 in-lbf for the 45° model. The maximum shearing stress computed using eq (1) was 363.0 psi and 57.0 psi for the 15° and 45° model respectively.

Factors of Safety

The ultimate factors of safety were computed based on the 4650 psi bond strength of the aluminum base epoxy. Using this property and eq (3) the factor of safety for section C-C was 9.51 for the 15° model and 19.1 for the 45° model.

Although a factor of safety of 4 is considered rather stringent, the large values attained in this analysis will insure safety of the tunnel and insure minimum aeroelastic effects on the data (Ref 13).

Model-Balance Dimensionsal Data

Fig. 16. Angle of Balance

$G = \overline{AB}$, distance between front and rear fitting

$a = \overline{BC}$, vertical distance between $\overline{AB}$ and rear fitting

$\overline{AC}$ = balance axis

α_0 = angle between balance axis and $\overline{AB}$

Table X

Model - Balance Dimensional Data

	G (in)	a (in)	α_0
15° model	14.781	0	J
30° model	14.435	0	0
45° model	16.938	0	0

Appendix D

Test Condition Computation

Reynolds Number

$$Re = \frac{\rho V \ell}{\mu}$$

$$\rho = \frac{P}{RT}$$

$$V = (2q/\rho)^{0.5}$$

$$\mu = (\beta/g)\, \frac{T^{1.5}}{T+S}$$

where

ρ = density (slugs/ft^3)

v = velocity (ft/sec)

ℓ = chord length (ft)

μ = viscostiy (lb-sec/ft^2)

R = gas constant (1716.55 lb$_f$ ft/R lbm)

β = bulk modulus of compression (7.3025×10^{-7} lb ft^{-1} sec^{-1} ($^\circ$R)$^{-0.5}$)

S = 109.72 R

g = gravity (32.174 ft/sec^2)

q = dynamic pressure (62.433/12) x in water

p = static pressure (2116.22/29.9213) x in Hg

Applying these relations, we obtain:

$$Re = 2.88487 \times 10^{-7} x \; \{p \times q\}^{0.5} \; \{\frac{F + 685.4}{(F + 458.67)^2} \cdot \ell$$

where

F is the static temperature in degrees F.

Although pressure and temperature are really measured as stagnation values rather than static, the error incurred by using these measurements is less than one percent for this tunnel. About a one percent error is incurred by not correcting the dynamic pressure for axial test section location.

Dynamic Pressure

From 1970 longitudinal static pressure gradient test data (data availability at tunnel), the dynamic pressure at the model location for these tests was 1.0189 times the manometer setting. Other corrections to dynamic pressure are discussed in Appendix E.

Mach Number

$$P_t = (2116.22/29.213) \ P_a$$

P_a = ambient pressure in in Hg

$$P = P_t - 1.0189q$$

$$q = (62.433/12)(\text{in water})$$

$$M = \{1.0189 \ q/.7P^{0.5}\}$$

which is within one percent of the value based on isentropic compressible flow relations. A maximum error of 2 percent is incurred by not applying boundary effects corrections (Ref 7).

Appendix E

Wind Tunnel Boundary Corrections

Dynamic Pressure

The dynamic pressure was corrected for solid and wake blockage by:

$$q_{corr} = (1 + \varepsilon_{wb} + \varepsilon_{sb})^2 \, q_u$$

where

q_{corr} = corrected q

q_u = 1.0189 times the manometer reading converted to psf

$\varepsilon_{wb} = 1/4 \; s/c \; C_{D_u}$

$\varepsilon_{sb} = \dfrac{\tau^1 \, k^1 \, (volume)}{c^{1.5}}$.

The constants used were

s = wing area (see Appendix A)

c = 19.635 ft^2 (test section cross-sectional area)

τ^1 = .81 ~.83 (depending on configuration) (Figure 6-16, Ref 4)

k^1 = .94 for t/c = .06 (Figure 6-14, Ref 4)

volume = wing volume in cu. ft. (see Appendix A).

The value of C_{D_u} was given by:

C_{D_u} = (measured drag - wire balance drag - bouyancy drag)/(q_u S)

Bouyancy drag was set to zero based on the following:

$\Delta D_b = -\dfrac{dp}{d\ell} \, (volume)$

where

ΔD_b = bouyancy drag(lbf)

$\dfrac{dp}{d\ell}$ = longitudinal pressure gradient of test section at model location (psf/ft)

volume = wing volume (ft^3)

From a 1970 test at the five foot tunnel, $\dfrac{dp}{d\ell}$ = -.00045 q (12).

Extension two presented the greatest bouyancy drag.

$$\Delta D_b = .00045 \ (25.58) \ (.056) \ (12)$$

$$= .0076 \ \text{lb}$$

This value was well within the drag scale accuracy for these tests.

In terms of C_D:

$$\Delta C_{D_b} = .0076/(25.58 \times 2.03)$$

$$= .000146$$

Drag

The drag coefficient was corrected for boundary induced upwash by:

$$C_D = C_{D_u} \left(\frac{q_u}{q_c}\right) + C_{D_i}$$

where

$$\Delta C_{D_i} = \left(\frac{S}{C}\right) C_L^{\ 2}$$

$$\delta = .125 \ (\text{Fig. } 6\text{-}28, \ \text{Ref } 4)$$

$$C_L = C_L \ \text{using } q_c$$

Angle of Attack

Angle of attack was corrected for flow angularity, streamline curvature and boundary induced upwash by:

$$\alpha = \alpha_{set} + (1 + \tau_2)\Delta\alpha_i + FA$$

$$\Delta\alpha_i = \delta(\frac{S}{C})C_L, \quad \text{upwash correction}$$

$\tau_2\Delta\alpha_i$ = streamline curvature correction

τ_2 = .05 (Fig. 6-54, Ref 4)

FA = tunnel flow angularity

Pitching Moment

The pitching moment was corrected for streamline curvature by:

$$C_m = C_{m_u} + \Delta C_m$$

$$C_{m_u} = M_{ac}/(q_c\ Sc)$$

M_{ac} = measured moment transferred to the areodynamic center

ΔC_m = .25 $\tau_2\Delta\alpha_1 a$

where

a = wing lift curve slope, $\dfrac{\Delta C_L}{\Delta\alpha}$

Appendix F

Wind Tunnel Data Reduction Program

Input Data:

Input data was run interactively from tape. (see sample input)

Line	Columun	Symbol	Discription
1	1-8	ALENGT	Model chord in inches
	9-16	G	Distance between front and rear attachment fittings
	17-24	SREF	Model reference area in sq. ft.
	25-32	VOL	Model volume in cu. ft.
	33-40	BETA	Angle between model reference line and balance reference line in degrees
	41-48	QH2OHT	Tunnel dynamic pressure in inches of water
	49-56	DELTA	Boundary correction factor from Fig. 6-28, Ref 4
2	1-2	DB	Bouyancy drag
	9-16	DWB	Wire balance drag
	17-24	ALPHAO	Angle between reference line and balance reference line in degrees
	25-32	DELAFA	Tunnel flow angularity in degrees
	33-40	AK1	Wing shape factor from Fig. 6-15, Ref 4
	41-48	TAU1	Solid blockage factor from Fig. 6-16, Ref 4
	49-56	TAU2	Downwash correction factor from Fig. 6-52, Ref 4

71

Line	Column	Symbol	Description
3	1-4	RUNNUM	Run number, integer
	5-8	NOP	Number of data points, integer
4	1-8	TFAR	Stagnation temperature in degrees F
	9-16	BARHT	Barometeric pressure in inches of mercury
5	(There are NOP line 5's for each run)		
	1-10	ALPHAB	Angle of the balance in degrees
	11-20	ZFS	Front lift static balance reading in pounds
	21-30	ZFWO	Front lift wind-on balance reading in pounds
	31-40	ZRS	Rear lift static balance reading in pounds
	41-50	ZRWO	Rear lift wind-on balance reading in pounds
	51-60	DS	Drag static balance reading in pounds
	61-70	DWO	Drag wind-on balnce reading in pounds

The remainder of the appendix contains the program listing and sample output.

Data Reduction Program Listing

```
1300:       CNTR(K)=CNTR(K)+DELCNTR(K)
1310-20     CONTINUE
1340-C      CDRC COMPUTATION
1350        DCRDCL=(CNTR(8)-CNTR(4))/(CL(8)-CL(4))
1370        DO 40 N=1,ND
1380        BCDBCL(4)=-.565
1390        BCDBCL(8)=-.565
1400        ALPHAG(N)=ALPHA(N)/57.3078
1410        A(N)=(1+(CD(N)B(1+(BLOK(N)B7.2)))BCOS(ALPHAG(N)))
1420        B(N)=1+BCDBCL(N)-(CL(N)B(1+(BLOK(N)B57.3)))BSIN(ALPHAG(N))
1430        C(N)=(BCDBCL(N)-(CL(N)B(1+(BLOK(N)B7.2)))BCOS(ALPHAG(N)))
1440        D(N)=1+(CD(N)B(1+(BLOK(N)B57.3)))BSIN(ALPHAG(N))
1450        E(N)=A(N)-B(N)
1460        F(N)=C(N)-D(N)
1470-40     CONTINUE
1480        X=(BCDBCL-(F(8)B(BCDBCL/F(4))))/
1500        (1+(-F(8)BE(4))/(E(4)BX(8))/F(4))
1510        V=(BCDBCL-(E(4)BX))/F(4)
1520        DO 50 N=1,ND
1530        ALPHAG(N)=ALPHA(N)/57.3
1540        CDRC(N)=CNTR(N)-(XB(CL(N)B(1+(BLOK(N)))))-
1550        (+(CD(N)BSIN(ALPHAG(N)))))-
1560-50     (VB(CD(N)BCOS(ALPHAG(N)))-(CL(N)BSIN(ALPHAG(N)))))
1570-C      CONTINUE
1580        WRITE REDUCED DATA
1590        PRINT'(//75,A,T13,A)','TITLE=','30-DEG BASIC FGN',
1600-415    WRITE(6,415)FORMULA
1610        FORMAT(1H0,GL,'RUN NO.-',I4)
1620        WRITE(6,430)RUN,APROCH
1630-410    WRITE(6,410)
1640        FORMAT(///,GX,'ALPHA',4X,'CL',BX,'CD',
1650        1BX,CDRC ,7X,'CNTR')
1660        DO 0 I=1,NDP
1670-400    WRITE(6,400)ALPHA(I),CL(I),CB(I),CDRC(I),CNTR(I)
1680-0      FORMAT(1H0,4X,F6.2,BX,F7.3,BX,F8.4,BX,F6.3,4X,F8.3)
1690        CONTINUE
1700-395    WRITE(6,395)
1710-390    FORMAT(1H0,4X,'POSITION OF CDRC FROM TRUN.')
1720        WRITE(6,390)X,V
1730        FORMAT(1H0,3X,'X= ',F15.7,BX,'V= ',F15.7,)
1740        STOP
            END
```

Data Reduction Program — Cont'd

75

RUN,FTN5

TITLE- 15-DEG BASIC PIN

MODEL SPECIFICATIONS:

REF-IN.	CBAR-IN.	B-IN.
7.800	7.800	14.781

SREF-SQ.FT.	VOL-CU.FT.	BETA-DEG.
1.030	.0000	0.0000

TUNNEL SPECIFICATIONS:

Q-PSF	DB-LBS	DWB-LBS	ALPHAO-DEG
25.5787	0.000	1.820	0.0000

DELAFA-DEG	AK1	TAU1	TAU5
.100	.0400	.300	.0800

RUN DATA: ALPHA-DEG,LOADS-LBS

RUN NO.	NO. POINTS	TEMP F	BAROIN. HG
8	14	81.50	29.189

REYNOLDS NO.- .5885E+06   MACH NO.- .135

ALPHA3	ZFVO	ZF5	ZFVO	BAO	DWO	D5
-4.00	46.65	36.58	81.30	19.58	18.16	80.06
-2.00	41.30	36.58	20.16	19.30	19.31	80.00
0.00	36.85	36.58	20.10	19.28	19.39	80.03
2.00	31.66	36.58	17.85	19.80	19.38	80.04
4.00	25.70	36.58	16.88	19.80	19.08	80.04
6.00	20.52	36.58	15.48	19.88	18.08	80.08
8.00	15.80	36.58	14.44	19.80	17.74	80.04
10.00	10.87	36.58	13.84	19.84	15.98	80.05
11.00	9.11	36.58	13.07	18.14	14.83	80.06
12.00	7.87	36.58	11.47	18.14	12.78	80.05
13.00	7.70	36.58	11.08	18.81	13.40	80.05
14.00	7.66	36.58	10.63	18.18	11.88	80.04
15.00	7.18	36.58	10.88	18.18	10.18	80.03
16.00	7.10	36.58	10.80	18.10	9.66	80.81

ENTER BCDBCL(4),

TITLE- 15-DEG BASIC PIN

RUN NO.- 8

REYNOLDS NO.- .5885E+06   MACH NO.- .135

ALPHA	CL	CD	CMAC	CNTR
-4.00	-.558	.0158	-.018	-.074
-1.99	-.118	.0077	-.007	-.034
0.00	-.013	.0065	.038	-.035
2.00	.148	.0064	.004	-.063
4.00	.306	.0141	.001	-.100
6.00	.413	.0141	.003	-.117
8.00	.537	.0447	.003	-.108
10.00	.710	.1086	-.018	-.186
11.05	.764	.1456	-.028	-.072
13.00	.766	.1671	-.041	-.056
14.00	.756	.1748	-.047	-.211
15.00	.756	.0841	-.065	-.267
16.00	.557	.0857	-.040	-.376
				-.335

POSITION OF CMAC FROM TRLM.

K= -.3480863   V= .0071768

STOP
27400 MAXIMUM EXECUTION FL.
.108 CP SECONDS EXECUTION EXECUTION TIME.

Sample Output

76

Appendix G

This appendix contains the remaining experimental data.
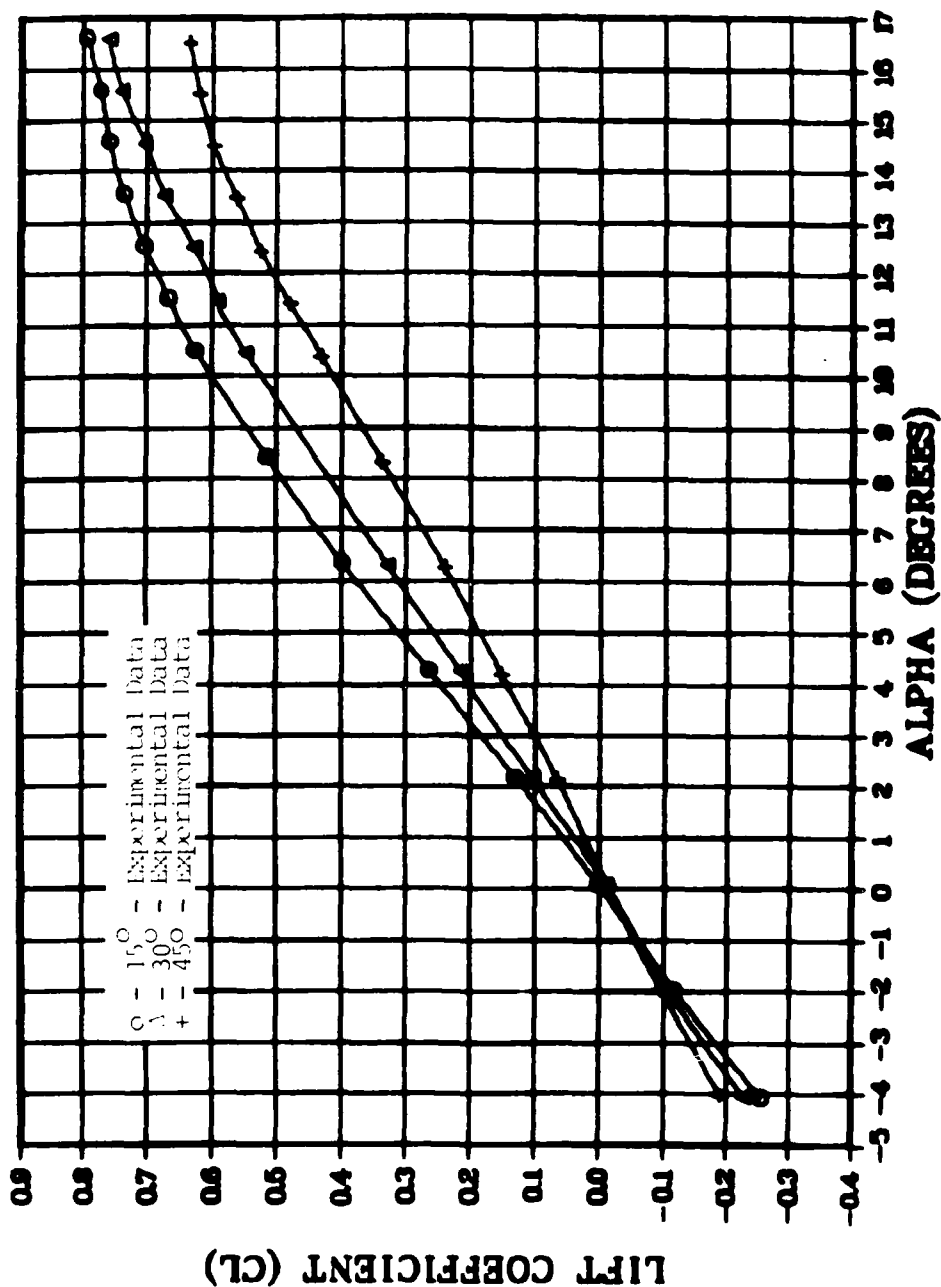
Fig. 17a. Lift Coefficient Versus Angle of Attack For Increasing
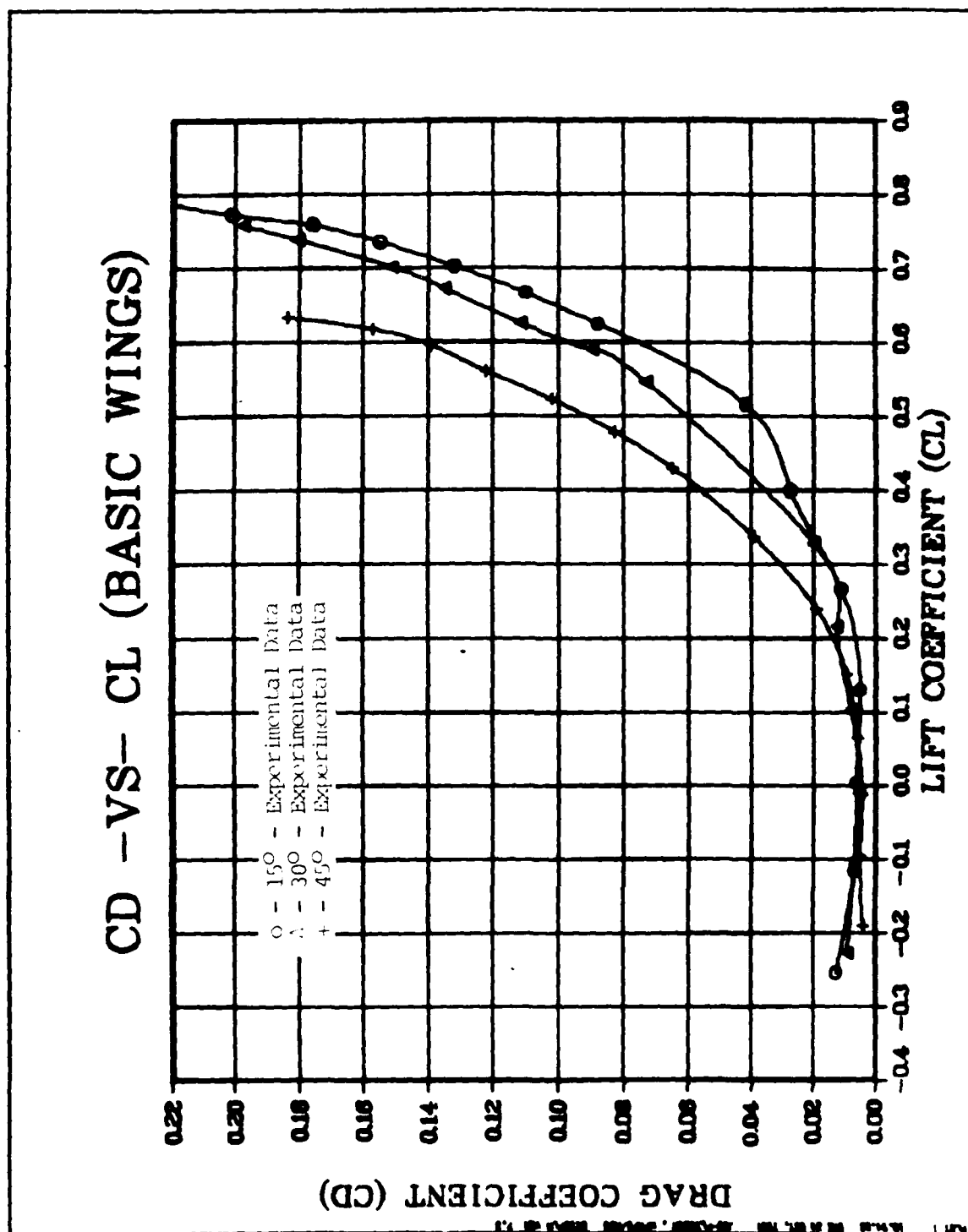Forward Sweep Angles (Basic Wings)

CD –VS– CL (BASIC WINGS)

o – 15° – Experimental Data
∆ – 30° – Experimental Data
+ – 45° – Experimental Data

LIFT COEFFICIENT (CL)

DRAG COEFFICIENT (CD)

Fig. 17b. Drag Coefficient Versus Lift Coefficient for Increasing
Forward Sw__ __ Angles (Basic Wings)

79
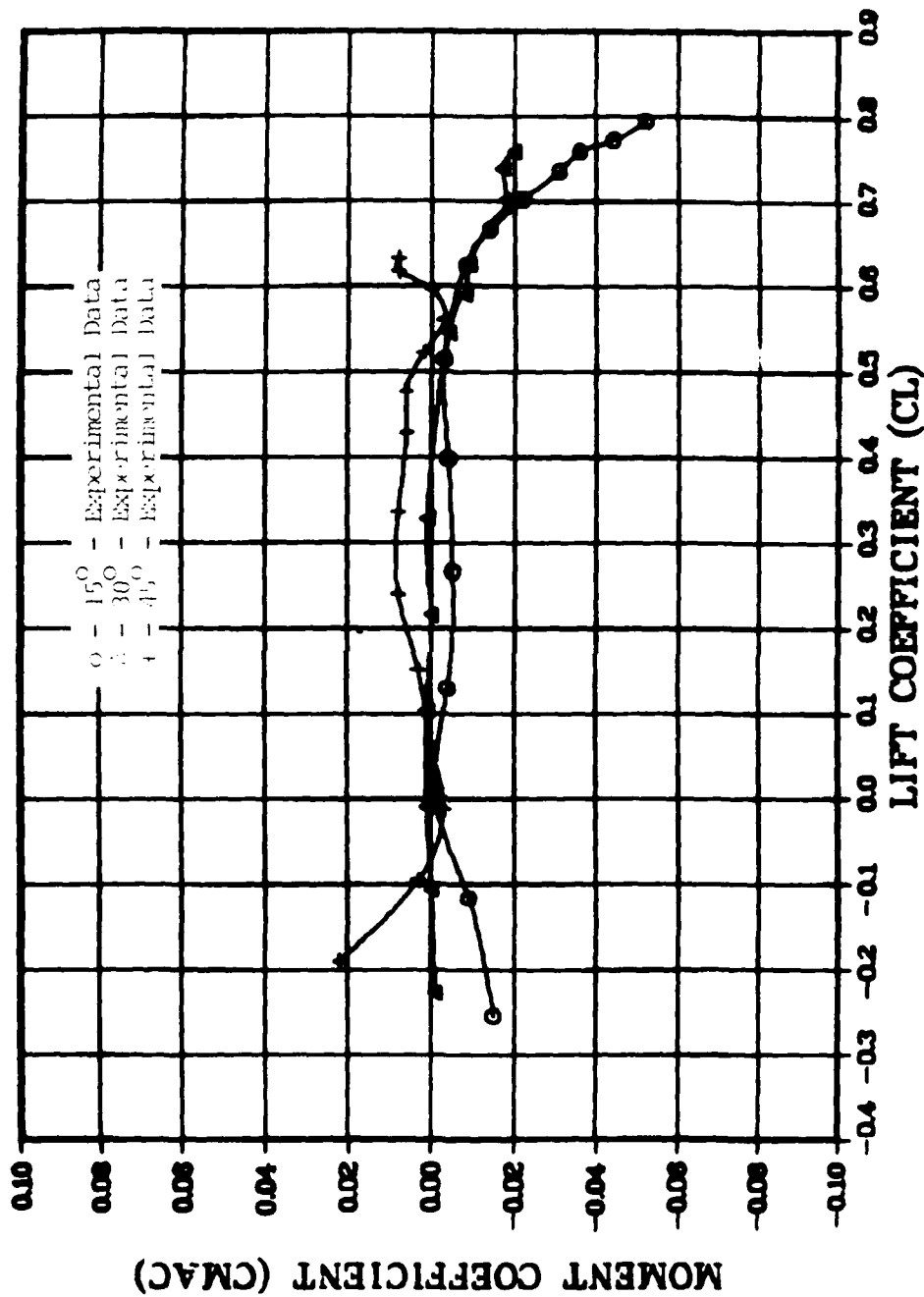
Fig. 17c. Moment Coefficient Versus Lift Coefficient for Increasing
Forward Sweep Angles (Basic Wings)

CL –VS– ALPHA (EXT-1)

o – 15° – Experimental Data
∆ – 30° – Experimental Data
+ – 45° – Experimental Data

ALPHA (DEGREES)

LIFT COEFFICIENT (CL)
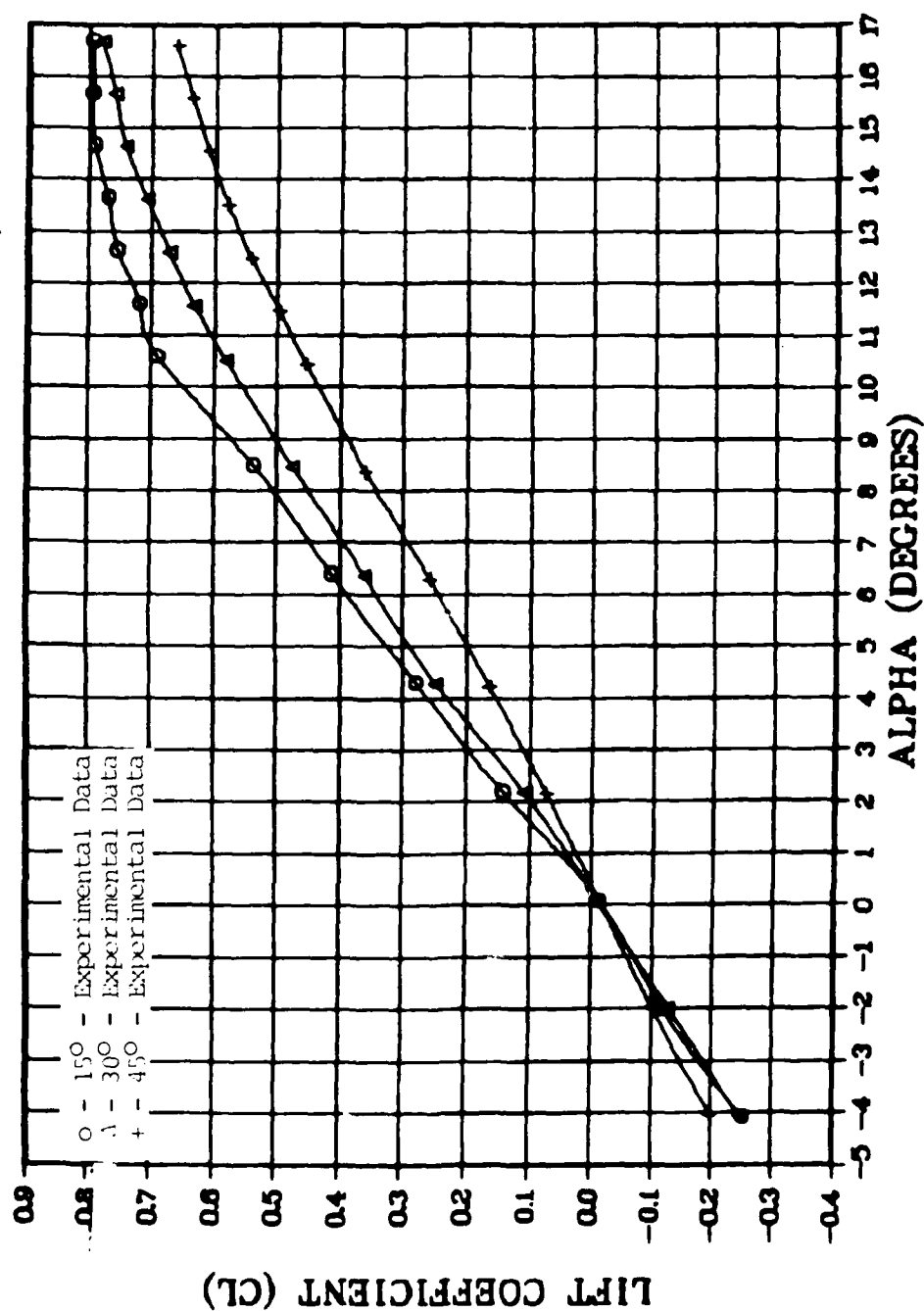
Fig. 18a. Lift Coefficient Versus Angle of Attack For Increasing Forward Sweep Angles (Extension-1 Mach 18)

CD –VS– CL (EXT–1)

LIFT COEFFICIENT (CL)

DRAG COEFFICIENT (CD)

○ – 15° – Experimental Data
△ – 30° – Experimental Data
+ – 45° – Experimental Data

Fig. 16d. Drag Coefficient Versus Lift Coefficient for Increasing Positive Sweep Angles (Extension–1 Model)

CMAC –VS– CL (EXT–1)

Legend (inside plot):
- ○ – 15° – Experimental Data
- △ – 30° – Experimental Data
- + – 45° – Experimental Data
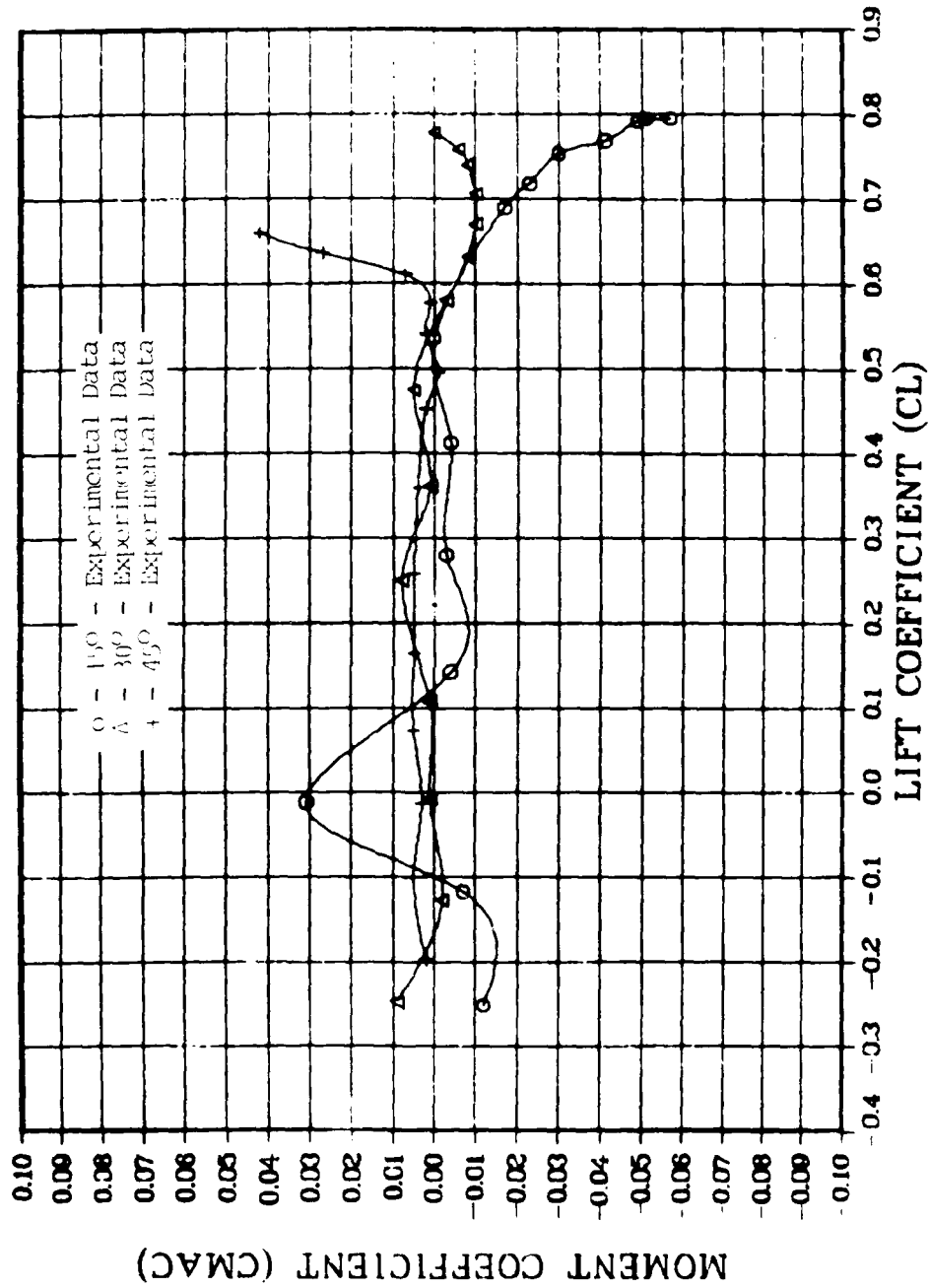
X-axis: LIFT COEFFICIENT (CL)
Y-axis: MOMENT COEFFICIENT (CMAC)

Fig. 18c. Moment Coefficient Versus Lift Coefficient For Increasing Forward Sweep Angles (Extension–1 Models)
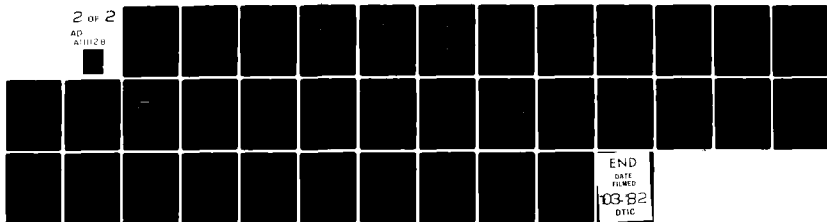
CL –VS– ALPHA (15 FSW)

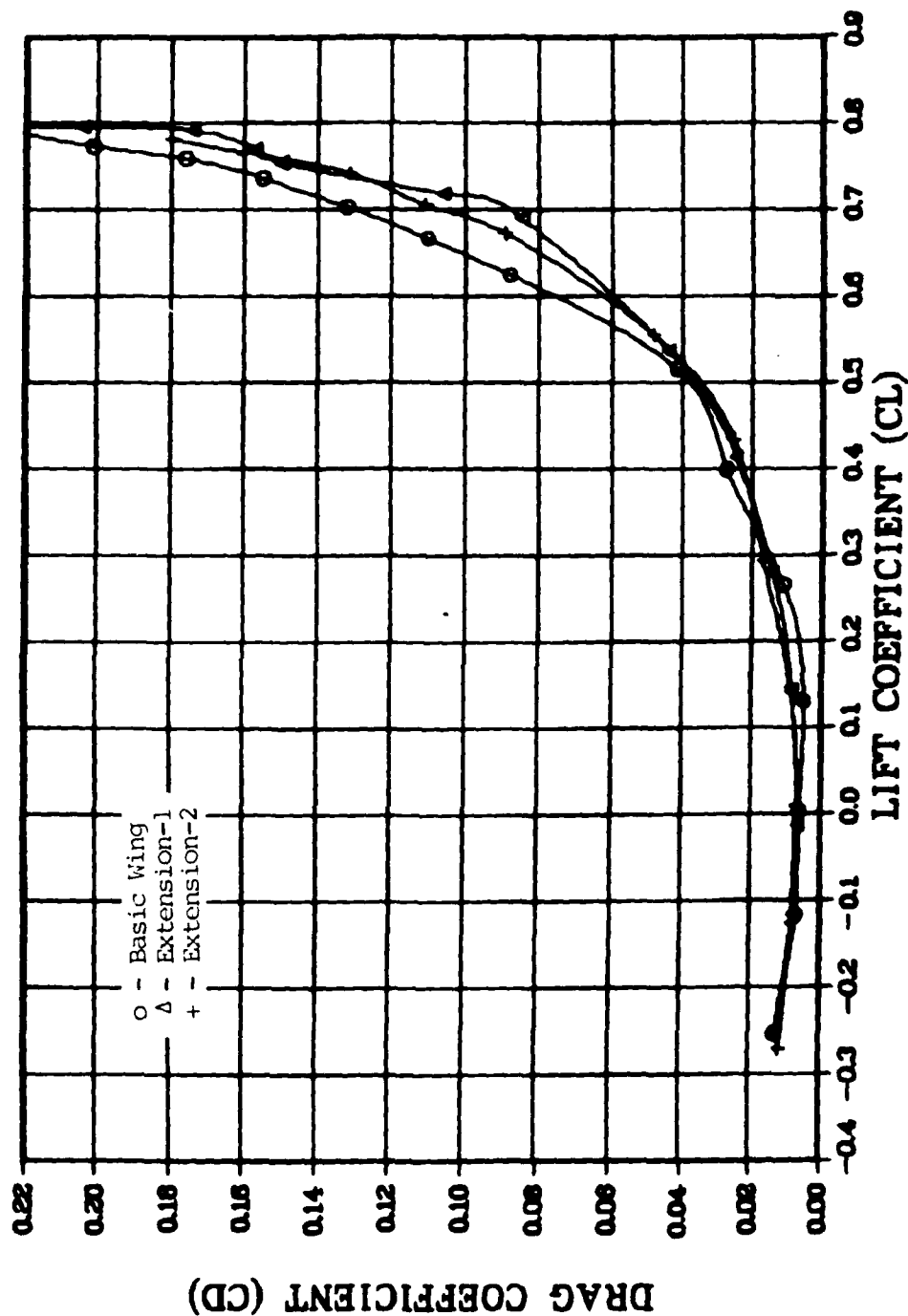Fig. 19a. Lift Coefficient Versus Angle of Attack For Increasing
Aspect Ratio (15 Degree Swept)

Fig. 19b. Drag Coefficient Versus Lift Coefficient For
Increasing Aspect Ratio (15 Degree Models)
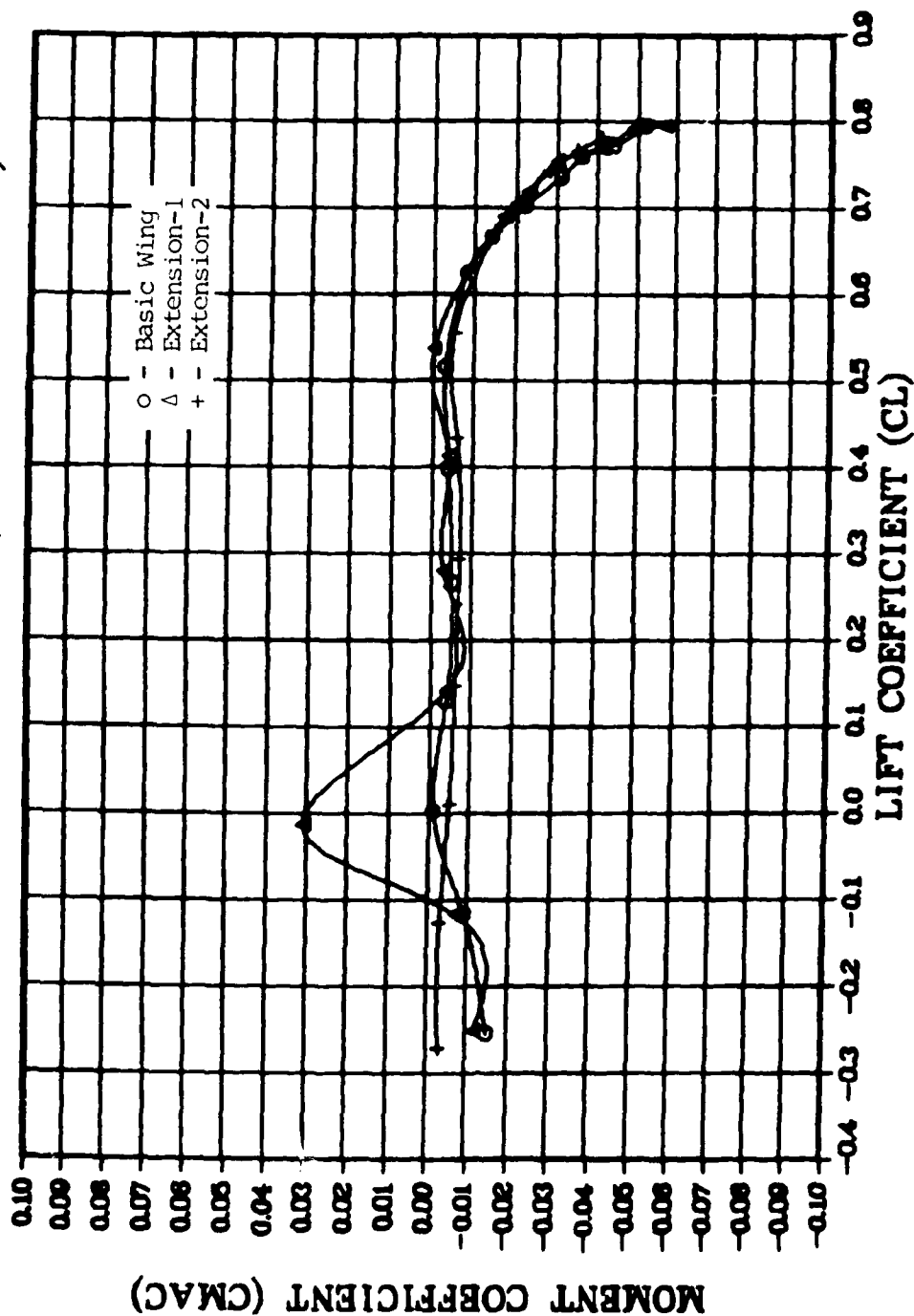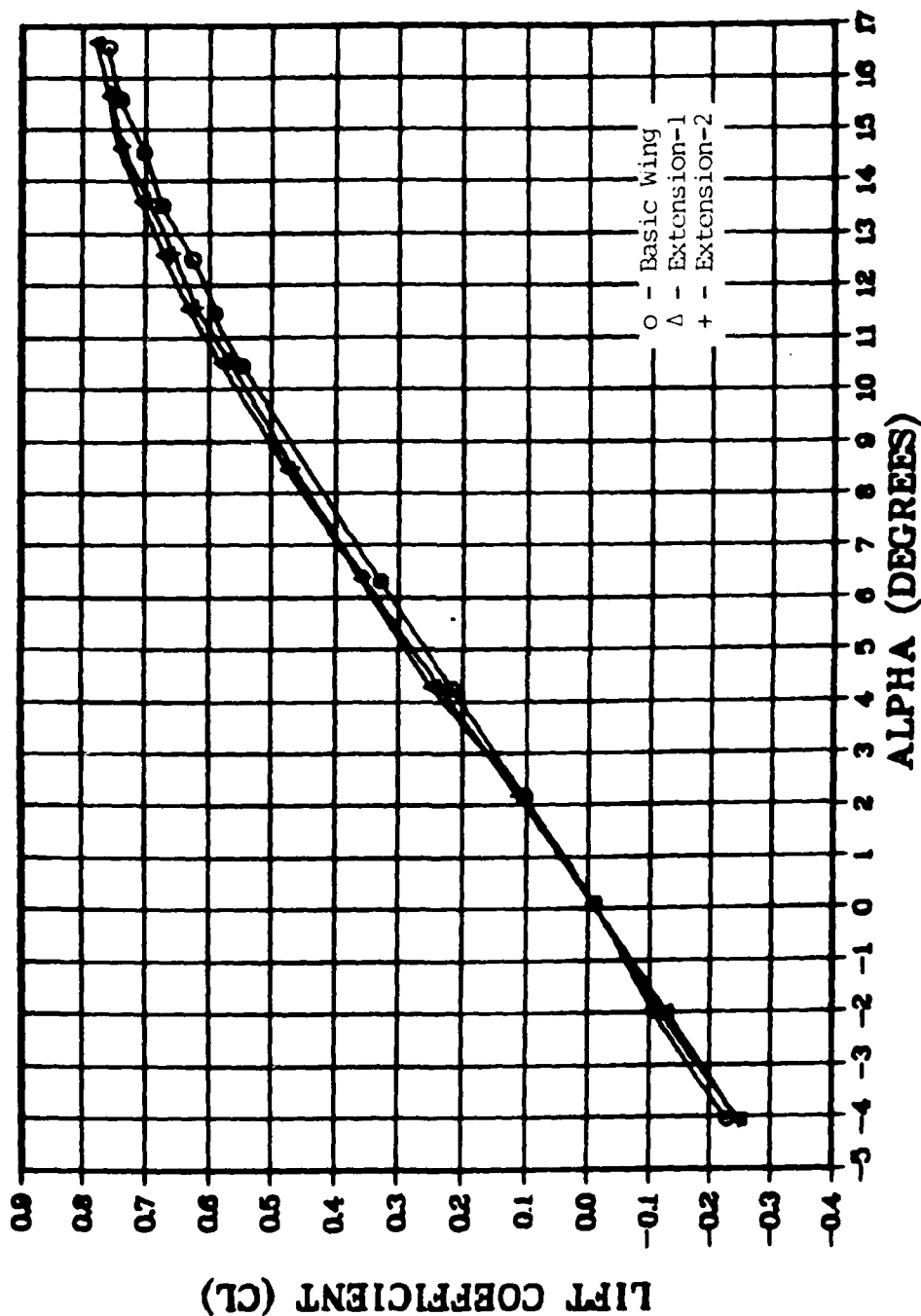
Fig. 19c. Moment Coefficient Versus Lift Coefficient For
Increasing Aspect Ratio (15 Degree Models)

Fig. 20a. Lift Coefficient Versus Angle of Attack For
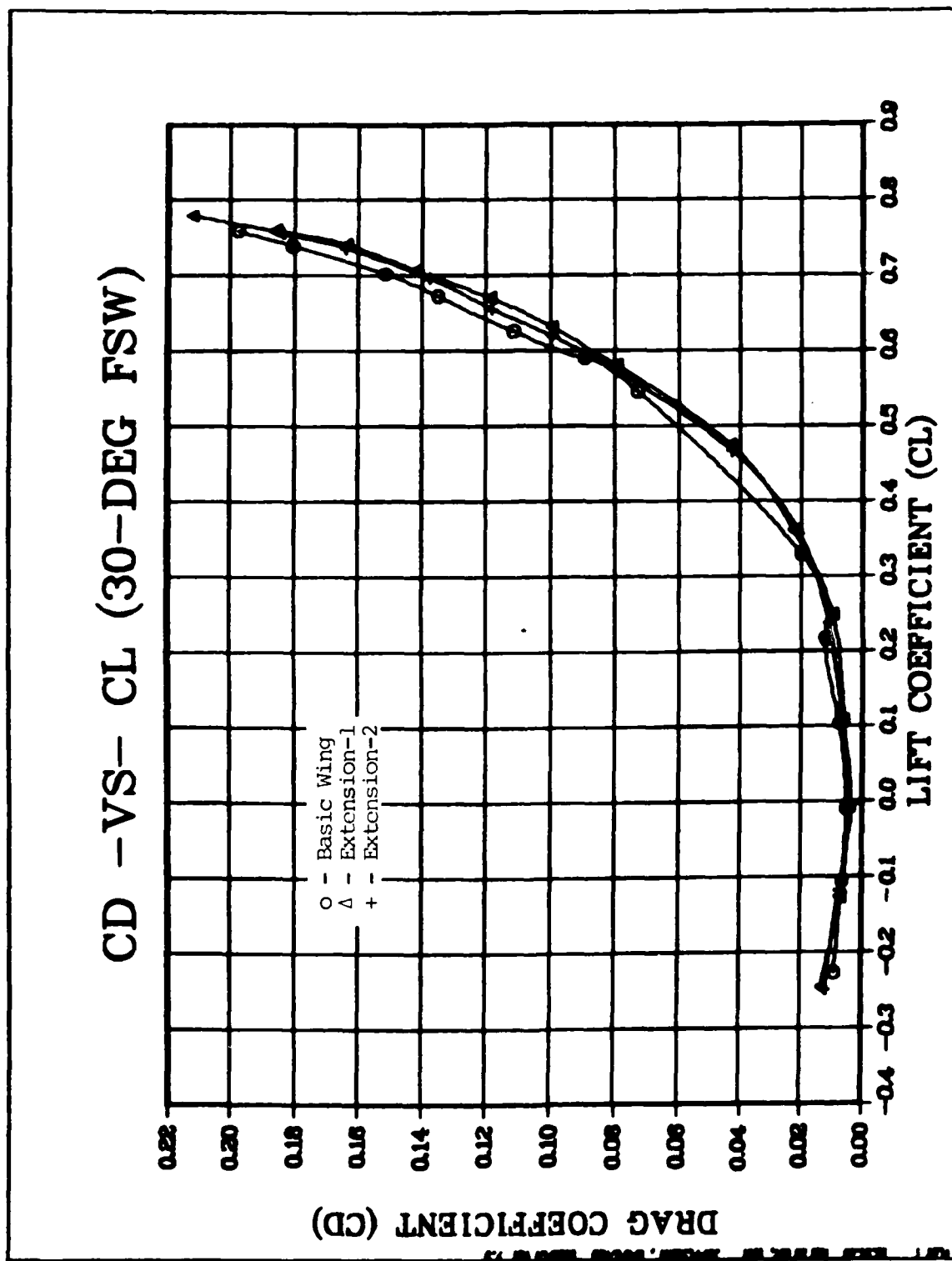Increasing Aspect Ratio (30 Degree Models)

CD -VS- CL (30-DEG FSW)

o - Basic Wing
Δ - Extension-1
+ - Extension-2

LIFT COEFFICIENT (CL)

DRAG COEFFICIENT (CD)

Fig. 20b. Drag Coefficient Versus Lift Coefficient For
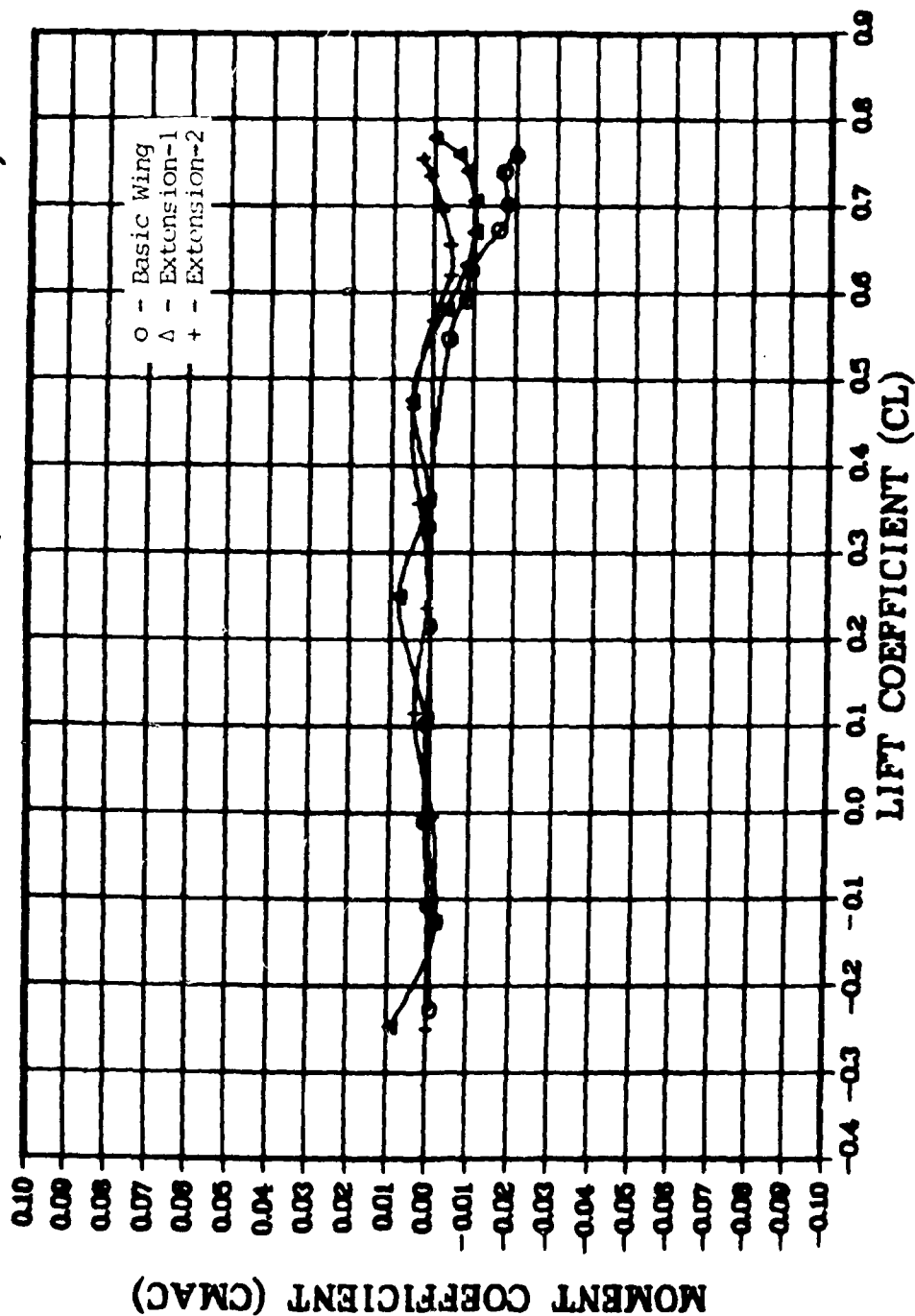Increasing Aspect Ratio (30 Degree Models)

88

Fig. 20c. Moment Coefficient Versus Lift Coefficient For
Increasing Aspect Ratio (30 Degree Models)

89

Appendix H

LACBIN Inputs and Geomerty

This appendix contains a variable definition, sample input tape and an
output listing for the empirically based performance prediction program
LACBIN, that was used for comparison to the experimental data.

This program was run interactively using NAMELIST input data, described
on page 24, Ref 6. The program must be run with a body (fuselage).
Therefore a small hump was added to the centerline of essentially a flying
wing (Figs 21 and 22). Friction drag for this hump was held to zero.
However, a small amount of interference drag could not be avoided. But this
quantity was an output of the program, hence its value was known.

The program was run for 18 configurations. Nine forward sweep angles
which matched each of the wind tunnel models and extensions and nine aft
sweep angles which also matched the models except for sweep angle.

NAMELIST Variables

Geometric values for forward and aft swept wings are described in
Figs 21 and 22.

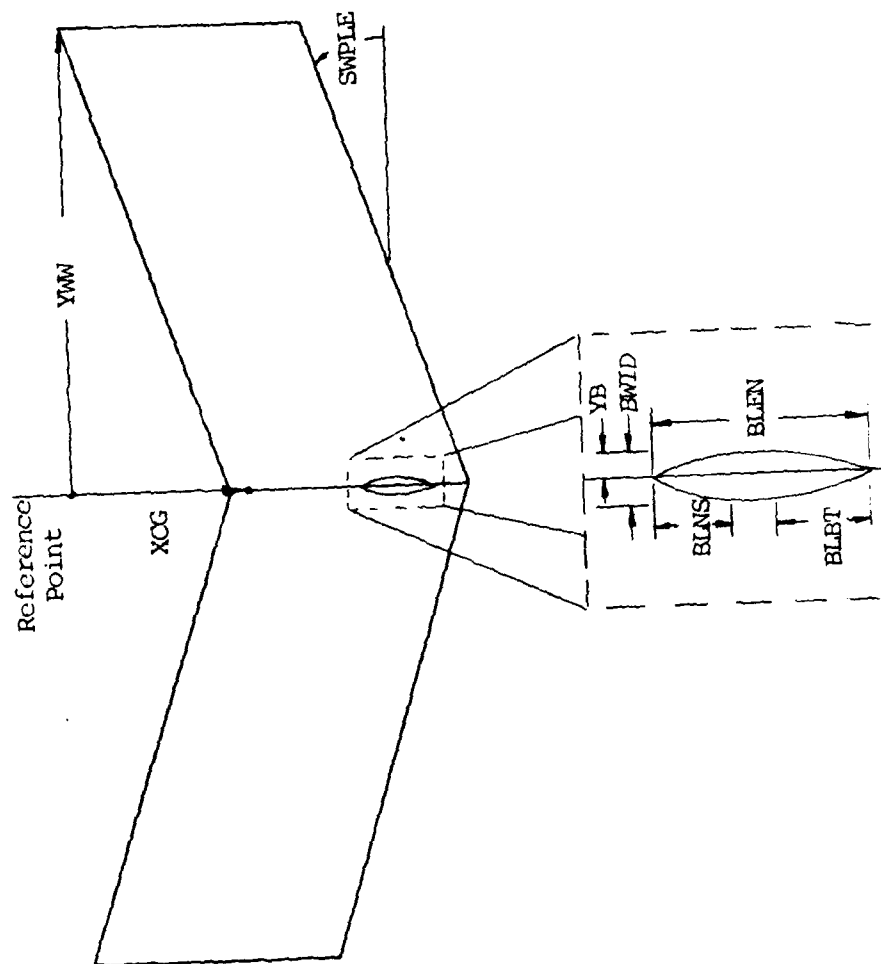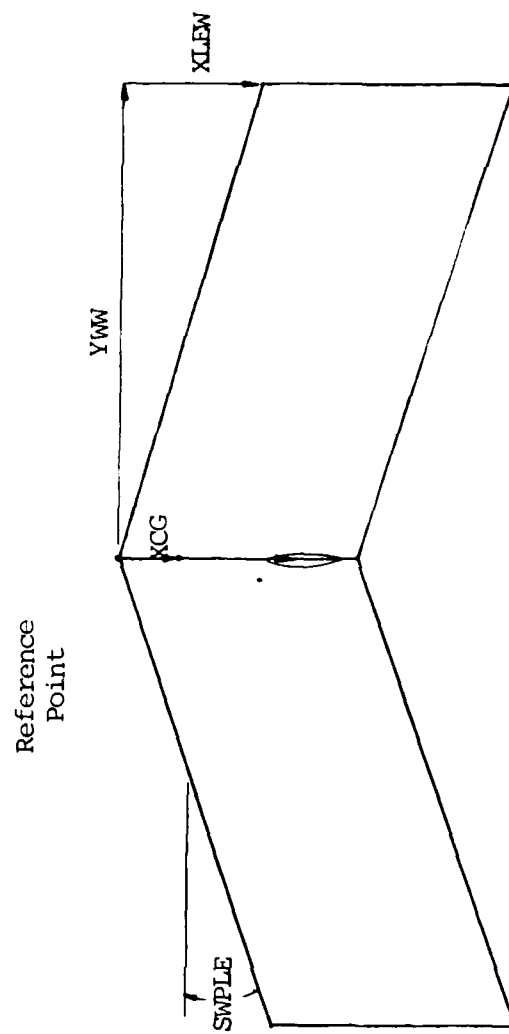| NAMELIST	Variable	Description
BODYS		Body Configuration(s)
	NBODYS	Total number of body tyupes used to represent the configuration – 1 used
	NNACS	Total number of nacelles used to represent the configuration – 0 used
	NSURFS	Total number of airfoil surfaces used to represent the confuration – 1 used
	IWSP	Variable swee indicator – 0-fixed wing geometry

Fig.21. Forward Sweep Geometry Model

Fig. 22. Aft Sweep Geometry Model

92

NAMELIST	Variable	Description
	NSURFS	Number of wing panels to represent wing surface – 1 used
	XCG	Fuselage station for moment reference point – default to MAC
	BLEN	Body length (in.)
	BWID	Body width (in.)
	BGHT	Body height (in.)
	BLNS	Nose length (in.)
	BLBT	Boattail length (in.)
NACEL		Nacelle configuration
	NNACS	Number of nacelles to be described
WING		Wing configuration parameters
	NSURFS	Total number of airfoil surface used to represent the wing – 1 used
	ISWP	Variable sweep indicator 0 used
	NPNLS	Number of wing panels to represent wing surface – 1 used
	AR	Aspect ratio
	TAPR	Taper ratio – 1 used
	SWPLE	Leading edge sweep (deg)
	SPLAN	Wing planform area (ft^2)
	TWIST	Wing twist (deg) – 0 used
	WINC	Wing incidence relative to fuselage line (deg) – 0 used
	TW	Type of wing section see Ref 6 page 26
	CAM	Wing chamber – 0 used
	TOC	Wing thickness – .06 used
	SREF	Reference area, same as SPLAN

NAMELIST	Variables	Description
	XLEW	X-position of point on wing leading edge (measurement from reference axis in inches)
	YWIW	Y-position of point on wing leading edge (measurement from reference axis in inches)
	YB	Y-distance of intersection of wing with fuselage (measured from reference axis in inches)
	SWMT	Sweep angle of mean thickness (deg)
	XCG	Moment reference position (measured from reference axis in inches)
	CONCL	Wing conical camber design C_L
SURFS		Other surface description
	NHT	Number of horizontal surfaces – used
	NVT	Number of vertical surfaces 0 – used
SURV		Data parameters list
	NSURV	Number of lift, drag and moment surveys – 1 used
	NCLAS	Number of evenly spaced C_L values in survey
	FMSURV(I)	Mach number for survey. $I = 1$ for this study
	CLLO(I)	Lowest C_L value for the survey condition
	CLHI(I)	Highest C_L value for the survey
	IT(1)	Transition location indicator, first survey, 1 used
	TRU(J, K3)	Transition location on upper surface of panel K3 (K3=1, NPLNS), J=1
	TRL(J, K3)	Transition location on lower surface of panel K3

NAMELIST	Variables	Description
STOL		STOL parameters
	IHLS	High lift system descriptor - used.
ADJUST		Aerodynamic variable input
	IVAL(1)	Adjust C_M as a function of Mach number - $C_M = 0$ used

The following is a typical input tape, and output of interest.

```
100-TEST IS FSU EXT-1
110-1
120-NAMELIST INPUT
130-GEOMS   NGOMS=1,BLEN(1)=3,
140-        BWID(1)=.85,BMAT(1)=.85,BLNB(1)=1.4,
150-        BASE(1)=0.,BLBT(1)=1.48
160-        NMMCS=00
170-BMMCEL  IGRP=0,NPML=1,AR=4.38,TAPR=1.,SMPLE=-18.,
180-SUTMO   SPLAN=1.83,SREF=1.83,TUIST=0.,UINC=0.,
190-        TU=11.,CAN(1)=0.,TOC(1)=.05,
200-        XLEU=0,YAW=15.,YP=185,SWA=-15.,
210-        XCO=4.27,CONC=-6.6
220-BSURFS  NSURFS=1,NAT=0,NUT=00
230-BSURU   NSURU=1,NHLSU=0,FMBUR U(1)=.135,
240-        ALT(1)=180.,CLLO(1)=180.,CLWI(1)=18.9,
250-        NCLAS=225
260-SSTOL   IHLS=05
270-SADJUST IVAL(1)=29208
280-END
```

Sample Input

Appendix I

This appendix contains the remaining computer program comparisons.

CL —VS— ALPHA (PROG. COMP)

15 - DEG BASIC WING
○ Experimental Data
—·— Neg. Sweep Angle (FSW)
——— Pos. Sweep Angle (ASW)
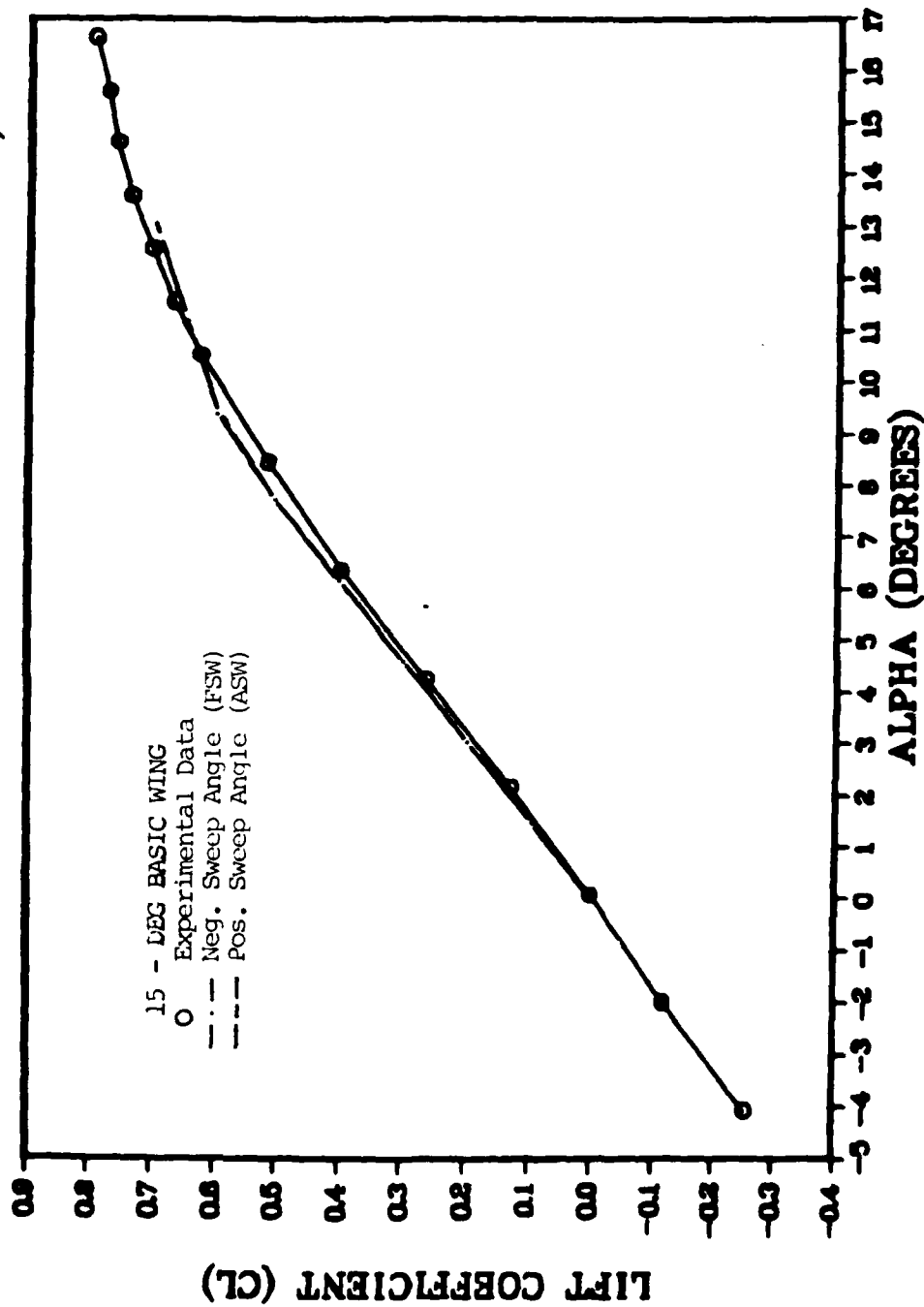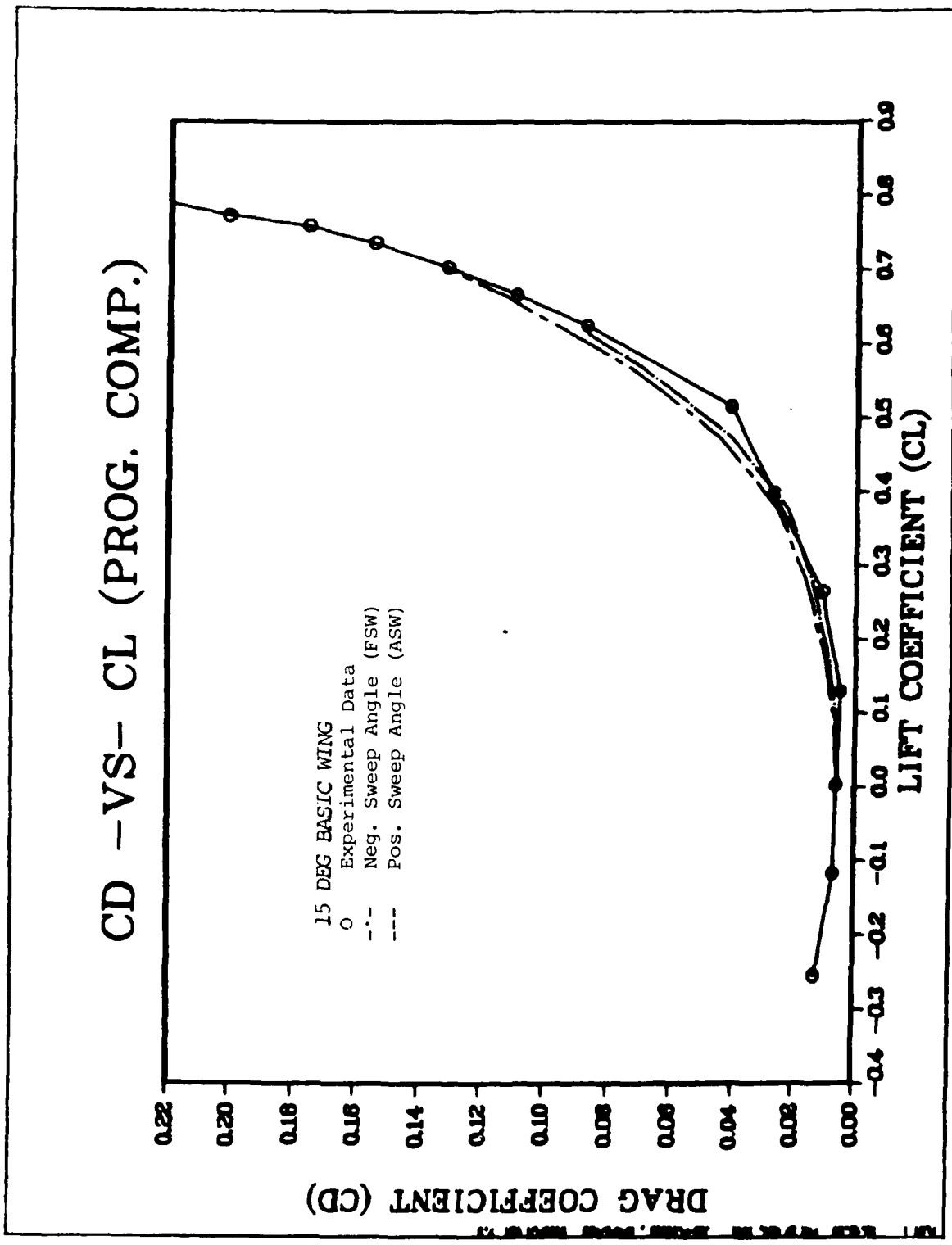
LIFT COEFFICIENT (CL)

ALPHA (DEGREES)

Fig. 23a. Program Comparison of Lift Coefficient Versus Angle of Attack For the 15 Degree Basic Model

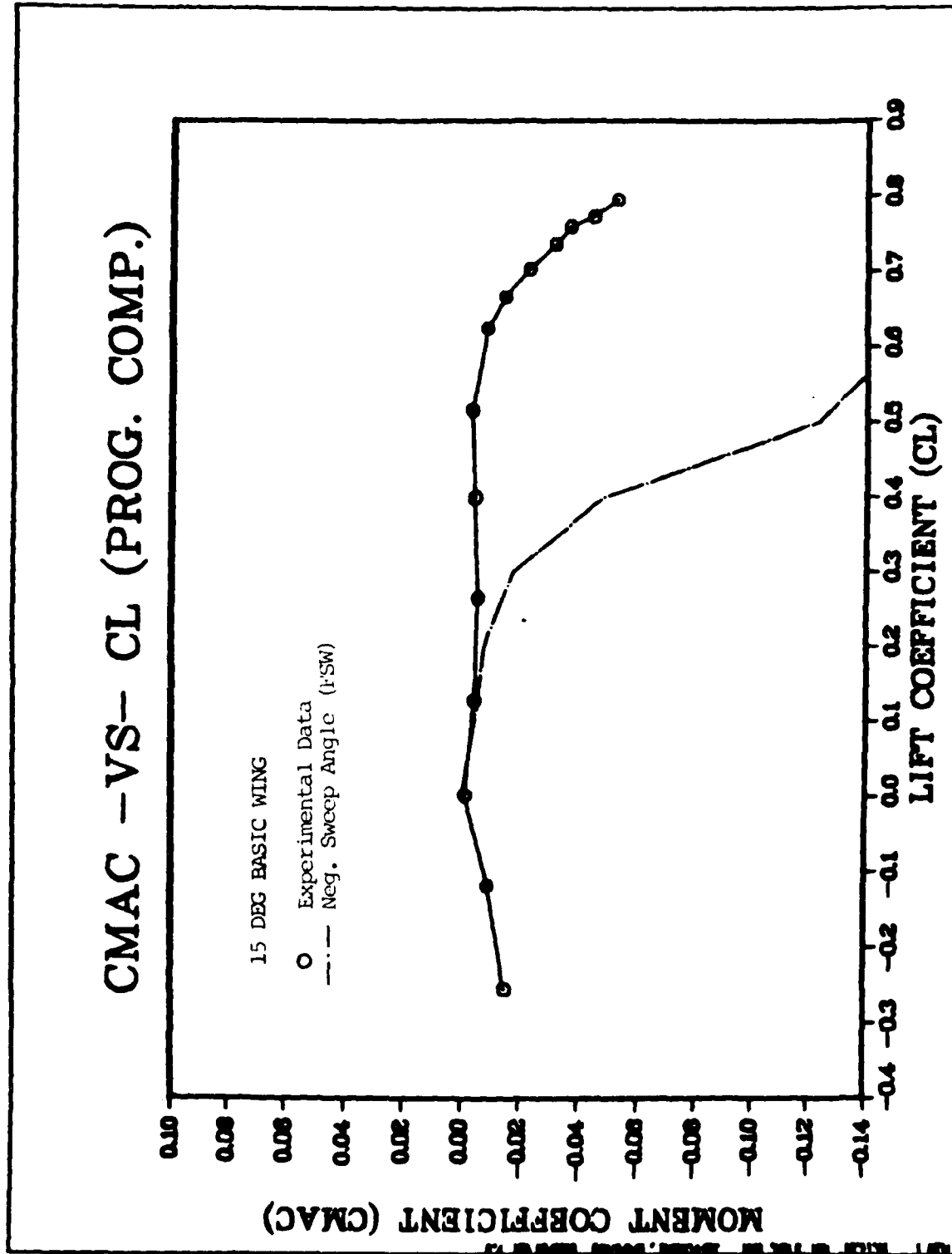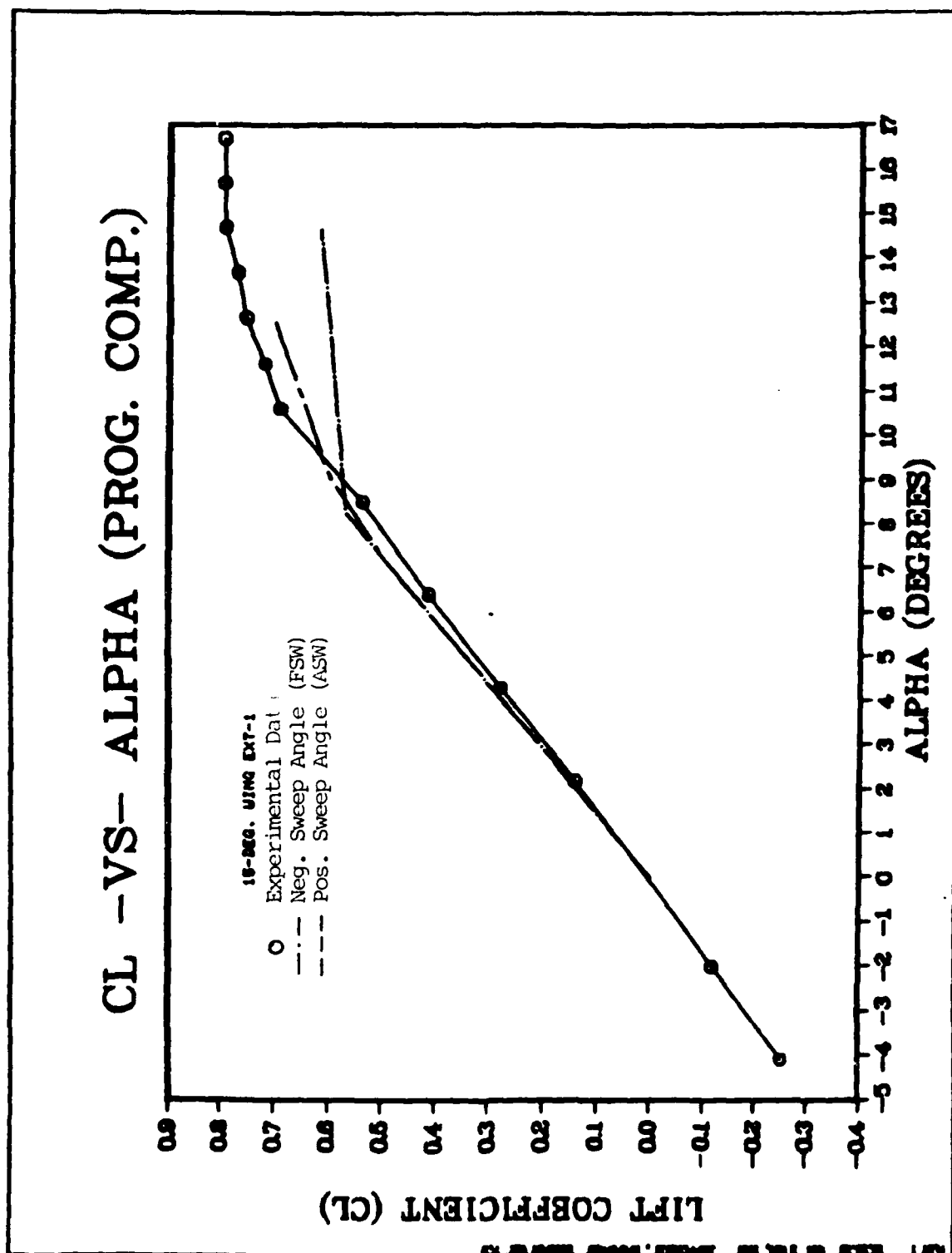Fig. 23b. Program Comparison of Drag Coefficient Versus Lift Coefficient for the 15 Degree Basic Model

101

CMAC —VS— CL (PROG. COMP.)

15 DEG BASIC WING

o   Experimental Data
—·— Neg. Sweep Angle (r·SW)

LIFT COEFFICIENT (CL)

MOMENT COEFFICIENT (CMAC)

Fig. 23c.   Program Comparison of Moment Coefficient Versus Lift Coefficient For the 15 Degree Basic Model

102

Fig. 24a. Program Comparison of Lift Coefficient Versus Angle of Attack for the 15 Degree Extension-1 Model
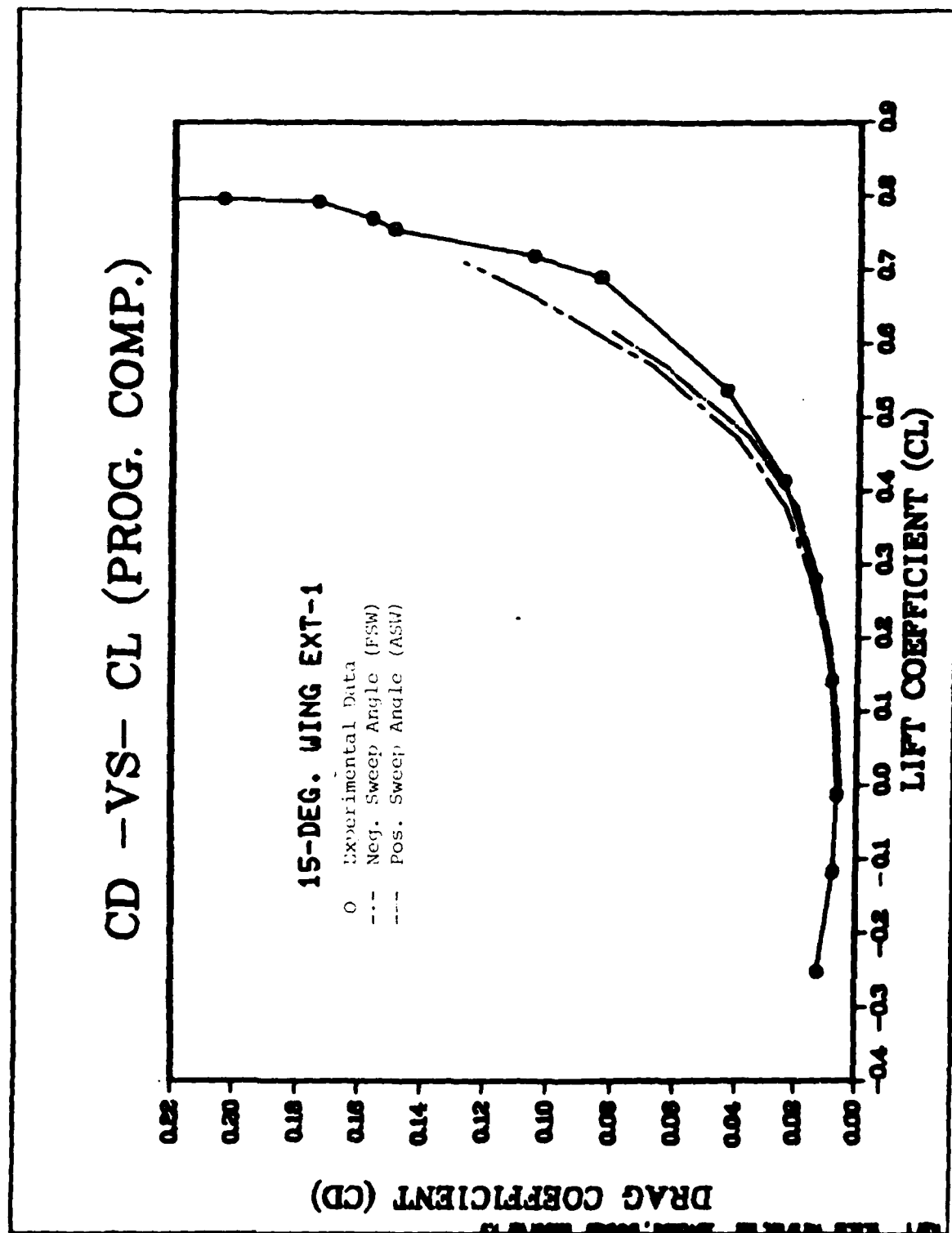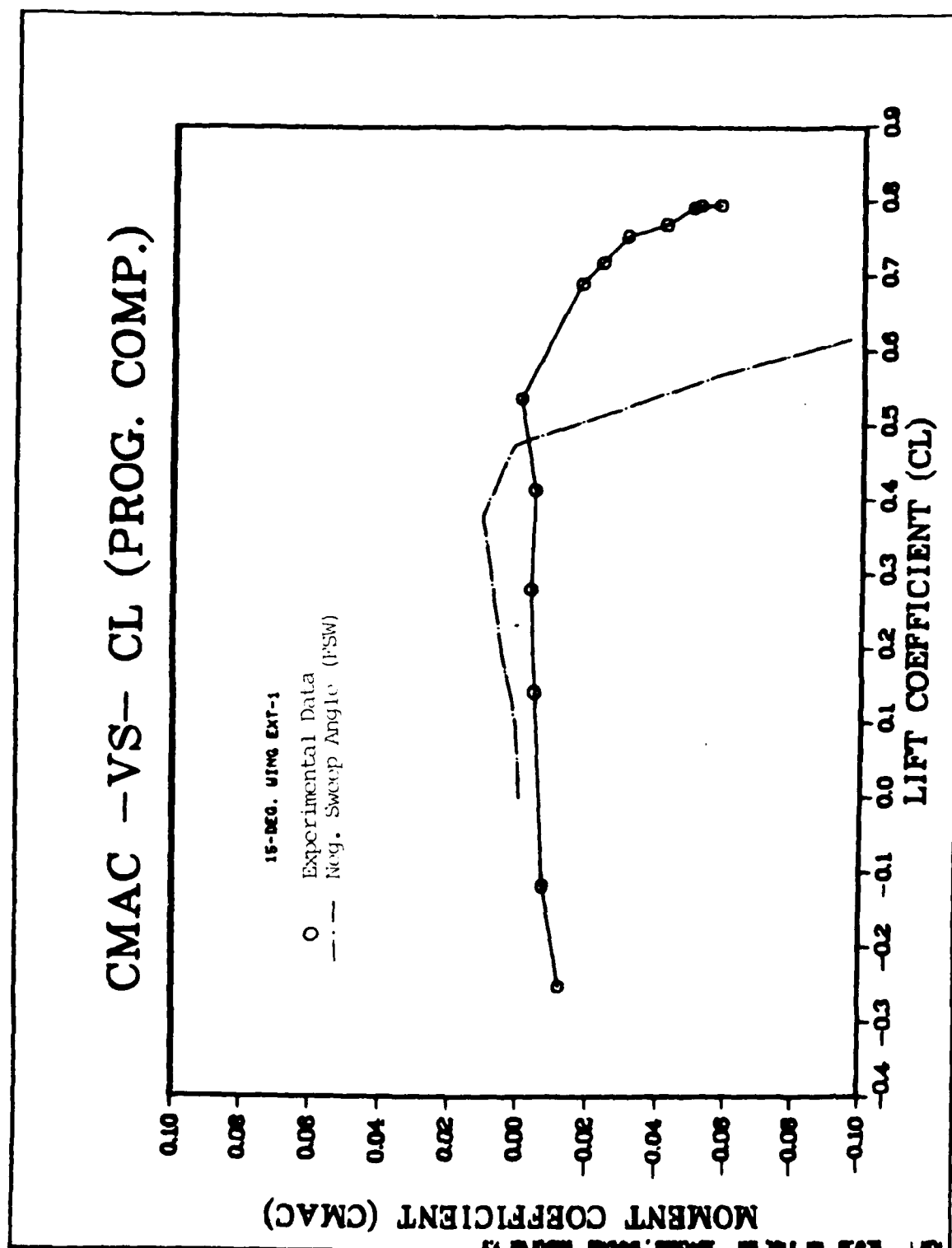
CD -VS- CL (PROG. COMP.)

15-DEG. WING EXT-1

O   Experimental Data
-·- Neg. Sweep Angle (FSW)
--- Pos. Sweep Angle (ASW)

Fig. 24b. Program Comparison of Drag Coefficient Versus Lift Coefficient For the 15 Degree Extension-1 Model

104

CMAC —VS— CL (PROG. COMP.)

Fig. 24c. Program Comparison of Moment Coefficient Versus Lift Coefficient For the 15 Degree Extension-1 Wing-1
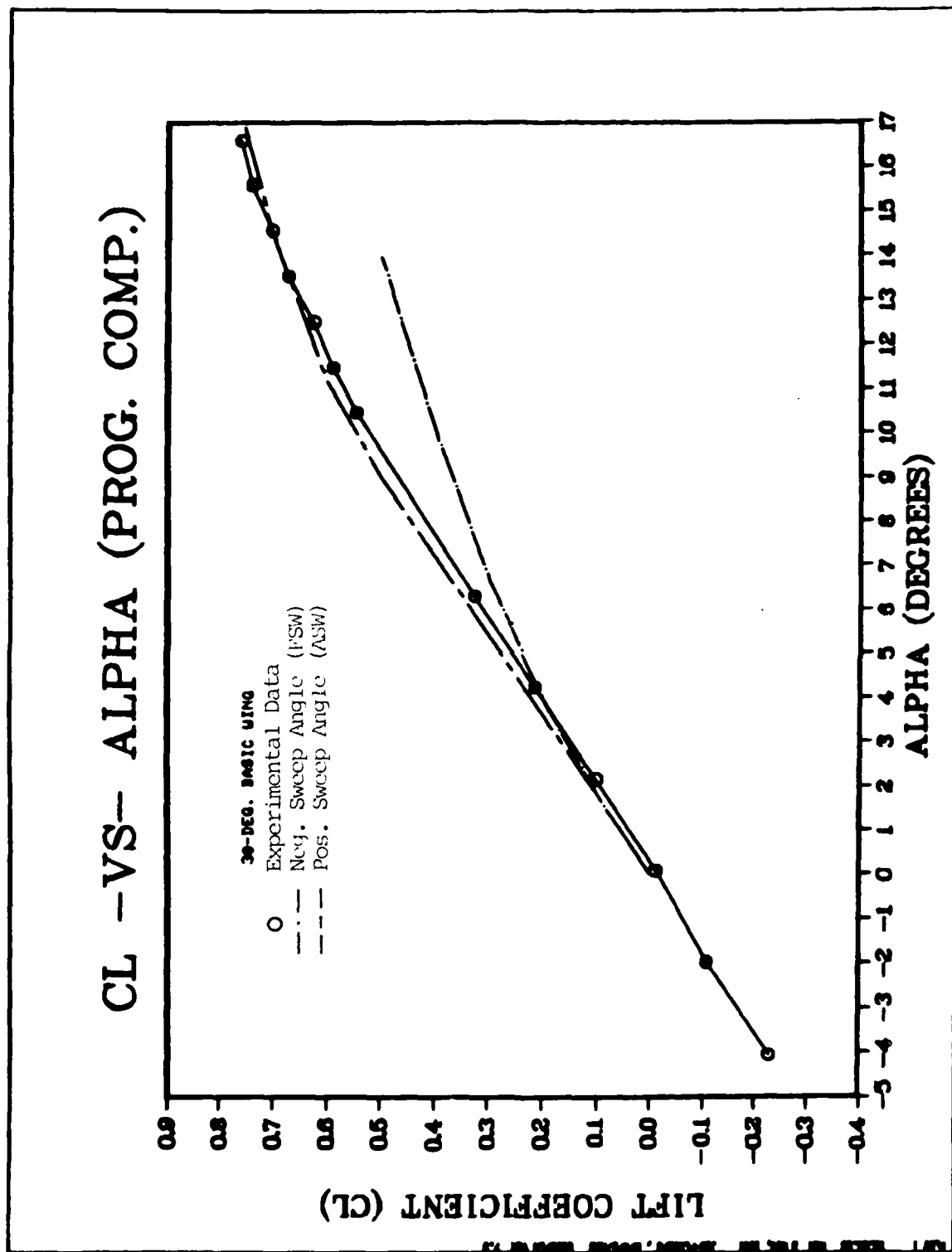
CL —VS— ALPHA (PROG. COMP.)

Fig. 75a.   Program Comparison of Lift Coefficient Versus Angle of Attack For the 30 Degree Basic Model
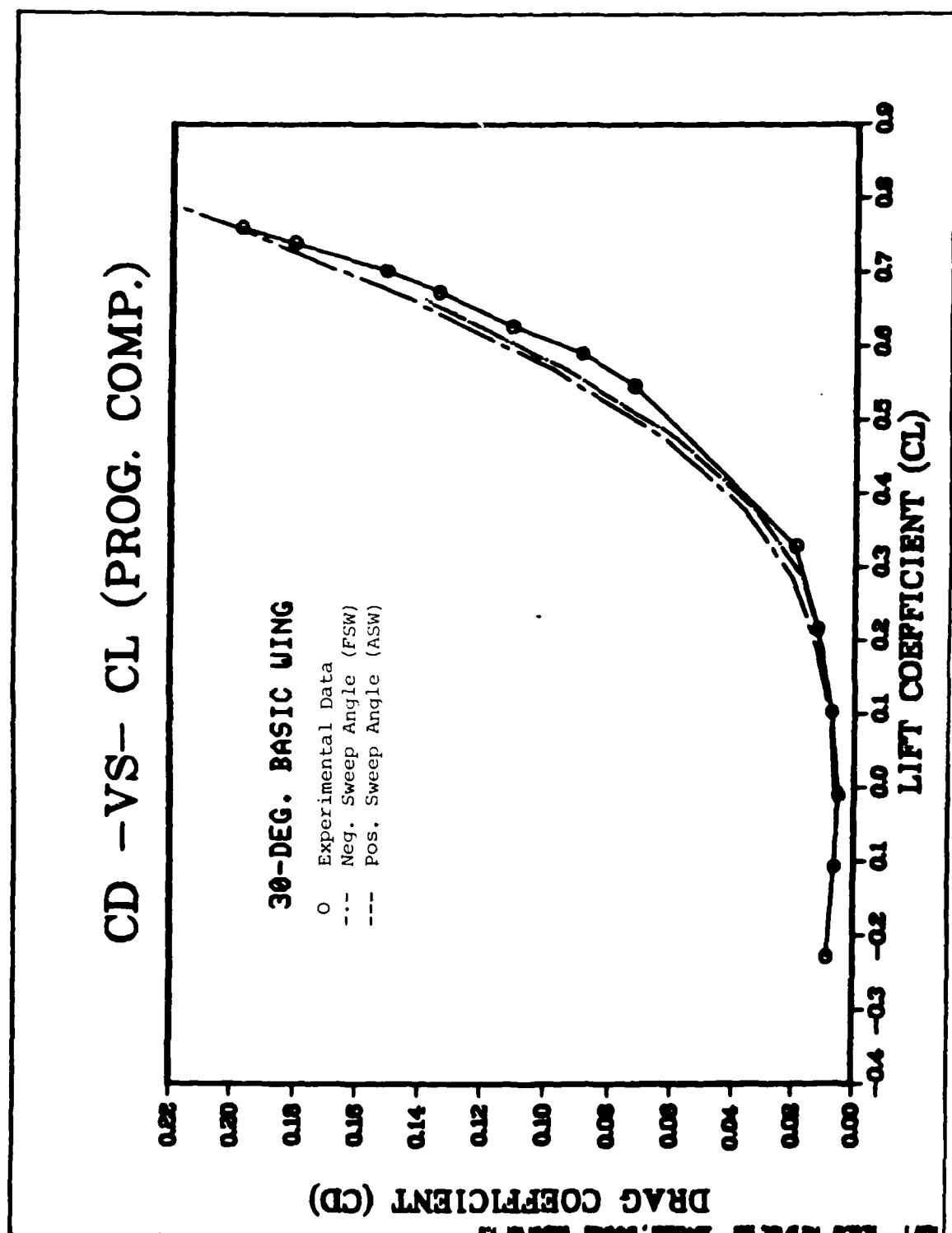
Fig. 25b. Program Comparison of Drag Coefficient Versus Lift Coefficient for the 30 Degree Basic Model
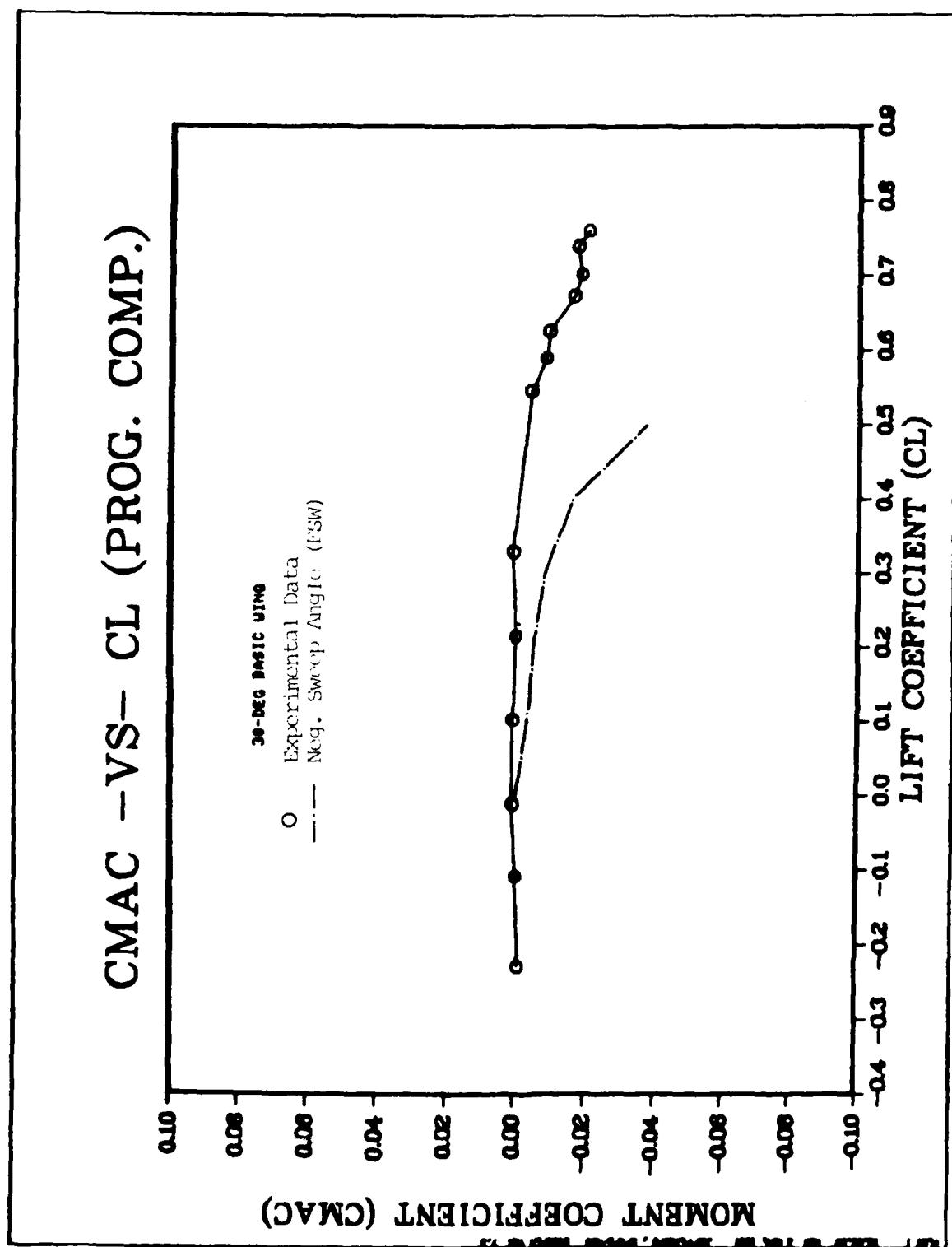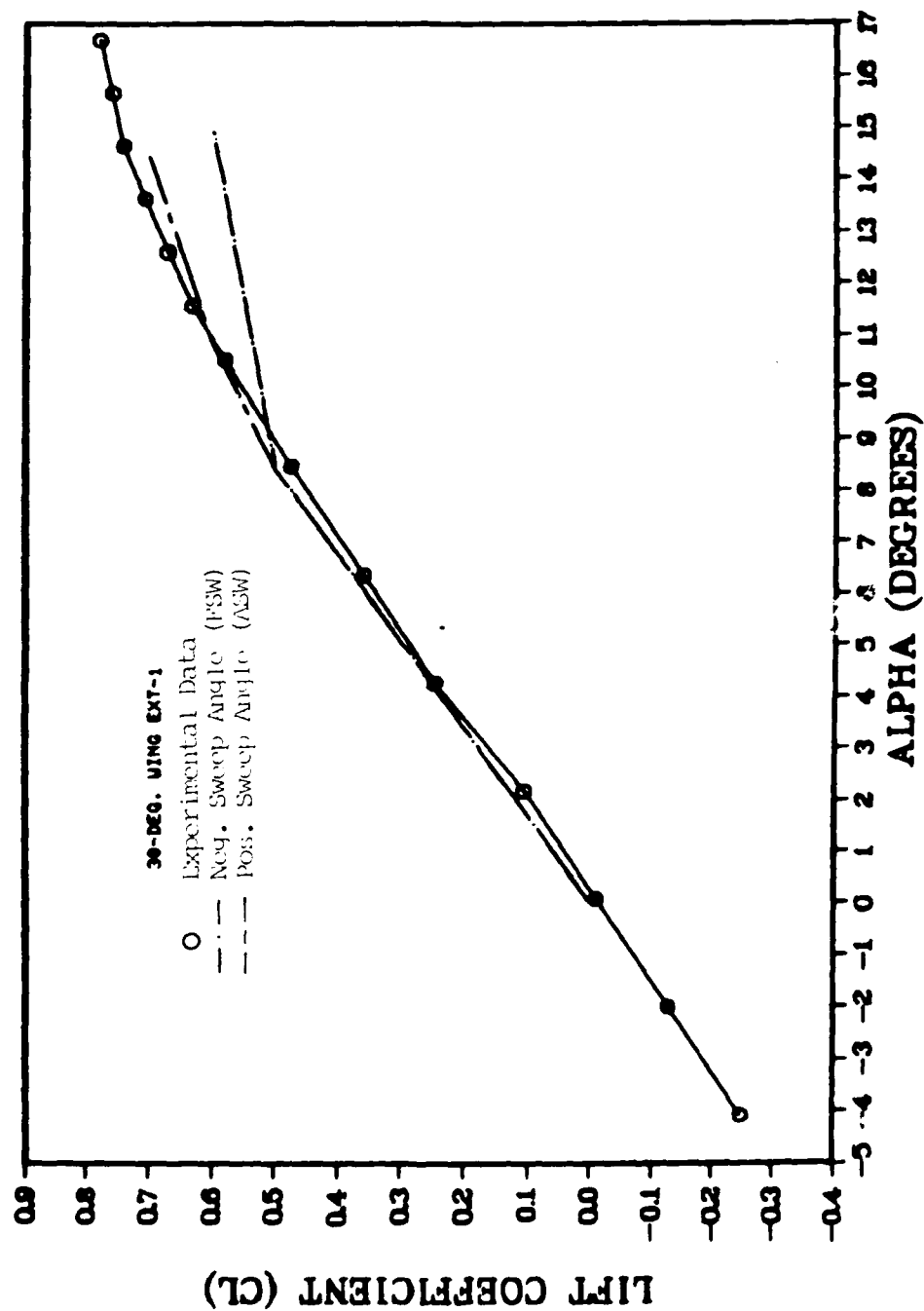
107

CMAC −VS− CL (PROG. COMP.)

30-DEG BASIC WING

O   Experimental Data
−·− Neg. Sweep Angle (FSW)

MOMENT COEFFICIENT (CMAC)

LIFT COEFFICIENT (CL)

Fig. 25c. Program Comparison of Moment Coefficient Versus Lift Coefficient For the 30 Degree Basic Model

CL –VS– ALPHA (PROG. COMP.)

LIFT COEFFICIENT (CL)

ALPHA (DEGREES)

30-DEG. WING EXT-1

O   Experimental Data
─·─ Neg. Sweep Angle (FSW)
─ ─ Pos. Sweep Angle (ASW)

Fig. 26a. Program Comparison of Lift Coefficient Versus Angle of Attack For the 30 Degree Extension–1 Wing.

CD –VS– CL (PROG. COMP.)

30-DEG. WING EXT-1

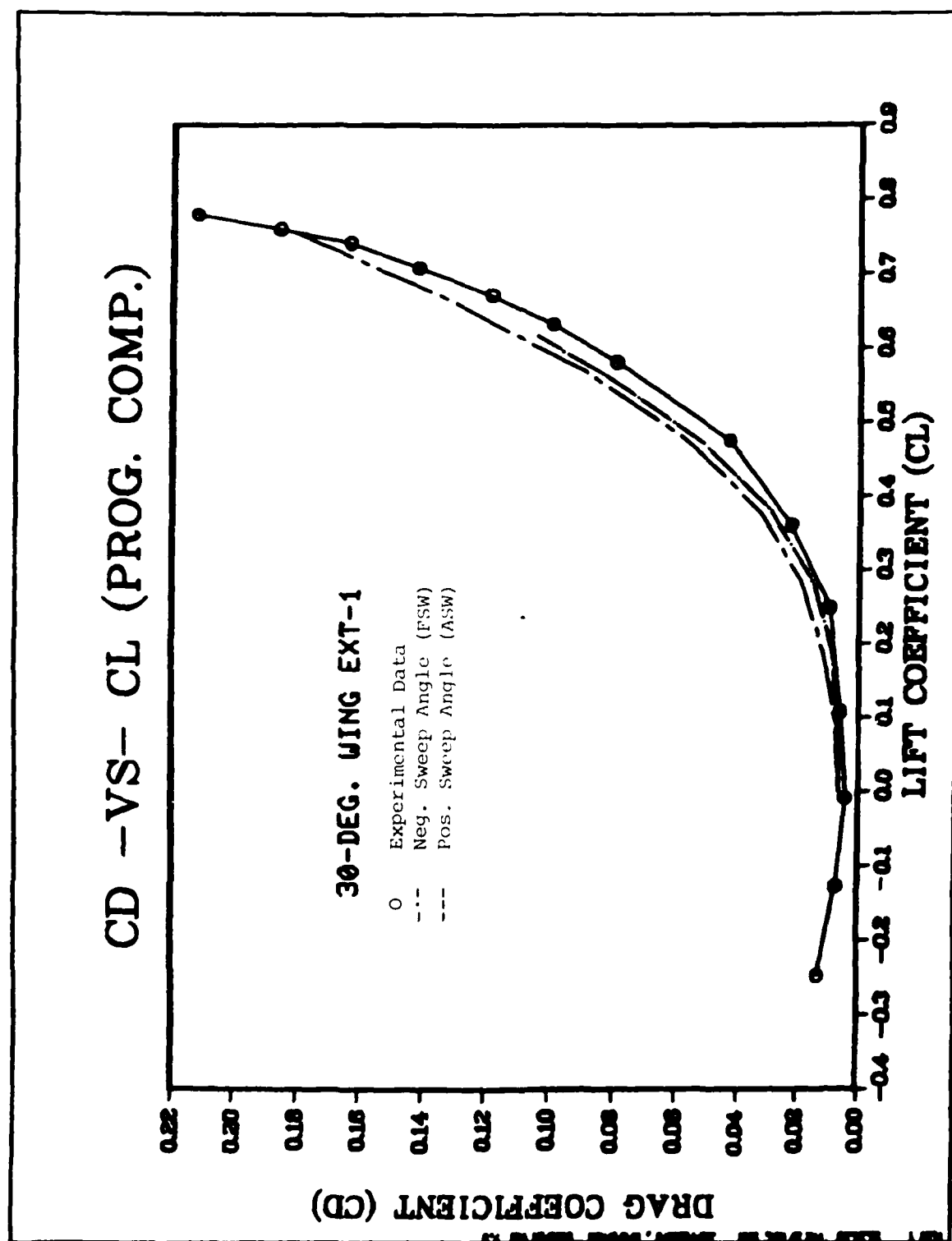|	
O	Experimental Data
–·–	Neg. Sweep Angle (FSW)
–––	Pos. Sweep Angle (ASW)

LIFT COEFFICIENT (CL)

DRAG COEFFICIENT (CD)

Fig. 26b.   Program Comparison of Drag Coefficient Versus Lift Coefficient For the 30 Degree Extension-1 Model
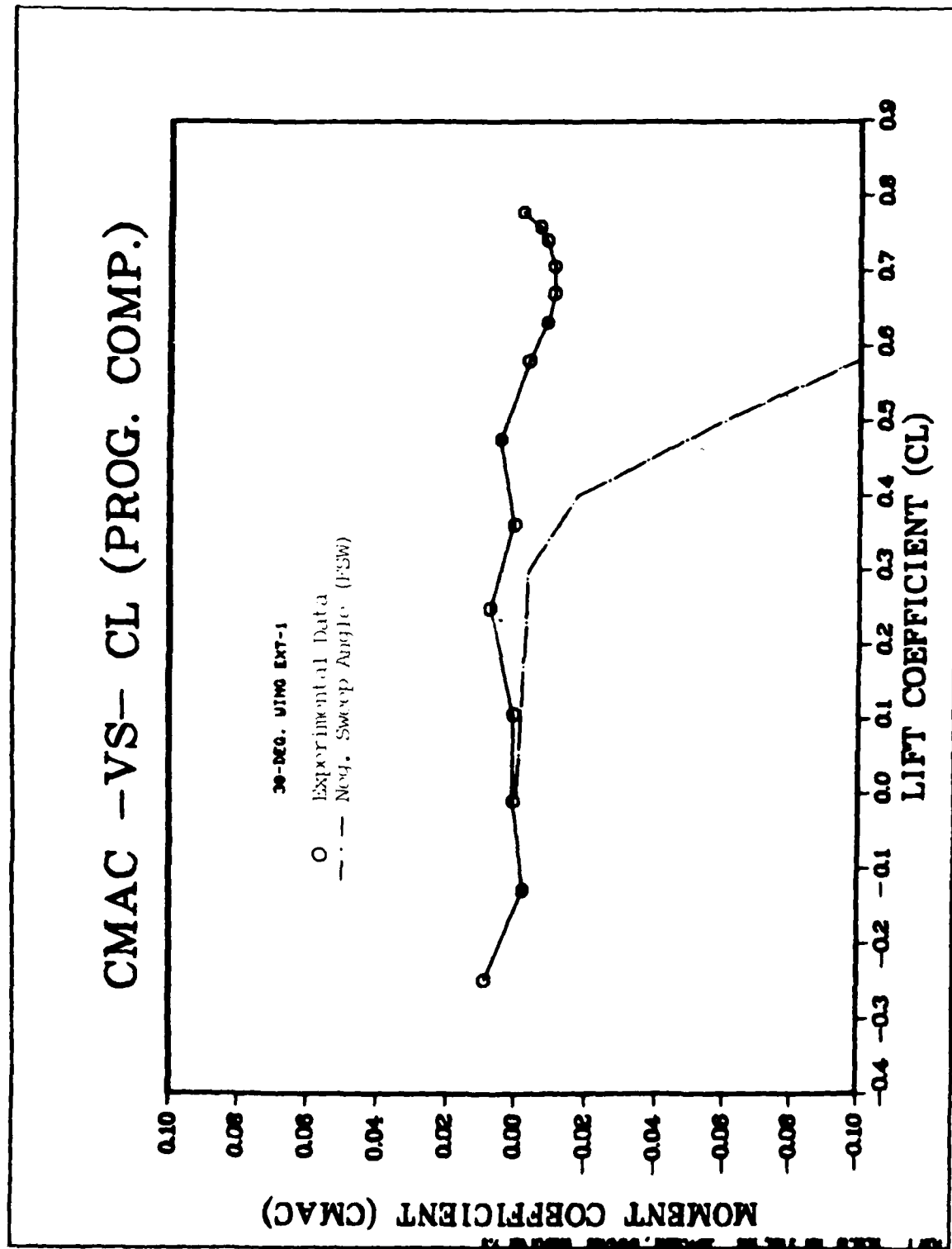
110

CMAC -VS- CL (PROG. COMP.)

Fig. 26c. Program Comparison of Moment Coefficient Versus Lift Coefficient For the 30 Degree Extension-1 Model
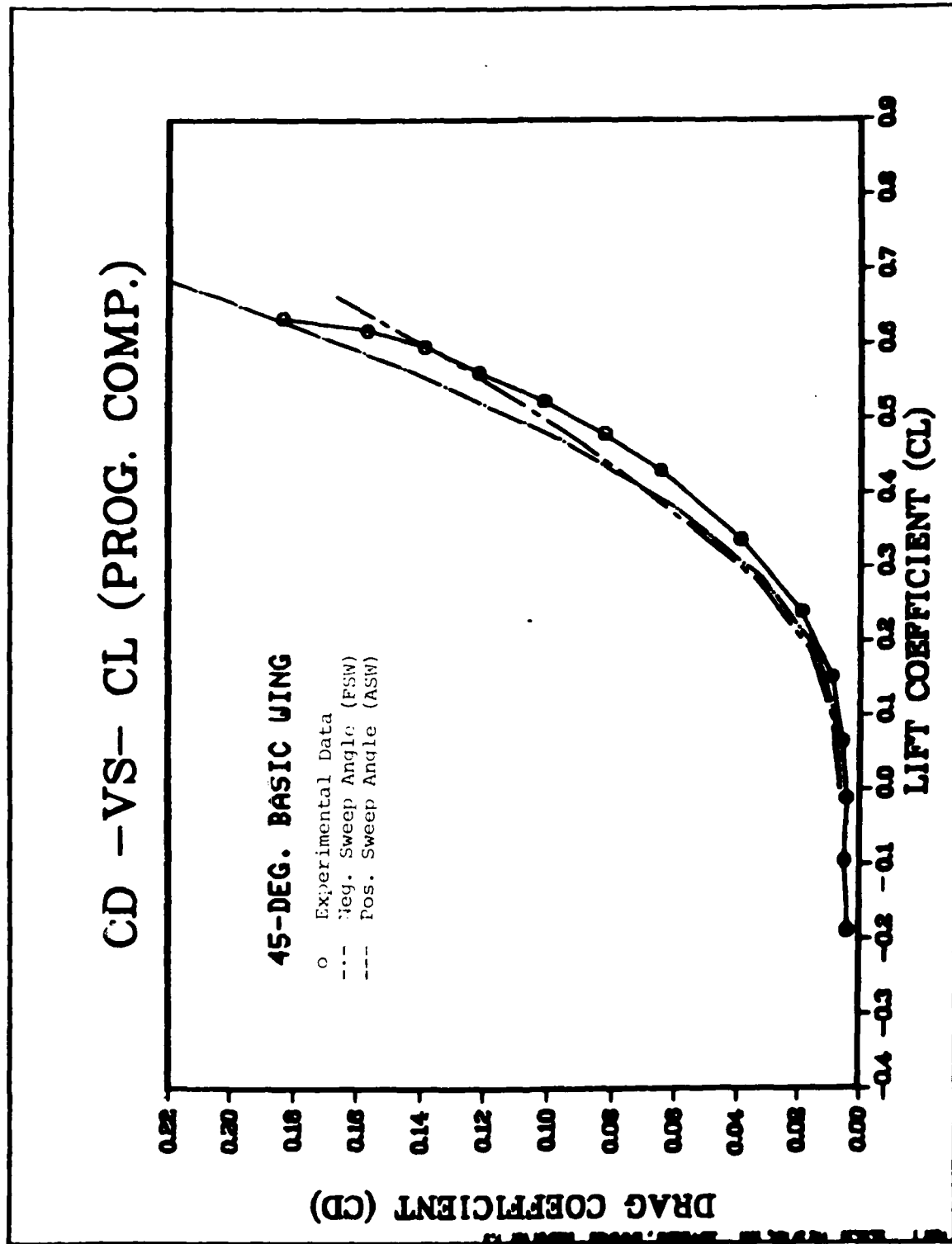
111

Fig. 27a. Progam Comparison of Drag Coefficient Versus Lift Coefficient For the 45 Degree Basic Model
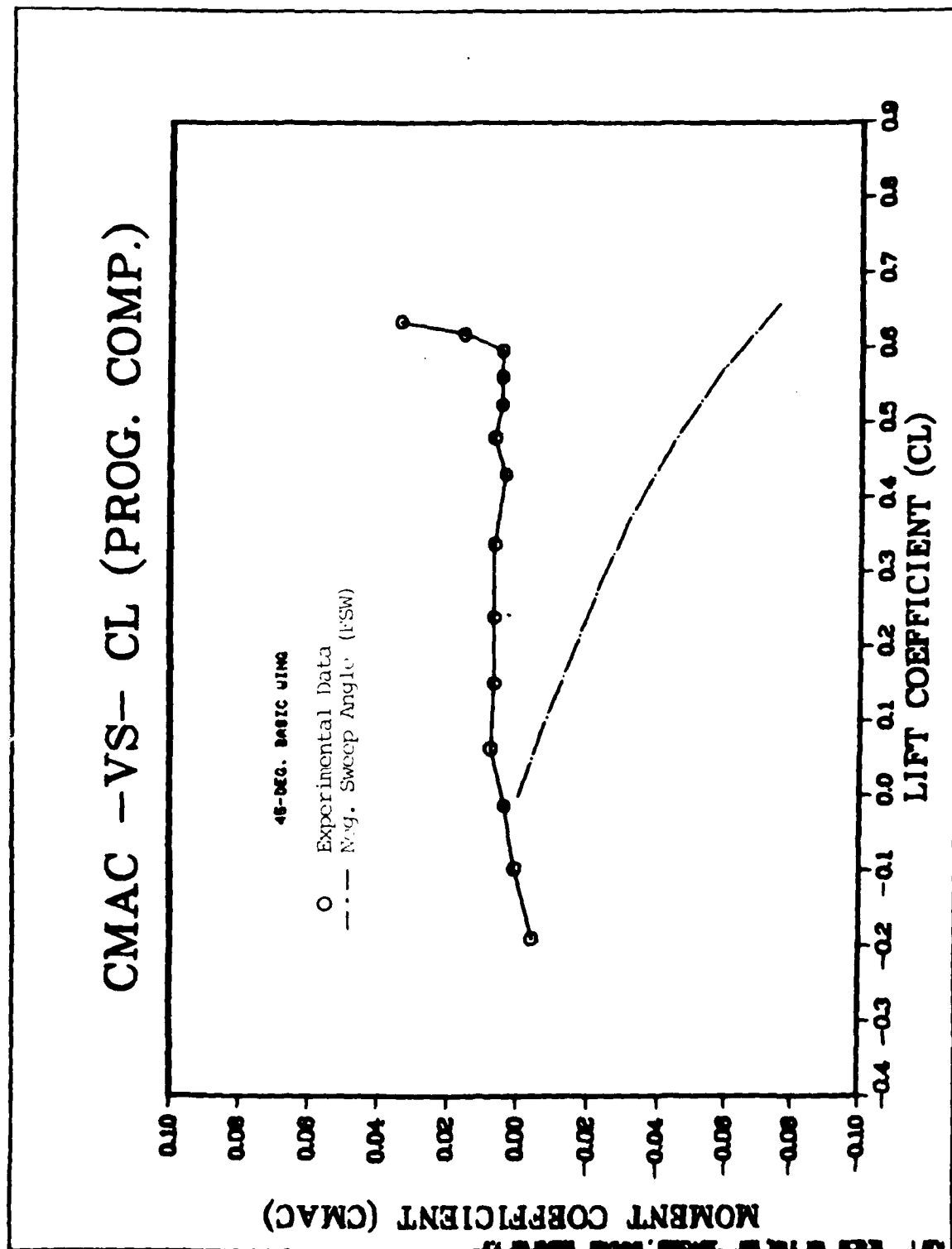
Fig. 27b. Program Comparison of Moment Coefficient Versus Lift Coefficient For the 45 Degree Basic Wing
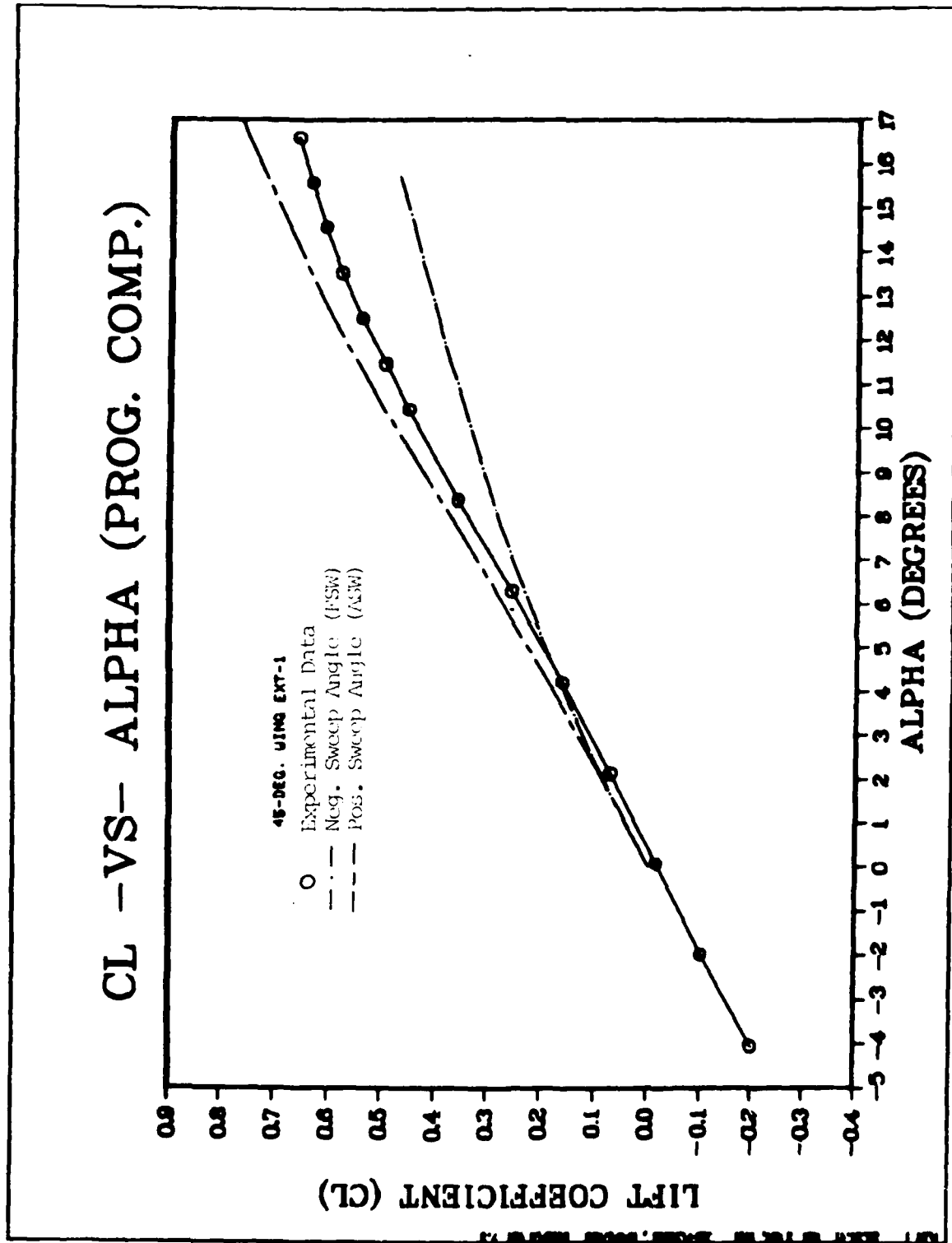
Fig. 28a. Program Comparison of Lift Coefficient Versus Angle of Attack For the 45 Degree Extended 1-1 Wing.
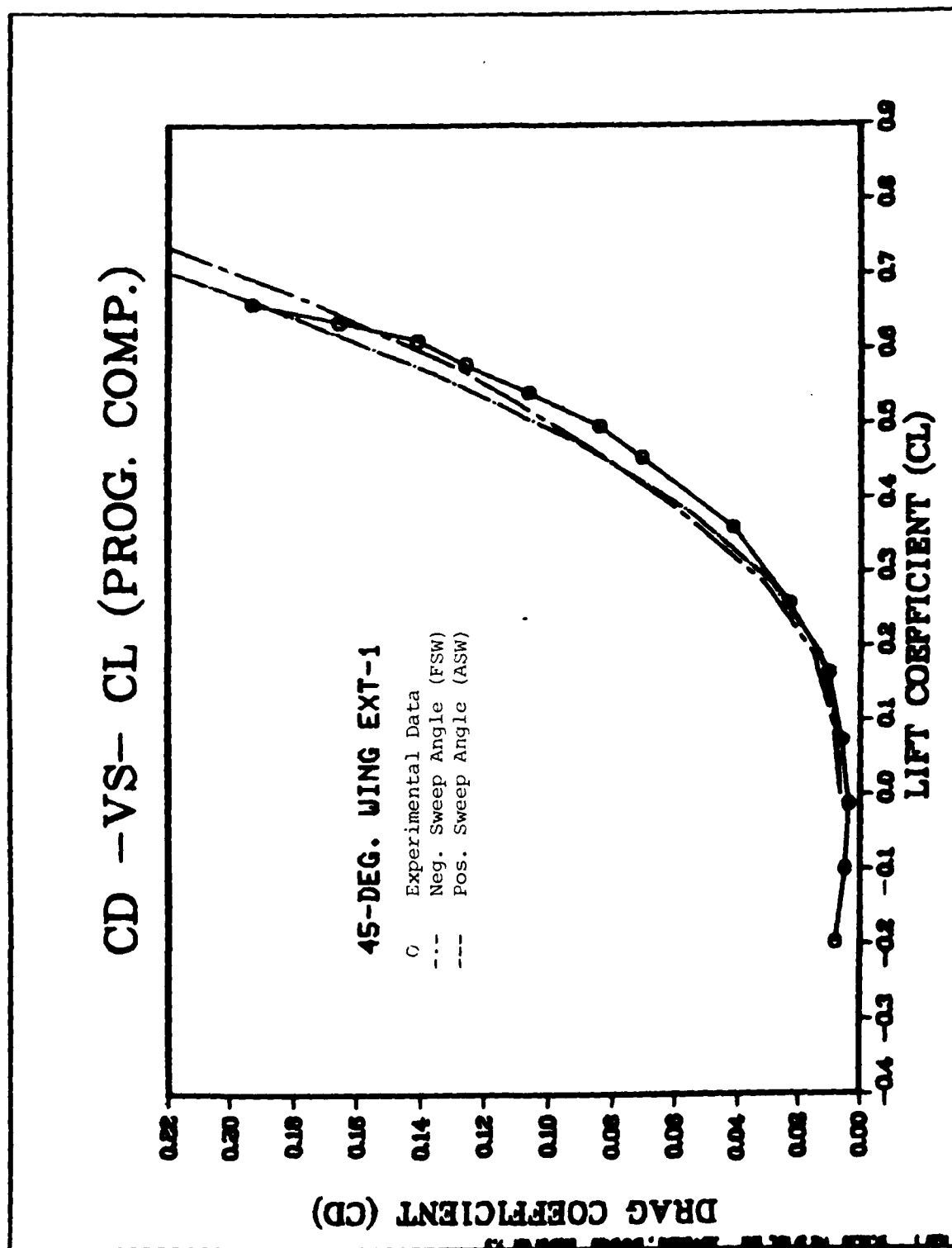
Fig. 28b.   Program Comparison of Drag Coefficient Versus Lift Coefficient For the 45 Degree Extension-1 Model
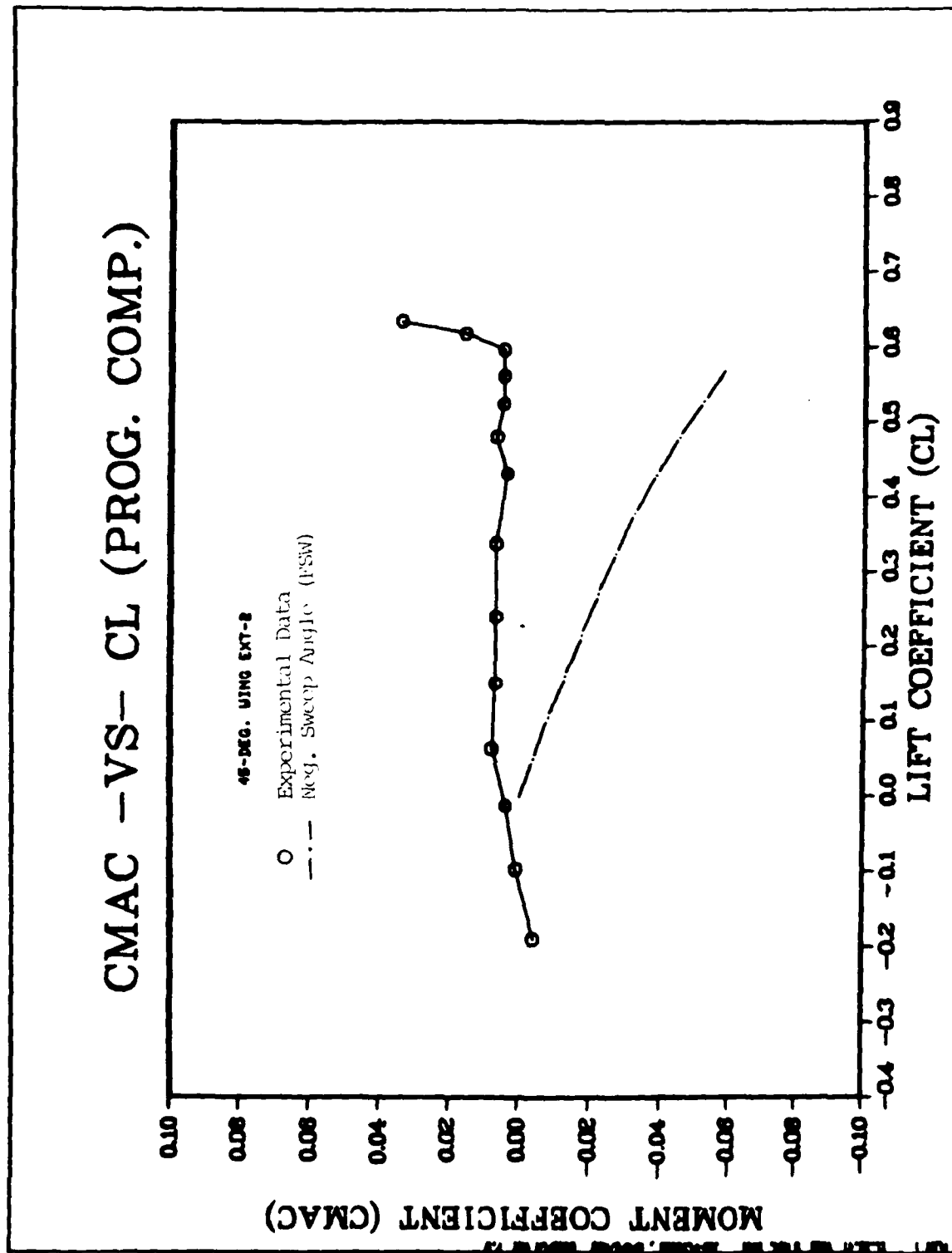
Fig. 28c. Program Comparison of Moment Coefficient Versus Lift Coefficient For the 45 Degree Extension-1 Model.

<u>Vita</u>

Paul W. Savage was born on 20 September 1956 in Mineapolis, Minnesota. He graduated with a *Bachelor of Science in Aeronautical Engineering* and a commission from the U.S.A.F. Academy in 1978. His first assignment was to the Foreign Technology Division at Wright-Patterson AFB where he served as a Foreign Aircraft Analyst for two years. He was then assigned to the A.F. Institute of Technology in June 1980.

SECURITY CLASSIFICATION OF THIS PAGE (When Data Entered)

REPORT DOCUMENTATION PAGE		READ INSTRUCTIONS BEFORE COMPLETING FORM
1. REPORT NUMBER AFIT/GAE/AA/81D-26	2. GOVT ACCESSION NO. AD-A111 128	3. RECIPIENT'S CATALOG NUMBER
4. TITLE (and Subtitle) EXPERIMENTAL ANALYSIS OF THE EFFECTS OF SWEEP AND ASPECT RATIO ON INCOMPRESSIBLE FLOW ABOUT FORWARD SWEPT WINGS		5. TYPE OF REPORT & PERIOD COVERED AFIT Thesis
		6. PERFORMING ORG. REPORT NUMBER GAE/AA/81D-26
7. AUTHOR(s) Paul W. Savage		8. CONTRACT OR GRANT NUMBER(s)
9. PERFORMING ORGANIZATION NAME AND ADDRESS Air Force Institute of Technology (AU) Wright-Patterson AFB, Ohio 45433		10. PROGRAM ELEMENT, PROJECT, TASK AREA & WORK UNIT NUMBERS
11. CONTROLLING OFFICE NAME AND ADDRESS Air Force Flight Dynamic Lab (FIMB) Wright-Patterson AFB, Ohio 45433		12. REPORT DATE December 1981
		13. NUMBER OF PAGES 128
14. MONITORING AGENCY NAME & ADDRESS(if different from Controlling Office)		15. SECURITY CLASS. (of this report) Unclassified
		15a. DECLASSIFICATION, DOWNGRADING SCHEDULE

16. DISTRIBUTION STATEMENT (of this Report)

Approved for public release; distribution unlimited.

17. DISTRIBUTION STATEMENT (of the abstract entered in Block 20, if different from Report)

28 JAN 1982

Air Force Institute of Technology (ATC)
Wright-Patterson AFB, OH 45433

18. SUPPLEMENTARY NOTES

Approved for public release; IAW AFR 190-17

FREDRIC C. LYNCH, Major, USAF
Director of Public Affairs

19. KEY WORDS (Continue on reverse side if necessary and identify by block number)

Forward Swept Wings
Incompressible
Windtunnel test
Aspect Ratio Variation
Sweep Angle Variation

20. ABSTRACT (Continue on reverse side if necessary and identify by block number)

Low speed wind tunnel tests were conducted on nine wing planforms to determine the effect of sweep and aspect ratio on forward swept wings in incompressible flow. Sweep angles tested were -15, -30 and -45 degrees. Aspect ratios ranged from 2.05 to 4.79. A NACA 0006 airfoil section perpendicular to the leading edge was used for all models. Results showed increasing negative sweep decreased lift curve slope and shifted the aerodynamic center rearward. Increasing aspect ratio increased lift curve slope, decreased drag coefficient and shifted the

DD FORM 1473 1 JAN 73   EDITION OF 1 NOV 65 IS OBSOLETE

SECURITY CLASSIFICATION OF THIS PAGE (When Data Entered)

SECURITY CLASSIFICATION OF THIS PAGE(When Data Entered)

aerodynamic center rearward. The wind tunnel aerodynamic data were compared to
the Air Force Flight Dynamics Laboratory's Large Aircraft Performance Prediction
Program to determine the program's ability to predict forward swept wing
aerodynamic coefficients. At incompressible Mach numbers, the program was found
to be accurate in predicting lift curve slope in the linear range using a
positive sweep input. Drag Polar slope and moment coefficient were accurately
predicted for lift coefficients below 0.4 using a negative sweep angle input.
Neither positive nor negative angle input predicted maximum lift coefficient
accurately.

UNCLASSIFIED